

Dissertation

**Submitted to the
Combined Faculty of Natural Sciences
and Mathematics
Heidelberg University, Germany
for the degree of
Doctor of Natural Sciences (Dr. rer. nat.)**

Presented by
Wenqian Feng
Born in Shanxi, P.R.China

Supervisor: Dr. Pavel A. Levkin
Prof. Dr. Oliver Trapp

Oral examination: June 17th, 2016

Spatial Surface Functionalization Based on Photo-induced Thiol Reactions

This dissertation was carried out at the
Organisch-Chemisches Institut
Ruprecht-Karls-Universität Heidelberg

Referees:

Prof. Dr. Oliver Trapp

Prof. Dr. Hans-Robert Volpp

Abstract

Surface functionalization is important for modern science, technology as well as human's daily life. To endow different surfaces with various unique properties, lots of effort has been devoted to develop innovative chemical methods utilized for surface functionalization. Due to the controllability both spatially and temporally, photo-based functionalization is one of the most convenient surface modification methods. This doctoral thesis mainly focuses on photo-induced thiol chemistries for surface functionalization.

In Chapter 1, an introduction is given to describe the recent progress in the field of surface patterning technologies as well as newly developed photo chemistries.

In Chapter 2, a fast (<15 s), initiator-free and versatile surface photopatterning method based on UV-induced thiol-yne click chemistry for creating precise superhydrophobic-superhydrophilic micropatterns is introduced. The method is based on the formation and modification of alkyne-functionalized polymer surfaces with porous structure. This alkyne surface can be modified with variety of thiol-containing chemicals under UV irradiation without any photoinitiator, in different solvents and even in water rapidly. Superhydrophobic-superhydrophilic micropatterns with feature resolution down to 10 μm could be created facilely on this polymer surface. Applications for the formation of microarrays of droplets as well as high-density microarrays of cells are also shown in the chapter.

In Chapter 3, a simple, rapid and convenient surface functionalization method based on UV-induced thiol-ene click chemistry to create transparent and mechanically robust micropatterns on smooth glass or flexible polymer films is described. These patterns enable the fabrication of high-density arrays of low surface tension liquid microdroplets via discontinuous dewetting. A wide range of organic solvents including ethanol, acetone, DMF, dichloromethane and even hexane (surface tension 18.4 mN/m), could be used to produce such microdroplet arrays with complex shapes. This unique method provides an important solution for ultra high-throughput chemical screening applications. The possibility of parallel addition of different chemicals into the individual organic

microdroplets is demonstrated. This approach is also employed to create high-density arrays of polymer microlenses with defined 3D shapes. In addition, this method is uniquely suited to create patterns of hydrophobic nanoparticles that can be only dispersed in organic solvents.

In Chapter 4, a UV-induced 1,3-dipolar nucleophilic addition of tetrazoles to thiols is demonstrated. Under UV irradiation the reaction proceeds rapidly at room temperature, with high yields, without a catalyst, and in both polar protic and aprotic solvents, including water. This UV-induced tetrazole-thiol reaction was successfully applied for the synthesis of small molecules, protein modification, and rapid and facile polymer--polymer conjugation. The reaction has also been demonstrated for the formation of micropatterns by site-selective surface functionalization. Superhydrophobic--hydrophilic micropatterns were successfully created by sequential modifications of a tetrazole-functionalized porous polymer surface with hydrophobic and hydrophilic thiols. In addition, a biotin-functionalized surface could be fabricated in aqueous solutions under long-wavelength UV irradiation.

In the last part of this thesis, a brief summary and outlook are present.

Zusammenfassung

Die Funktionalisierung von Oberflächen ist in der modernen Wissenschaft, der Technologie sowie im alltäglichen Leben von großer Bedeutung. Dabei liegt das Interesse in der Entwicklung innovativer, chemischer Methoden, die zur wirksamen Funktionalisierung von Oberflächen genutzt werden können und somit die unterschiedlichen Oberflächen mit diversen, einmaligen Eigenschaften ausstatten. Die photo-basierende Funktionalisierung ist aufgrund ihrer zeitlichen sowie räumlichen Kontrollierbarkeit eine der leistungsfähigsten Oberflächen-Modifizierungs-Methoden. Das Ziel dieser Doktorarbeit ist die Nutzung von photo-induzierbarer Thiol-Chemie zur Funktionalisierung von Oberflächen.

Kapitel 1 beschreibt den aktuellen Fortschritt der Oberflächen-Patterning-Technologie sowie kürzlich entwickelte Methoden der Photo-Chemie.

In Kapitel 2 wird eine schnelle (<15 s), Initiator-freie und vielseitige Oberflächen Photopatterning Methode vorgestellt, durch die präzise superhydrophobe-superhydrophile Micropatterns, mittels UV-induzierter Thiol-yne Click Chemie, hergestellt werden können. Die Methode basiert auf der Bildung und Modifizierung Alkyne-funktionalisierter Polymer Oberflächen mit poröser Struktur. Diese Alkyne Oberflächen können mit einer Vielfalt an Thiol-haltigen Chemikalien unter UV Bestrahlung und ohne Photo-Initiatoren, sowie in unterschiedlichen Lösungsmitteln und ebenso in Wasser schnell modifiziert werden. Dabei konnten superhydrophobe-superhydrophile Micropatterns, mit einer Merkmalauflösung bis zu $10\ \mu\text{m}$, auf einfachste Weise auf diesen Polymer Oberflächen hergestellt werden. In Kapitel 2 werden außerdem Anwendungen für die Bildung von Tropfen-Microarrays sowie die von high-density Microarrays von Zellen gezeigt.

Kapitel 3 beschreibt eine einfache, schnelle und praktische Oberflächen-Funktionalisierungs Methode zur Herstellung transparenter und mechanisch robuster Micropatterns auf glatter Glasoberfläche oder auf flexiblen Polymer-Filmen, mittels UV-induzierter Thiol-ene Click Chemie. Diese Patterns ermöglichen die Fertigung von high-density Tropfen-Microarrays aus Flüssigkeiten mit geringer

Oberflächenspannung durch diskontinuierlicher Entnetzung. Eine große Auswahl organischer Lösungsmittel, einschließlich Ethanol, Acetone, DMF, Dichloromethane und sogar Hexane (Oberflächenspannung 18.4 mN/m), konnte genutzt werden, um solche Tropfen-Microarray mit komplexen Formen zu erzeugen. Diese einzigartige Methode bietet einen bedeutenden Lösungsansatz für Ultra-High-Throughput Chemikalien Screening Anwendungen und die Möglichkeit der parallelen Zugabe unterschiedlicher Chemikalien in die individuellen, organischen Microtropfen. Dieser Ansatz wird ebenso zur Herstellung von high-density Arrays aus Polymer Microlinsen mit definierten 3D Formen verwendet. Dieser Vorgang ist besonders geeignet Patterns aus hydrophoben Nanopartikeln herzustellen, die nur in organischen Lösungsmitteln dispergiert werden können.

In Kapitel 4 ist die UV-induzierte 1,3-dipolare Nukleophile Addition von Tetrazole zu Thiole gezeigt. Die Reaktion verläuft, unter UV Bestrahlung, bei Raumtemperatur schnell, mit hoher Ausbeute, ohne Katalysator, sowohl in polar protischen als auch in aprotischen Lösungsmitteln, einschließlich Wasser ab. Diese UV-induzierte Tetrazole-Thiol Reaktion konnte erfolgreich für die Synthese von niedermolekularer Verbindungen, für Protein Modifikationen und einer schnellen und einfachen Polymer-Polymer Konjugation verwendet werden. Ebenso wurde die Nutzung dieser Reaktion für die Bildung von Micropatterns mit lagenselektiver Oberflächen-Funktionalisierung gezeigt. Superhydrophobe-hydrophile Micropatterns wurden erfolgreich mittels sequenzieller Modifikation einer Tetrazol-funktionalisierten, porösen Polymer Oberfläche mit hydrophoben und hydrophilen Thiolen gebildet. Außerdem konnte eine biotin-funktionalisierte Oberfläche in einer wässrigen Lösung, unter Bestrahlung mit langwelligem UV-Licht hergestellt werden.

Abschließend werden in Kapitel 5 dieser Thesis eine kurze Zusammenfassung sowie Perspektiven aufgezeigt.

Acknowledgement

I am very thankful to my PhD mentor, Dr. Pavel Levkin, for offering the opportunity to perform research work in his group, for his consistent interest in the progress of my work, and for lots of valuable suggestions and discussions. His encouragement and thoughtfulness are precious to me.

I am grateful to Prof. Dr. Oliver Trapp for supervising during my PhD period and reviewing my PhD thesis.

I would also like to thank Prof. Dr. Hans-Robert Volpp for taking his time to be my second reviewer.

I thank Dr. Alex Welle for his measurements and helpful discussions of Time-of-Flight Secondary Ion Mass Spectrometry in the Institut für Funktionelle Grenzflächen, Karlsruhe Institute of Technology.

I thank Stefan Heissler for his kind help with Raman spectroscopy in the Institut für Funktionelle Grenzflächen, Karlsruhe Institute of Technology.

I thank Dr. Olaf Fuhr for his kind support on the mass spectrometry in the Institute of Nanotechnology, Karlsruhe Institute of Technology.

I thank Sven Stahl for his help with NMR Bruker AMX 5000 spectrometer in the Institute of Nanotechnology, Karlsruhe Institute of Technology.

I thank Dr. Tim Scharnweber for his kind support on the fluorescent microscopy in the Institut für Biologische Grenzflächen, Karlsruhe Institute of Technology.

I thank Chengwu Yang and his colleagues for their generous supports and measurements of X-ray photoelectron spectroscopy in the Institut für Funktionelle Grenzflächen, Karlsruhe Institute of Technology.

I thank Hualong Yan and Dr. Christine Blattner for help with the SDS-PAGE measurements in the Institut für Toxikologie und Genetik, Karlsruhe Institute of Technology.

I thank Dr. Blanco-Jaimes for the help with the manuscript writing.

I would like to thank Prof. Dr. Frank Breitling, Prof. Dr. Andrew Cato, Dr. Cornelia Lee-Thedieck and Dr. Alex Welle for being my TAC members and for their valuable scientific suggestions.

Special thanks to my colleagues in the Institut für Toxikologie und Genetik, particularly Dr. Linxian Li, Dr. Junsheng Li, Dr. Xin Du, Dr. Erica Boles, Dr. Victoria Nedashkivska, Dr. Girish Shankara, Dr. Alexander Efremov, Dr. Anna Popova, Dr. Danuta Kuzmicz, Tina Cruz, Konstantin Demir, Dr. Qing Chen, and Dr. Ping Zhang for their generous support both academic and personal. It was great to work with these lovely people.

I want to thank Helmholtz Association's Initiative and Networking Fund (Grant VH-NG-621) and China Scholarship Council to support my PhD research and studies.

I would like to thank Prof. Fengbao Zhang, a respected academic who guided me in scientific research during my master period in Tianjin University.

I am especially grateful to my parents and my wife, for their consistent encouragement and support to my academic career.

Publications

Refereed Publications

Wenqian Feng, Linxian Li, Xin Du, Alexander Welle, and Pavel A. Levkin. Single-Step Fabrication of High-Density Microdroplet Arrays of Low Surface Tension Liquids. *Advanced Materials*. 2016, DOI: 10.1002/adma.201505972.

Wenqian Feng, Linxian Li, Chengwu Yang, Alexander Welle, Oliver Trapp and Pavel A. Levkin. UV-Induced Tetrazole-Thiol Reaction for Polymer Conjugation and Surface Functionalization. *Angewandte Chemie International Edition*. 2015, 54, 8732.

Wenqian Feng, Linxian Li, Erica Ueda, Junsheng Li, Stefan Heißler, Alexander Welle, Oliver Trapp, Pavel A. Levkin. Surface Patterning via Thiol-Yne Click Chemistry: An Extremely Fast and Versatile Approach to Superhydrophilic-Superhydrophobic Micropatterns. *Advanced Materials Interfaces*. 2014, 1, 1400269.

Michael Hirtz¹, **Wenqian Feng**, Harald Fuchs, and Pavel A. Levkin. Click-Chemistry Immobilized 3D-Infused Microarrays in Nanoporous Polymer Substrates. *Advanced Materials Interfaces*. 2016, DOI: 10.1002/admi.201500469.

P. Lindemann, A. Schade, L. Monnereau, **W. Feng**, K. Batra, H. Gliemann, P. Levkin, S. Bräse, C. Wöll and M. Tsotsalas. Surface functionalization of conjugated microporous polymer thin films and nanomembranes using orthogonal chemistries. *Journal of Materials Chemistry A*. 2016, DOI: 10.1039/C5TA09429A.

Xin Du, Junsheng Li, Alexander Welle, Linxian Li, **Wenqian Feng**, Pavel A. Levkin. Reversible and Rewritable Surface Functionalization and Patterning via Photodynamic Disulfide Exchange. *Advanced Materials*. 2015, 27, 4997.

Junsheng Li, Linxian Li, Xin Du, **Wenqian Feng**, Alexander Welle, Michael Grunze, Oliver Trapp, Michael Hirtz and Pavel A. Levkin. Reactive Superhydrophobic Surface and Its Photoinduced Disulfide-ene and Thiol-ene (Bio)functionalization. *Nano Letter*. 2015, 15, 675.

Manuel Tsotsalas, Himanshu Maheshwari, Sophia Schmitt, Stefan Heißler, **Wenqian Feng** and Pavel A. Levkin. Freestanding MOF Microsheets with Defined Size and Geometry Using Superhydrophobic–Superhydrophilic Arrays. *Advanced Materials Interfaces*. 2015, DOI: 10.1002/admi.201500392

Muling Zeng, Anna Laromaine, **Wenqian Feng**, Pavel A. Levkin and Anna Roig. Origami magnetic cellulose: controlled magnetic fraction and patterning of flexible bacterial cellulose. *Journal of Materials Chemistry C*. 2014, 2, 6312.

Michael Hirtz, Marcus Lyon, **Wenqian Feng**, Andrea E. Holmes, Harald Fuchs and Pavel A. Levkin. Porous polymer coatings as substrates for the formation of high-fidelity micropatterns by quill-like pens. *Beilstein J. Nanotechnol.* 2013, 4, 377.

Oral Presentation

Wenqian Feng and Pavel A. Levkin. Single-Step Fabrication of High-Density Microdroplet Arrays of Low Surface Tension Liquids. The 2nd International Symposium on Bioinspired Interfacial Materials with Superwettability 2016. Shanghai, China.

Poster Presentations

Wenqian Feng and Pavel A. Levkin. UV-Induced Tetrazole-Thiol Reaction for Polymer Conjugation and Surface Functionalization. Deutsche- Bunsen-Gesellschaft für physikalische Chemie 2015. Bochum, Germany.

Wenqian Feng and Pavel A. Levkin. Superhydrophobic–Superhydrophilic Micropatterning via Click Chemistry. Fourth International Conference on Multifunctional, Hybrid and Nanomaterials 2015. Sitges, Spain.

Wenqian Feng and Pavel A. Levkin. A Fast and Versatile Approach to (Super)hydrophilic-(Super)hydrophobic Micropatterns via Thiol-ene Click Chemistry.

555th Wilhelm and Else Heraeus Seminar 2014. Hanau, Germany.

Wenqian Feng, Linxian Li, and Pavel A. Levkin. Superhydrophobic–Superhydrophilic Micropatterning via Click Chemistry. 539th Wilhelm and Else Heraeus Seminar 2013. Hanau, Germany.

Patents

Pavel Levkin, Linxian Li, Junsheng Li, Xin Du, **Wenqian Feng**. Reactive superhydrophobic surfaces, patterned superhydrophobic surfaces, methods for producing the same and use of the patterned superhydrophobic surfaces.

Pavel Levkin, **Wenqian Feng**, Linxian Li. Einschnittverfahren zur Herstellung hochdichter Droplet Microarrays von Flüssigkeiten mit geringer Oberflächenspannung. Submitted.

Abbreviations

°C	degree celsius
ACN	acetonitrile
BSA	bovine serum albumin
BMA	butyl methacrylate
CA	contact angle
CDCl ₃	chloroform, deuterated
δ	chemical shift
DIC	<i>N,N'</i> -diisopropylcarbodiimide
DCM	dichlormethane
DMAP	4-dimethylaminopyridine
DMF	dimethylformamide
DMPA	2,2-dimethoxy-2-phenylacetophenone
DMSO	dimethylsulfoxide
DMSO- <i>d</i> ₆	dimethylsulfoxide, deuterated
DPN	dip-pen nanolithography
EDMA	ethylene dimethacrylate
EtOAc	ethyl acetate
e.g.	exempli grātiā (for example)
eq.	equivalents
ESI	electrospray Ionization
Et	ethyl
<i>et al.</i>	et altera (and others)
FBS	fetal bovine serum
h	hour
HEMA	2-hydroxyethyl methacrylate
Hz	hertz
IR	infrared
<i>J</i>	coupling constant

min	minutes
MS	mass spectrometer
nm	nanometer
NMR	nuclear magnetic resonance
PBS	phosphate buffered saline
PDMS	poly(dimethylsiloxane)
PEG	poly(ethylene glycol)
PFDT	1 <i>H</i> ,1 <i>H</i> ,2 <i>H</i> ,2 <i>H</i> -perfluorodecanethiol
Ph	phenyl
rt	room temperature
SDS-PAGE	sodium lauryl sulfate-polyacrylamide gel electrophoresis
SEM	scanning electron microscope
TEA	triethylamine
THF	tetrahydrofuran
UV	ultraviolet
μCP	microcontact printing
μm	micrometer

Table of contents

Abstract	I
Acknowledgement.....	V
Publications	VII
Abbreviations	XI
Chapter 1. Introduction	1
1.1 Spatial surface modification.....	2
<i>1.1.1</i> Printing technologies.....	3
<i>1.1.2</i> Photolithography	6
1.2 Photo-induced (click) chemistry	10
<i>1.2.1</i> Photo-induced azide-alkyne reactions	11
<i>1.2.2</i> Photo-induced tetrazole-ene reactions	13
<i>1.2.3</i> Photo-induced thiol-ene/yne reactions	17
<i>1.2.4</i> Other photo-induced reactions	19
1.3 Superhydrophobic surfaces	27
<i>1.3.1</i> Theoretical background.....	27
<i>1.3.2</i> Superhydrophobic surfaces	29
<i>1.3.3</i> Porous polymethacrylate monoliths.....	31
Chapter 2. Surface Patterning via Thiol-Yne Click Chemistry: A Fast and Versatile Approach to Superhydrophilic-Superhydrophobic Micropatterns.....	35
2.1 Introduction	36
2.2 Results and discussions	37
2.2.1 Fabrication of alkyne surface	37
2.2.2 Kinetics of the thiol-yne reactions on alkyne surface	41
2.2.3 Thiol-yne reactions in different solvents.....	44
2.2.4 Stability of the superhydrophobic surface.....	45
2.2.5 Superhydrophobic-superhydrophilic micropatterns on alkyne surface.....	46
2.2.5 Inverse micropatterns	48
2.2.6 Hela-GFP cells array on superhydrophobic-superhydrophilic micropatterns...	50
2.3 Conclusions	50
2.4 Experimental details.....	51
2.4.1 Materials.....	51

2.4.2 Preparation of 12.5 μm -thin porous HEMA-EDMA films.....	51
2.4.3 Preparation of alkyne modified HEMA-EDMA.....	52
2.4.4 Thiol-yne “click” reactions on the porous polymer layer.....	52
2.4.5 Preparation of superhydrophobic-superhydrophilic micropatterns via thiol-yne click photopatterning	53
2.4.6 Preparation of inverse patterns	53
2.4.7 Using the thiol-yne patterning method for creating peptide patterns	53
2.4.8 Fabrication of cell microarray	54
Chapter 3. Single-Step Fabrication of High-Density Microdroplet Arrays of Low Surface Tension Liquids	55
3.1 Introduction.....	56
3.2 Results and discussions.....	57
3.2.1 Glass surface modification via silanation and UV-induced thiol-ene click reactions	57
3.2.2 Dewetting ability	61
3.2.3 Fabrication of microdroplet arrays via discontinuous dewetting	62
3.2.4 Smooth and rough surfaces.....	64
3.2.5 Transparency.....	66
3.2.6 Mechanical stability	67
3.2.7 High-throughput screening	68
3.2.8 Nanoparticles arrays	70
3.2.9 Polymer micropads arrays	71
3.2.10 Flexible polymeric substrate.....	72
3.3 Conclusions.....	72
3.4 Experimental details	73
3.4.1 Materials	73
3.4.2 Characterization	73
3.4.3 Preparation of dewetting-wetting pattern on bare glass	74
3.4.4 Preparation of superhydrophobic porous polymer surface	74
3.4.5 Preparation of poly(ethylene dimethacrylate) micropad arrays.....	74
3.4.6 Preparation of flexible and smooth HEMA-EDMA polymer layer.....	75
Chapter 4. UV-Induced Tetrazole-Thiol Reaction for Polymer Conjugation and Surface Functionalization	77

4.1 Introduction	78
4.2 Results and discussions	79
4.2.1 Kinetics of the UV-induced tetrazole-thiol reaction	79
4.2.2 Isolated yield of the UV-induced tetrazole-thiol reaction under different conditions.	86
4.2.3 Protein modification via UV-induced tetrazole-thiol reaction in water.....	87
4.2.4 UV-induced tetrazole-thiol reaction for polymer conjugation.....	91
4.2.5 UV-induced tetrazole-thiol reaction for surface functionalization	92
4.2.6 Patterning biomolecules in water under long-wavelength UV irradiation.....	100
4.3 Conclusions	101
4.4 Experimental details.....	101
4.4.1 Materials.....	101
4.4.2 Preparation of 4-(2-phenyl-2H-tetrazol-5-yl)benzoic acid	102
4.4.3 Preparation of methyl 4-(2-phenyl-2H-tetrazol-5-yl)benzoate 1	102
4.4.4 Kinetic study of UV-induced 1,3-dipolar nucleophilic addition with 1 and 2	103
4.4.5 Yield of UV-induced 1,3-dipolar nucleophilic addition with 1 and 2 under different conditions	103
4.4.6 Preparation of PEG-tetrazole 4	104
4.4.7 UV-induced 1,3-dipolar nucleophilic addition in water	104
4.4.8 Modification of bovine serum albumin (BSA) by PEG-tetrazole.....	104
4.4.9 Polymer-polymer coupling	105
4.4.10 Preparation of tetrazole-modified HEMA-EDMA films (tetrazole surface)	105
4.4.11 UV-induced tetrazole-thiol reactions on tetrazole surface.....	106
4.4.12 Preparation of superhydrophobic-hydrophilic micropatterns via tetrazole-thiol reaction.....	106
4.4.13 Designing a cell microarray on produced superhydrophobic-hydrophilic micropattern	107
4.4.14 Immobilization of biotin-PEG-thiol on tetrazole surface and Streptavidin binding	107
Chapter 5. Summary and outlook	109
References	113

Chapter 1. Introduction

1.1 Spatial surface modification

Surfaces are universal and have been widely used in our daily lives. The ability to control chemical properties of a surface, such as hydrophobicity,^[1, 2] antibacterial property,^[3-5] antifouling property,^[6, 7] anti-icing property,^[8-10] biocompatible property,^[11-13] stimuli-responsibility^[14, 15] *etc.*, is crucial in most of the applications. To introduce or to vary a specific functionality in a substrate, many surface modification methods have been explored by incorporating selected elements or functional groups to a surface. A classic example is the mussel-inspired polydopamine coating. Messersmith *et al.* demonstrated that dopamine could polymerize in basic water solutions and resulted in polydopamine coating on various surfaces immersed in the solution.^[16] Moreover, the polydopamine coating could, in turn, react with thiols, amines and metal ions to introduce further functionalities (see Figure 1.1), offering a simple and versatile strategies for surface modification of multiple classes of materials.

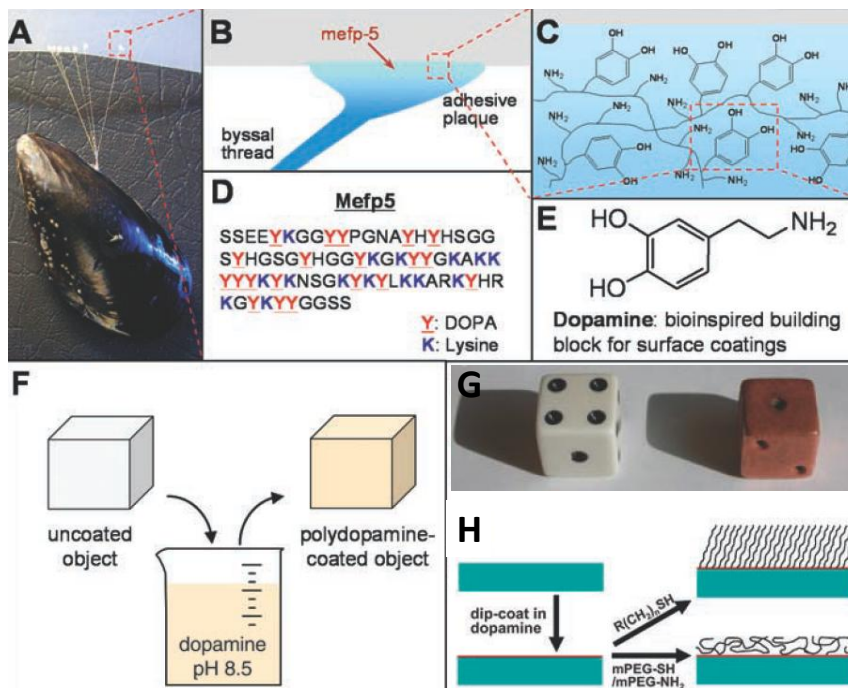


Figure 1.1. Mussel-inspired polydopamine coating. (A) Photograph of a mussel attached to commercial poly(tetrafluoroethylene) surface. (B and C) Schematic illustrations of the interfacial location of Mytilus edulis foot protein 5 (Mefp-5) and a simplified molecular representation of characteristic amine and catechol groups. (D) The amino acid sequence of Mefp-5. (E) Dopamine contains both amine and catechol functional groups found in

Mefp-5. It was used as a molecular building block for polymer coatings. (F) A schematic illustration of thin film deposition of polydopamine by dip-coating an object in an alkaline dopamine solution. (G) Polydopamine-assisted electroless metallization of plastic object. (H) Schematic illustration of thiol monolayer and polyethylene glycol (PEG) polymer grafting on polydopamine-coated surfaces. Adapted from Ref.^[16]

Spatial surface modification which could be used to create well-controlled chemical patterns, otherwise known as surface patterning, has attracted great interest in the past decades. Patterned surfaces have a wide range of applications in both research and industrial fields including microfluids,^[17] bioarrays,^[18-20] medicinal science^[21] and the development of optics^[22, 23] and electronics.^[24] To achieve the control needed during surface patterning, a number of techniques have been optimized to introduce target chemicals at the specified place on substrate. Basically these technologies can be categorized into two strategies. In the first strategy, the contact between the substrate and the modification chemical is controlled. Target chemical is delivered onto the substrate, and the reaction only takes place on where the modification chemical is present. This type of patterning methods also can be described as printing technologies, and several kinds of frequently used techniques in lab, including microcontact printing,^[25, 26] inkjet printing,^[27] dip-pen nanolithography,^[28] are based on this strategy. The second strategy of surface patterning is to control the initiation of the modification reaction. In this case, the reaction is only initiated in the selected areas even the whole surface is in contact with the modification chemical. Electron-beam lithography,^[29] laser writing,^[30] two-photon polymerization^[31, 32] and the important photolithography^[33] fall into the second strategy.

1.1.1 Printing technologies

Microcontact printing (μ CP), pioneered by the Whitesides group in the 1990s, has proven to be a useful technique in the spatial functionalization of certain chemicals and biological materials onto surfaces.^[34-37] In traditional μ CP, a poly(dimethylsiloxane) (PDMS) stamp with bas relief features is used to transfer an 'inked' material to the substrate (Figure 1.2A). By decreasing the printed zones of structures on a PDMS stamp below 100 nm and by diluting the molecules in the ink, single protein molecules was patterned on a bare glass (Figure 1.2 B,C).^[38]

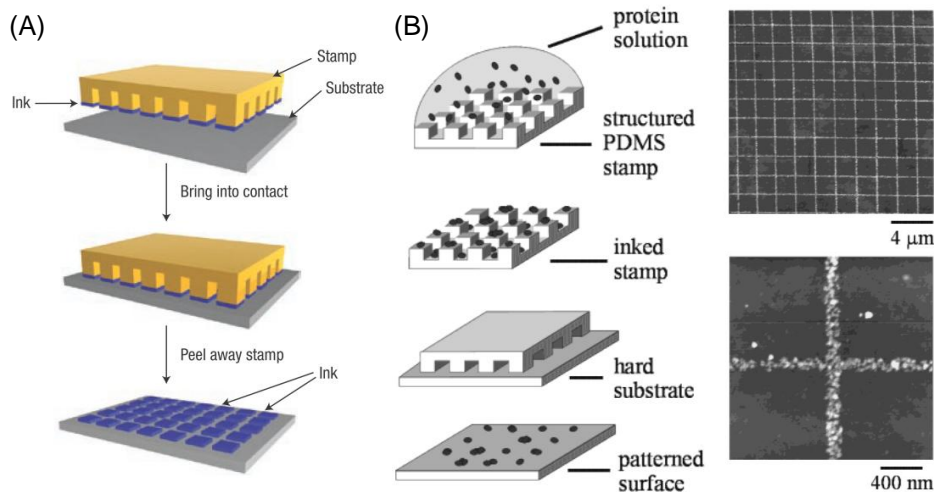


Figure 1.2. (A). Schematic of surface patterning via μ CP. Adapted from Ref. ^[39] (B) Fabricating high-resolution patterns of proteins using μ CP. Fabrication starts with depositing proteins from solution onto the surface of a stamp during an inking step and transferring the proteins to a substrate in the area of contact to yield a patterned substrate once the stamp has been removed. (C) AFM images of antibodies microcontact printed on glass using high-resolution PDMS stamps. Adapted from Ref. ^[38]

In recent years, the technology of contact and non-contact printing has progressed enough to be used for the surface patterning.^[40] Li et al. developed a simple method for creating superhydrophilic-superhydrophobic micropatterns using a contact printer.^[41] An “ink”, an ethanol solution of a phospholipid, was printed onto a porous polymer superhydrophobic surface and transformed the spots into superhydrophilic areas (Figure 1.3). The lipid molecules were absorbed on solid substrate physically, hence a single washing of the lipid-coated superhydrophilic surface with organic solvents could make it again superhydrophobic. As a special inkjet technology, a filament of an ink material could also be extruded from a nozzle continuously and is deposited on a substrate to yield 2D or 3D patterns.^[42]

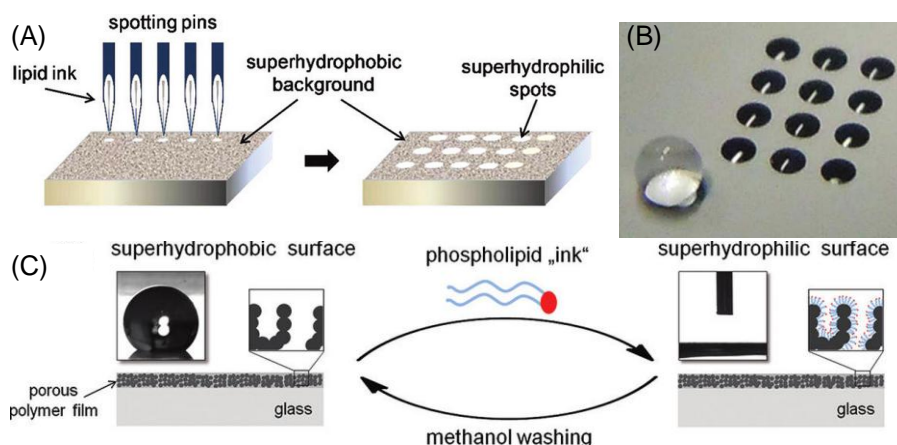


Figure 1.3. (A) Schematic illustration of the creating an array of superhydrophilic microspots by printing a lipid/ethanol solution as an ink on a superhydrophobic background. (B) Image of an array of superhydrophilic spots filled with water and a water droplet on the superhydrophobic background. (C) Schematic representation of switching from superhydrophobicity to superhydrophilicity by applying an “ink” containing a phospholipid. Adapted from Ref.^[41]

Similar to ink-jet printing, scanning probe microscope lithography such as dip-pen nanolithography (DNP) is another branch of direct writing techniques.^[43, 44] With the aid of atomic-force microscopy (AFM) tip, the ink molecules transfer from the tip to the underlying substrate as a result of chemical or physical adsorption of the ink to the surface (Figure 1.4A). The resolution of patterning depends on the scanning speed, the volume of meniscus, the surface chemistry, the temperature as well as the ambient humidity.^[39] By using quill-like microcantilevers attached to a DPN platform, Hirtz et al. compared the microarray printing on different solid supports that are typically used in microspot printing, including paper, polymeric nitrocellulose, nylon membranes as well as porous poly(2-hydroxyethyl methacrylate-co-ethylene dimethacrylate) (HEMA-EDMA) layer.^[45] The size distribution of spots patterns on the HEMA-EDMA was narrow and symmetrical, while the size of the spots can be tuned by varying the dwell time (Figure 1.4B-D).

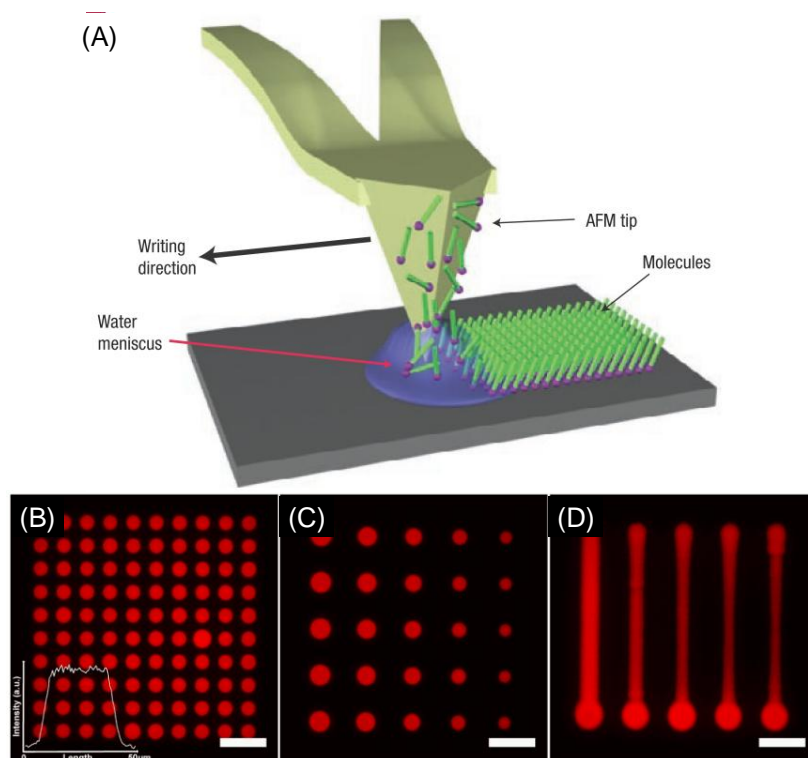


Figure 1.4. (A) Schematic illustration of the patterning process by using dip-pen nanolithography. Adapted from Ref. ^[39]. Fluorescent micrographs of (B) a spot pattern with 0.5 s dwell time, the inset shows the intensity profile of a typical spot; (C) spot pattern with varying dwell time (from left column to right 2.0 s, 1.5 s, 1.0 s, 0.5 s, and 0.1 s, respectively), and (D) lines written with different speeds (from left to right 50 $\mu\text{m/s}$, 100 $\mu\text{m/s}$, 150 $\mu\text{m/s}$, 200 $\mu\text{m/s}$, and 250 $\mu\text{m/s}$, respectively). Lines were written from bottom to top. Scale bars, 100 μm . Adapted from Ref. ^[45].

1.1.2 Photolithography

Since light-induced modifications can be spatially controlled by focusing photons onto a given area and controlled temporally by varying exposure time, wavelength, or intensity, photolithography is one of the most convenient techniques for surface patterning.^[39, 46] The principle of photolithography is that the modification reactions are triggered by light in the exposed areas. Site-specific exposure is usually achieved by illuminating the substrate through a photomask or by direct laser writing. The resolution of patterns varies from micrometres to sub-100 nanometres.^[39]

UV-induced polymerizations have been employed to generate patterns on surfaces.^[19, 47] Zahner et al. created superhydrophilic patterns in superhydrophobic porous polymer

films by UV-initiated photografting (Figure 1.5).^[19] A porous poly(butyl methacrylate-*co*-ethylene dimethacrylate) (BMA-EDMA) film was wetted with a photografting mixture composed of a hydrophilic methacrylate monomer, photoinitiator, and a mixture of tert-butanol/water. The monomer polymerized on the surface under UV light through a photomask, transforming the irradiated superhydrophobic surface into a highly wettable superhydrophilic surface.

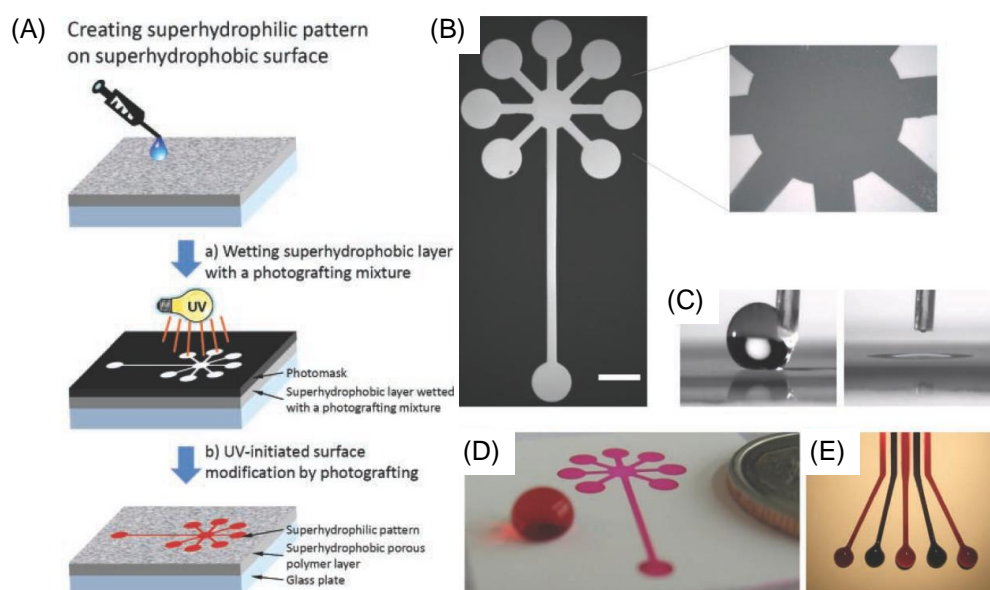


Figure 1.5. (A) Schematic representation of the method for creating superhydrophilic micropatterns by UV-initiated photografting. (B) Optical microscopy images of a superhydrophilic pattern after wetting with water. (C) Water droplets on the superhydrophobic BMA-EDMA before (left) and after photografting (right). (D) and (E) Superhydrophilic patterns with different geometries filled with water dye solutions. Adapted from Ref.^[19]

Hydrogels with designed geometry could be generated on surface after selective photocrosslinking (Figure 1.6).^[48] Upon 365 nm UV irradiation, 4-arm poly(ethylene glycol)-methacrylate (PEG-4-MA) and 4-arm poly(ethylene glycol)-tetrazole (PEG-4-Tet) could be crosslinked via tetrazole-alkene reaction and form hydrogels in situ. By selective exposure to UV light, patterned hydrogels with strong fluorescence at around 460 nm were formed.

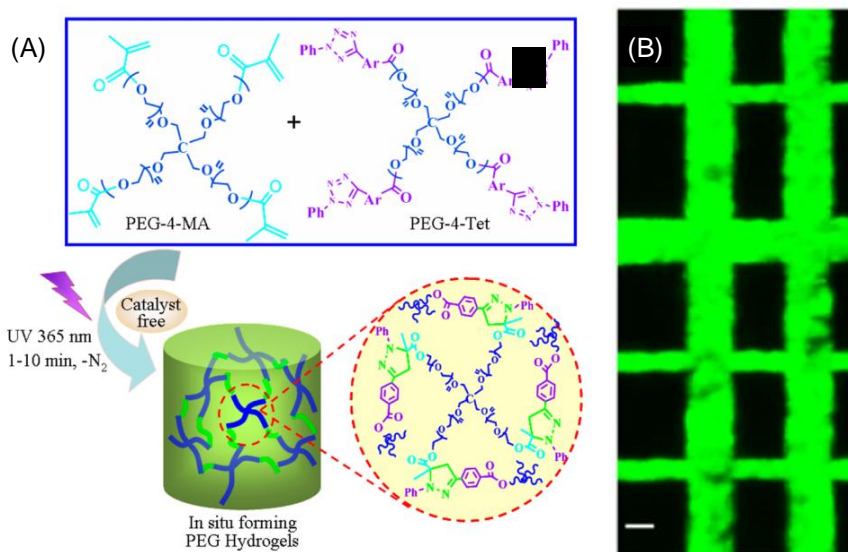


Figure 1.6. (A) Schematic representation of the in situ formation of poly(ethylene glycol) (PEG) hydrogels prepared from PEG-4-MA and PEG-4-Tet derivatives via catalyst-free UV-induced tetrazole-alkene reaction. (B) Fluorescence image of patterned PEG hydrogels formed under UV irradiation through a photomask. Scale bar: 100 μm . Adapted from Ref.^[48]

UV-induced decomposition reactions can also be utilized to pattern surfaces.^[49-51] As an example, Lai et al. fabricated a superamphiphobic surface based on *1H, 1H, 2H, 2H*-perfluorodecyltriethoxysilane (PFDS) modified pinecone-like anatase TiO_2 particles film.^[51] TiO_2 is a photosensitive material which possesses the excellent photocatalytic activity to decompose the PFDS layer under UV light.^[52] Thus, patterned superoleophilic surfaces with desired geometry could be easily constructed by controlling the site-selective exposure of UV light.

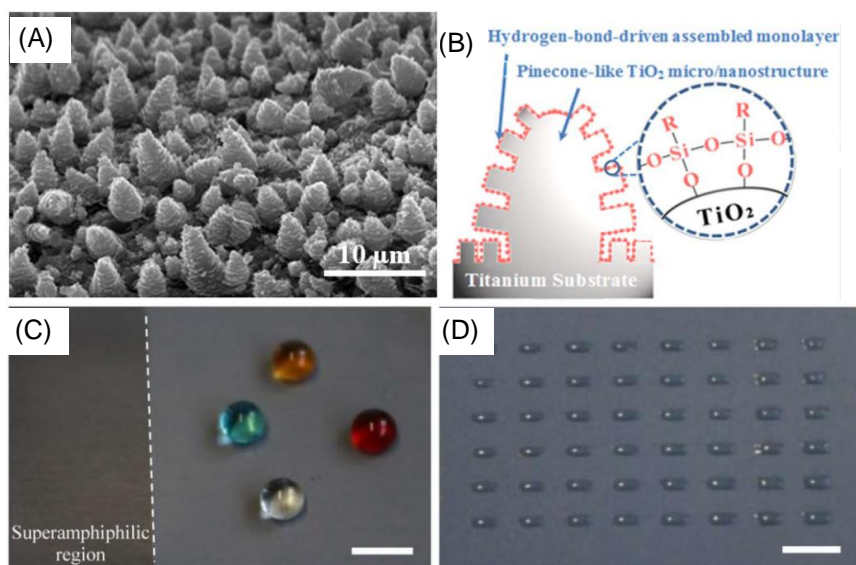


Figure 1.7. (A) SEM image of the as-anodized hierarchical pinecone-like structure TiO_2 film. (B) The PFDS surface modification with a hydrogen-bonding-driven self-assembled process on the hydroxylated TiO_2 substrate. (C) PFDS modified pinecone-like TiO_2 that was exposed to UV light (left area, superamphiphilic) and un-exposed area on the right (superamphiphobic). (D) Self-assembly of hexadecane droplets within the superamphiphilic arrays after dipping in hexadecane. Scale bars: 5 mm. Adapted from Ref.^[51]

Furthermore, a series of light-induced ligation reactions were developed to create patterns on surfaces. Most of these reactions are based on small molecule, which means the morphology of substrate doesn't change after the ligation reactions. As an example, Hensarling et. al. demonstrated that sequential thiol-yne reactions in conjunction with simple UV photolithography could be applied to afford micropatterned, multicomponent surfaces (Figure 1.8).^[53] A photomask was firstly placed in direct contact with the polymer surface containing alkyne groups, immersed in thiol solution, and irradiated with UV light. The alkyne groups in the exposed surface reacted with the thiol yielding a patterned thiol/alkyne surface. After removing the photomask and washing the surface, the unexposed and unreacted alkyne groups were then subjected to a second thiol-yne reaction with another thiol affording the patterned surface. More light-induced ligation reactions will be introduced in Chapter 1.2.

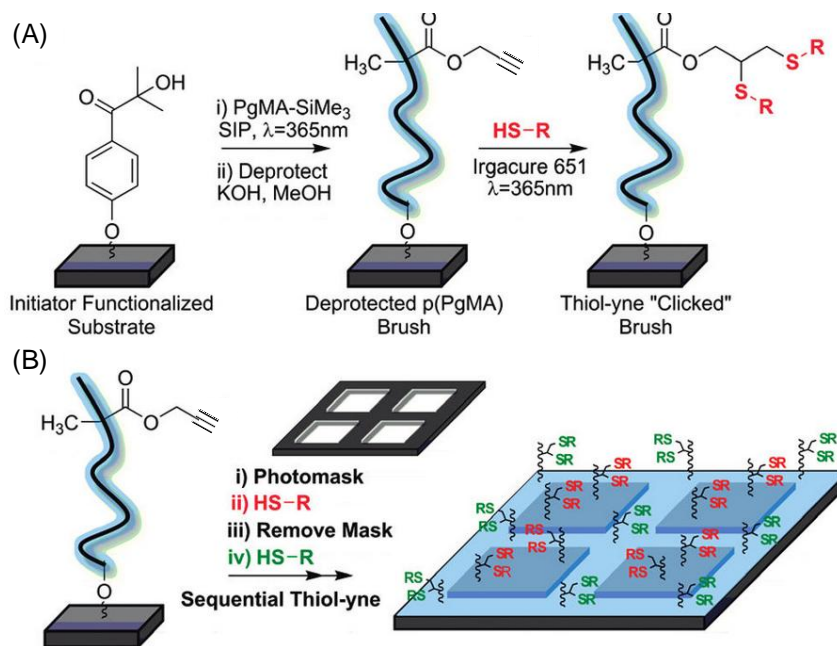


Figure 1.8. (A) Schematic procedure of poly(propargyl methacrylate) brushes fabrication and subsequent thiol-yne functionalization. (B) Schematic procedure for photopatterning alkyne-containing polymer brush surfaces with sequential thiol-yne reactions. Adapted from Ref.^[53]

1.2 Photo-induced (click) chemistry

Ever since the first reported photoreaction of an organic compound, santonin, in 1834 by Trommsdorf,^[54] the spatially and temporally controllable photochemistry has found diverse and widespread applications.^[55] In 2001, Sharpless and co-workers introduced a new concept in synthetic chemistry, named “click chemistry”.^[56] Click reactions occur in one pot, are not disturbed by water, generate minimal and inoffensive byproducts, react quickly and irreversibly to high yield of a single reaction product, and are with high reaction specificity.^[9] Those photo-induced reactions which have been adapted to fulfill these criteria could be seen as light-induced click reactions, effectively combining the classical benefits of click reactions with the advantages of a photochemical process. Although some light-induced reactions fail to meet the strict click criteria completely, it is worthwhile to note that these reactions are still of importance and could provide simple and efficient methods for the surface patterning.

1.2.1 Photo-induced azide–alkyne reactions

Copper(I)-catalyzed azide–alkyne 1,3-dipolar cycloaddition (CuAAC) reactions between azides and terminal alkynes are the most popular click reactions to date (Figure 1.9A).^[57] CuAAC presents several advantages such as: 1) the reactants are typically nonreactive to many other functional groups; 2) cycloadditions are not influenced by molecular oxygen to give undesired side reactions; 3) cycloadditions proceed in both aqueous and organic media with a high efficiency. However, as the Cu(I) catalyst is typically generated by the chemical reduction of Cu(II) to Cu(I), or added as a Cu(I) salt, the CuAAC reaction could not be controlled spatially. To achieve the spatial control of the CuAAC reaction, Yagci^[58] and Bowman^[59] demonstrated catalysis of the CuAAC reaction via the photochemical reduction of Cu(II) to Cu(I). Under light irradiation radicals are generated by a photoinitiator and reduce Cu(II) to Cu(I) which then catalyses the 1,3-dipolar cycloaddition between alkyne and azide groups (Figure 1.9 B), affording spatial and temporal control of the CuAAC reaction using photolithographic techniques (Figure 1.9C).^[59, 60]

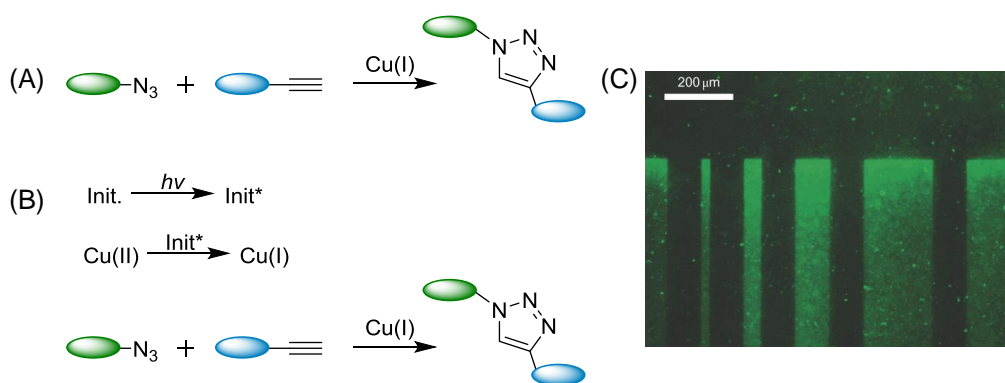


Figure 1.9. (A) Scheme for copper(I)-catalyzed azide–alkyne cycloaddition reaction. (B) Scheme for photo-catalyzed copper(I)-catalyzed azide–alkyne cycloaddition reaction. (C) Fluorescent patterning of a hydrogel by the photo-catalyzed CuAAC reaction between the pendant alkyne groups and azide-functionalized fluorophore. Adapted from Ref^[59].

One drawback of the CuAAC is the toxicity of Cu(I), restricting the range of practical applications of CuAAC in biological systems. To avoid toxicity of copper(I), Bertozzi et al. developed strain-promoted azide–alkyne cycloadditions (SPAAC) based on cyclooctynes (Figure 1.10A).^[61] SPAAC has been successfully applied for catalyst-free

bio-conjugation, *in vivo* imaging^[62, 63] and in the field of the surface functionalization.^[64] Interestingly, Locklin and coworkers reported a cyclopropenone masked dibenzocyclooctyne compound to spatial control the SPAAC reactions by light (Figure 1.10B).^[65] This photoremovable cyclopropenone moiety can be rapidly activated upon irradiation with UV light (350 nm) yielding reactive C≡C bond which then immobilizes azido-containing molecules without any catalyst; on the other hand, the cyclopropenone moiety is fully stable in the dark (Figure 1.10C).

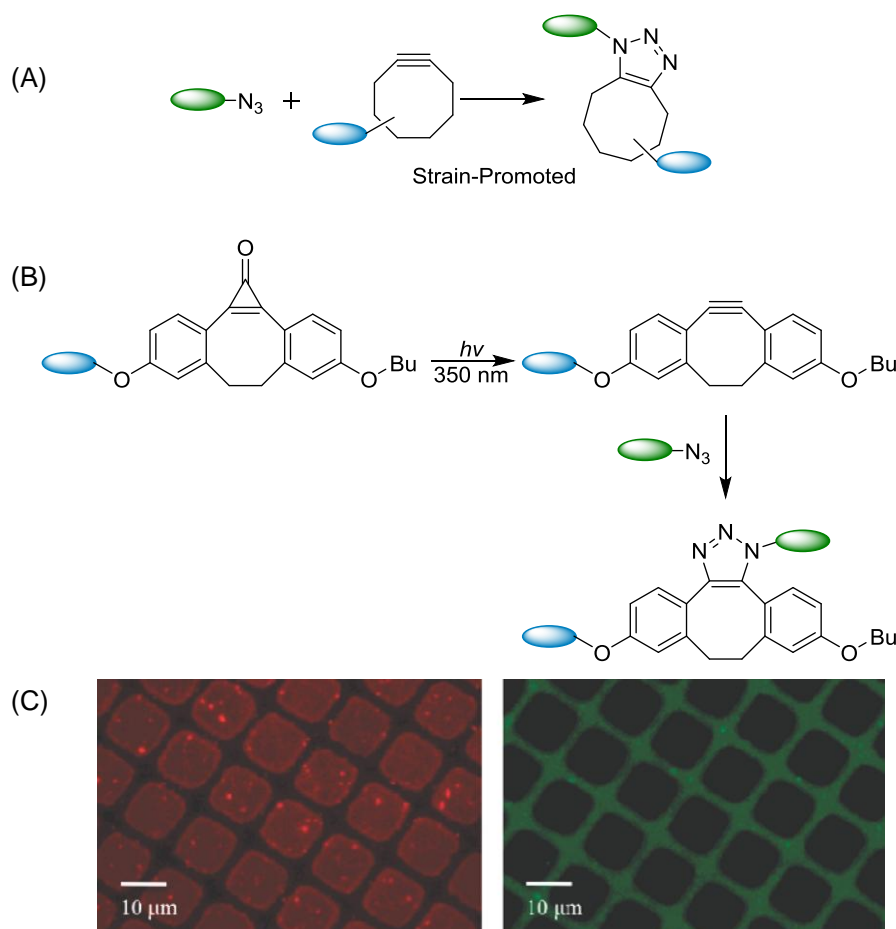


Figure 1.10. (A) Scheme for strain-promoted azide–alkyne cycloaddition reaction. (B) Scheme for subsequent photo-activation of dibenzocyclooctyne by removing cyclopropenone moiety upon UV irradiation, and functionalization of dibenzocyclooctyne by strain-promoted azide–alkyne cycloaddition (SPAAC) reaction. (C) Fluorescence microscope images of a photo-patterned surface fabricated by sequential photo-activation of dibenzocyclooctynes and functionalized with azido-Rhodamine B (left) and azido-fluorescein (right) via SPAAC reactions. Adapted from Ref^[65].

1.2.2 Photo-induced tetrazole-ene reactions

Another type of photoclick chemistry based on 1,3-dipolar cycloaddition is termed light-induced tetrazole-ene cycloaddition reactions.^[66, 67] Fifty years ago, Huisgen and co-workers reported a 1,3-dipolar cycloaddition reaction between 2,5-diphenyltetrazole and methyl crotonate under heating.^[68] In 1988 the reaction between 2,5-diphenyltetrazole with methyl methacrylate under UV was also reported.^[69] The proposed mechanism is shown in Figure 1.11A, whereby the diaryl tetrazole undergoes a cycloreversion reaction under UV irradiation to release N_2 and *in situ* generate a reactive nitrilimine intermediate which would react with an alkene spontaneously to afford a pyrazoline cycloadduct.^[68] The tetrazole-ene reactions present several advantages such as: 1) it is simple to implement the tetrazole-based molecules; 2) The photolysis of diaryl tetrazoles is extremely efficient upon UV irradiation, and only a simple hand-held UV lamp is required for activation; 3) catalyst is not needed, 4) these 1,3-dipolar cycloaddition reactions proceed fast; 5) they possess bio-orthogonality; 6) the generated pyrazoline cycloadducts show strong fluorescence. Thus, the tetrazole-ene chemistry has been employed as a powerful tool to protein and DNA modification (Figure 1.11B),^[70-72] cell labeling,^[73, 74] polymer-polymer conjugation^[75] and surface patterning (Figure 1.11C).^[76, 77]

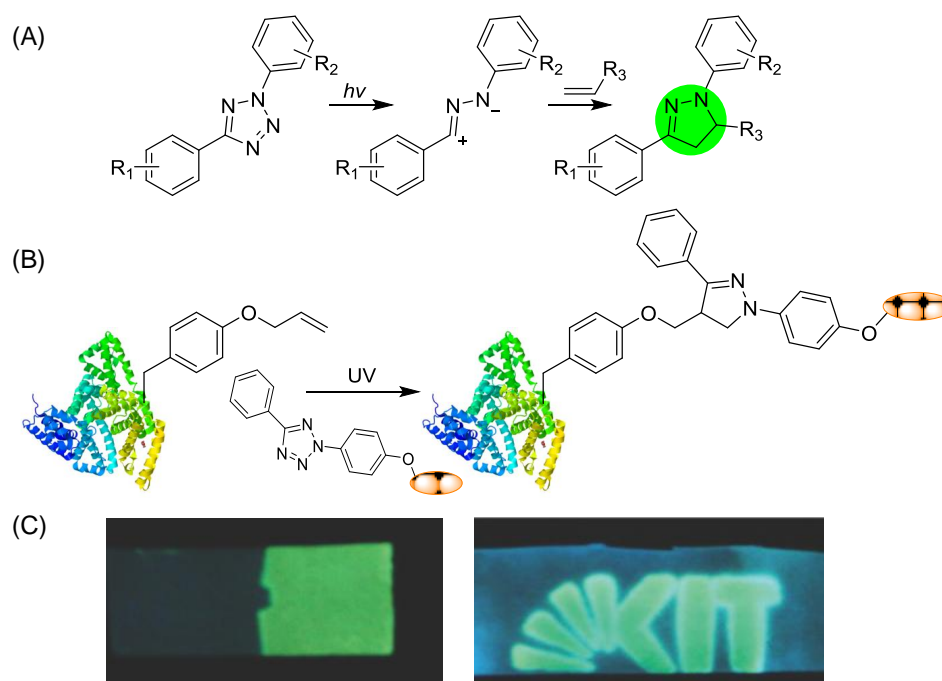


Figure 1.11. (A) Scheme for UV-induced formation of the nitrilimine intermediate from diaryl tetrazole and subsequent 1,3-dipolar cycloaddition with alkene. (B) Scheme for

modification of O-allyltyrosine-encoded protein by tetrazoles. (C) Photographs of pieces of tetrazole-modified cellulose membranes after photografting of maleimide-terminated polymers. The exposed areas show strong green fluoresce after tetrazole-ene reactions. Adapted from Ref^[75].

Since the tetrazole-ene cycloaddition comes under the category of type-I 1,3-dipolar cycloadditions,^[78] the cycloaddition reaction rate is inversely related to free-energy gap between the highest occupied molecular orbital (HOMO) of the dipole and the lowest unoccupied molecular orbital (LUMO) of the dipolarophile. This means that the tetrazole-ene cycloaddition reaction could be accelerated by raising the HOMO energy of the dipole or by lowering the LUMO energy of the dipolarophile. For example, in the photo-induced cycloaddition reactions of tetrazoles with 4-penten-1-ol (Figure 1.12A), electron-donating group (EDG) on the C5 phenyl ring as the X substituent or on the N2 phenyl ring as the Y substituent generally accelerates the cycloaddition rate due to the HOMO-lifting effect, whereas the presence of an electron-withdrawing group (EWG) results in rate decrease.^[67] For another example, the kinetics of 1,3-dipolar cycloaddition of diazomethane with a series of dipolarophiles is shown in the Figure 1.12B. Diazomethane reacts with the electron-poor ethyl acrylate more than a million folds faster than the electron rich butyl vinyl ether.^[79] In this case, EWG on the dipolarophile accelerates the reaction by lowering the LUMO.

These photo-induced tetrazole-ene addition reactions can be activated by single-photon UV light with different wavelengths. Lin and co-workers demonstrated that parts of diaryl tetrazoles were long-wavelength photo-activatable after placing auxochromic and conjugative substituent on the N2 phenyl ring (Figure 1.13).^[80] Diaryltetrazoles bearing amino and dimethylamino at the *para* position of the N2 phenyl ring give rise to excellent conversions under 365-nm UV irradiation. Apart from the UV-induced photolysis, naphthalene-based tetrazoles can even be efficiently activated by two-photon excitation with a 700 nm femtosecond pulsed laser (Figure 1.14), which offer a tool to dissect protein function in living organisms.^[81]

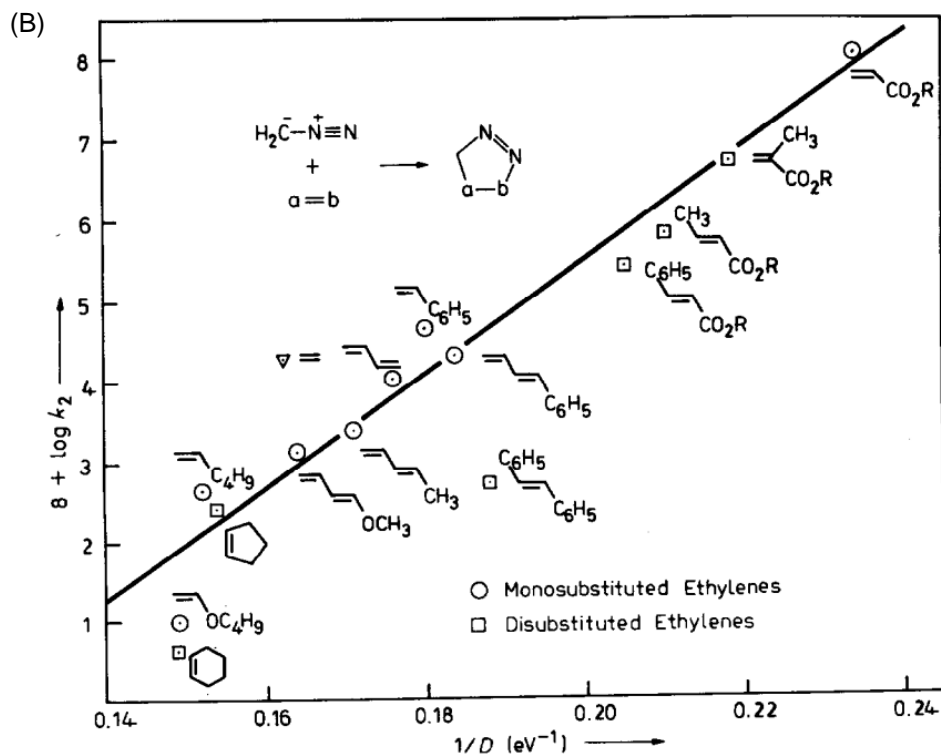
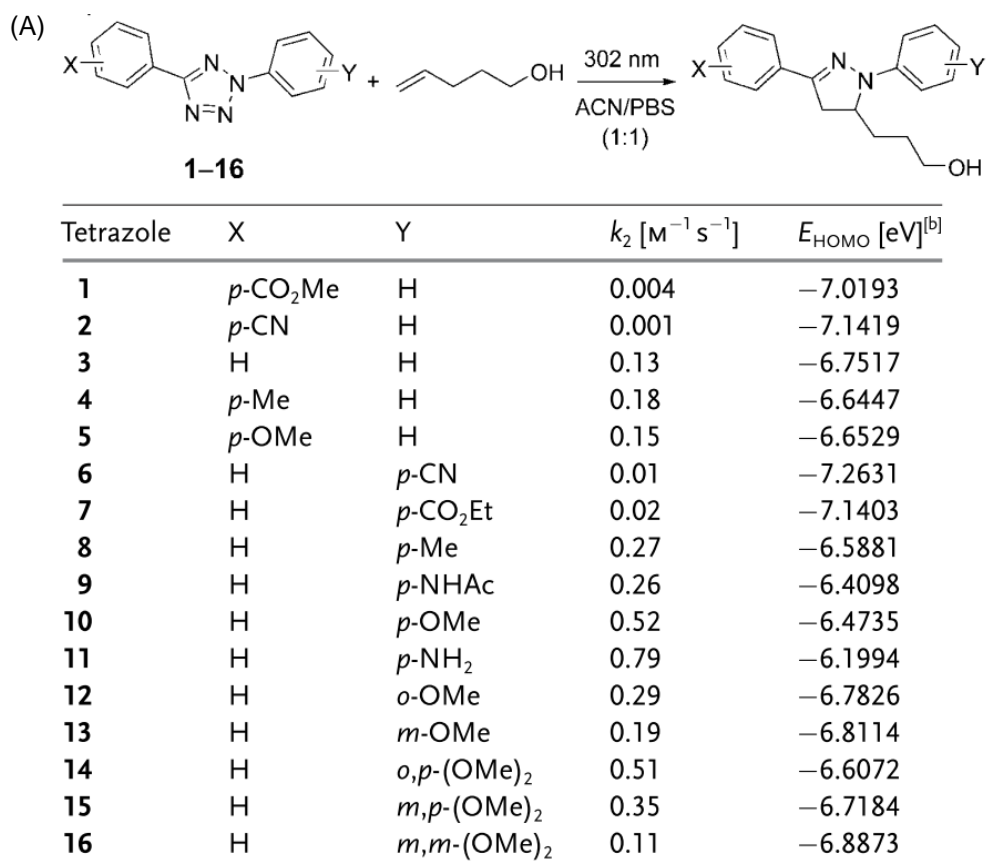


Figure 1.12. (A) Photoinduced cycloaddition reactions of tetrazoles with 4-penten-1-ol. K_2 is the cycloaddition rate constants, and E_{HOMO} is the HOMO energy of the nitrilimine

intermediate. Adapted from Ref^[67]. (B) The kinetics of 1,3-dipolar cycloaddition of diazomethane with a series of dipolarophiles. The cycloaddition rate is dependent on the $1/D$. Here K_2 is the cycloaddition rate constants and $1/D$ is the reciprocal HOMO(dipole)-LUMO(dipolarophile) D . Adapted from Ref^[79].

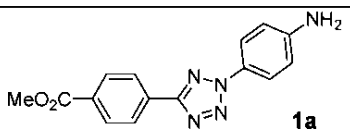
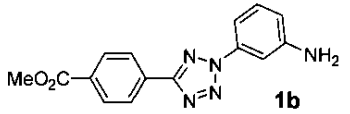
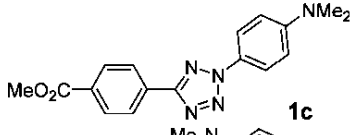
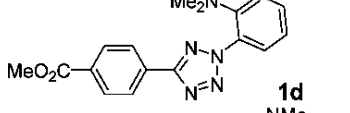
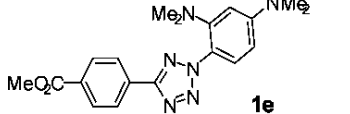
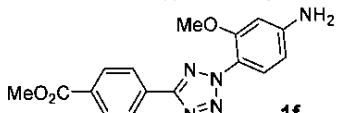
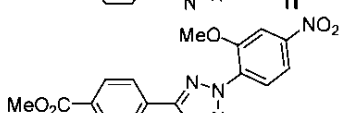
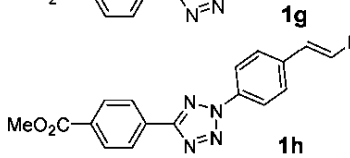
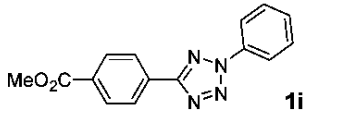
diaryltetrazole	λ_{\max} (nm)	ϵ_{302} ($M^{-1}cm^{-1}$)	ϵ_{365} ($M^{-1}cm^{-1}$)
 1a	310	20,500	3,500
 1b	268	14,000	600
 1c	336	20,000	18,700
 1d	258	2,900	400
 1e	258	15,300	7,600
 1f	254	15,900	1,000
 1g	264	13,400	3,400
 1h	304	4,700	2,100
 1i	276	7,100	900

Figure 1.13. Absorption maxima and molar absorption coefficients for various diaryltetrazoles. Adapted from Ref^[80].

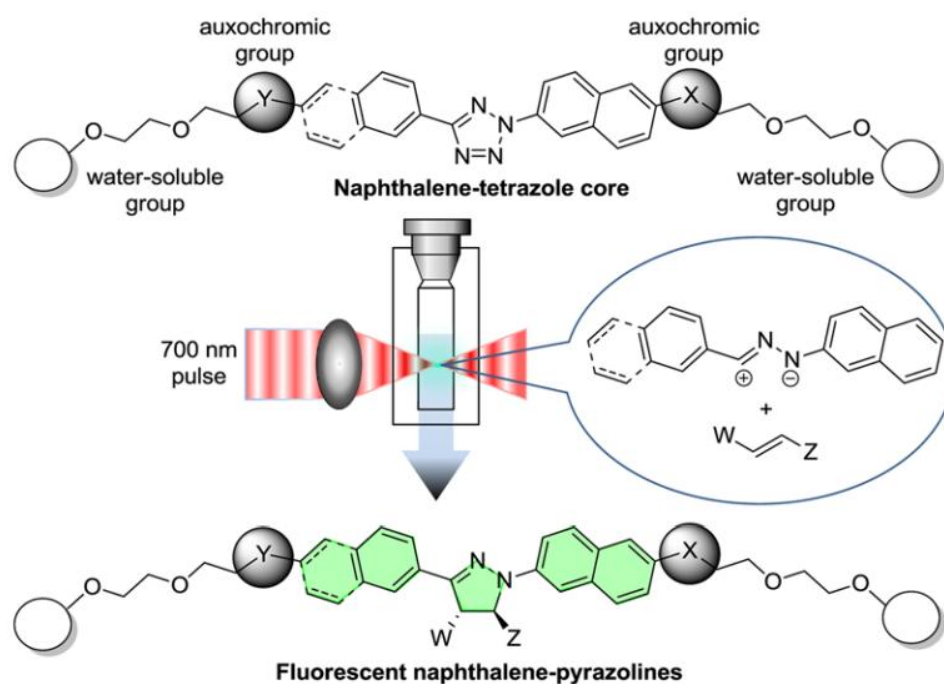


Figure 1.14. Scheme for the fluorogenic, two-photon-triggered photoclick chemistry between naphthalene-based tetrazoles and alkenes. Adapted from Ref^[81].

1.2.3 Photo-induced thiol-ene/yne reactions

Another reaction that is emerging as an attractive metal-free click process is the addition of thiols to alkenes (Figure 1.15A). This reaction was first reported in 1905,^[82] but it gained prominence in the last two decades for its feasibility and wide range of applications.^[83, 84] Two thiol-ene reactions of particular note emerged during the last century: the radical thiol-ene reaction and catalyzed thiol Michael addition.^[84] In both idealized reactions, a single thiol reacts with a single ene to yield the thioether product that exhibits a high degree of anti-Markovnikov selectivity.^[83] Although thiol-ene Michael addition reactions are also considered as click reactions, thiol-ene free-radical addition reactions show many advantages comparatively, such as catalyst free, and simple reaction conditions. Importantly, since both heat and light can generate radicals to initiate the thiol-ene reaction, the radical thiol-ene reactions are allowed to be controlled spatially and temporally when light is applied.

The ideal light-induced thiol-ene reaction revolves around the alternation between thiyl radical propagation and the chain-transfer reaction (Figure 1.15B), where the carbon-centered radical abstracts a hydrogen radical from the thiol to generate thioether product

without homopolymerization. The relatively weak sulfur-hydrogen bonds of thiols would result in a plethora of chemical reactions with nearly quantitative yields.^[84] The rate of the thiol-ene reaction is largely dependent upon the chemical structure of the alkene. In radical thiol-ene reactions, electron-rich alkenes or strained alkenes normally react with thiol more rapidly than electron-poor alkenes.

The light-induced thiol-ene reaction could proceed straightforwardly at room temperature in the absence of a metal catalyst or a photoinitiator,^[85] and tolerates a number of functional groups as well as mild reaction conditions (aqueous solution, molecular oxygen). As a result, thiol-ene click reactions have been widely utilized in the chemical synthesis^[86], spatial surface functionalization^[87] and bio-conjugation.^[88]

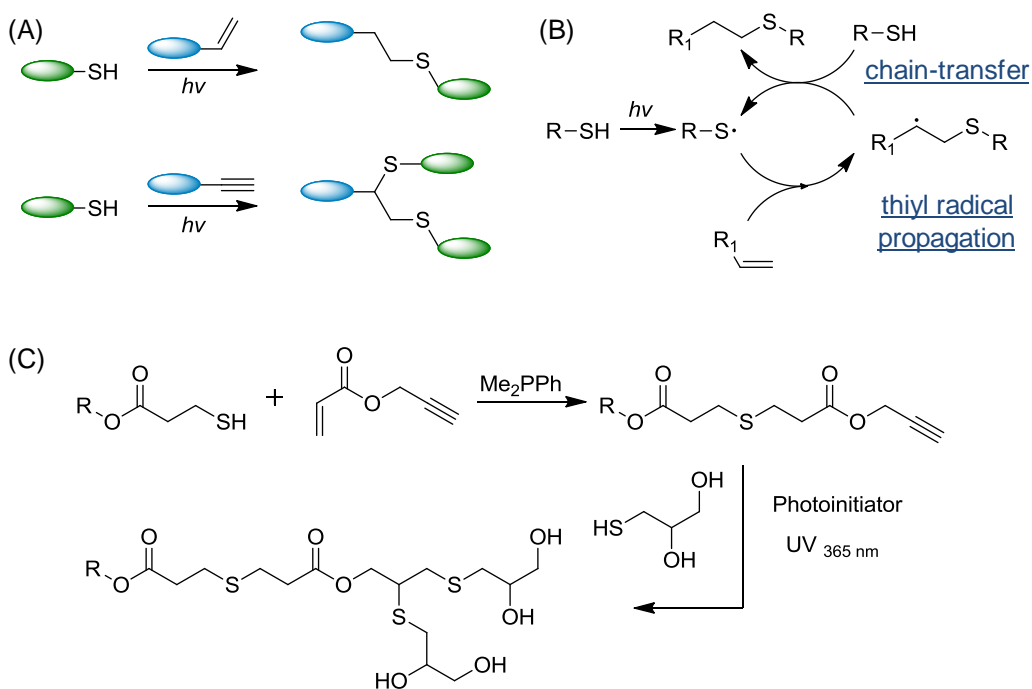


Figure 1.15. (A) Scheme for light-induced thiol-ene and thiol-yne click reactions. (B) Scheme for ideal light-induced thiol-ene reaction with alternating chain transfer and propagation. (C) Sequential nucleophilic thiol-ene reaction (Michael addition) and light-induced radical thiol-yne reaction. Dimethylphenylphosphine (Me_2PPh) was employed to generate a strong enolate base.

Inspired by almost forgotten reports on multiple radical additions of thiols to alkynes,^[89] the radical-mediated thiol-yne coupling was introduced as a new and powerful click chemistry by Bowman and co-workers in 2009.^[90, 91] In this procedure,

two thiols could be coupled to one alkyne group efficiently under UV irradiation or even sunlight (Figure 1.15A), facilitating for the synthesis of multifunctional polymer structures such as dendrimers^[92] and hyperbranched polymers.^[93] In addition, the radical mechanism of the thiol–yne reaction also makes it a robust and versatile method that tolerates different functional groups. Interestingly, Lowe and coauthors demonstrated the orthogonality of the radical thiol–yne reaction with a nucleophilic thiol–ene reaction (Michael addition), and employed sequential thiol–ene/thiol–yne reactions to fabricate multifunctional thioethers (Figure 1.15C).^[94] Initially, thiol group would rapidly react with an activated alkene in 100% yield under nucleophile-initiated conditions. Subsequently, the terminal propargyl group was reacted with 2 equiv of thioglycerol in the presence of a photoinitiator at 365 nm under ambient environment. The light-induced radical thiol–yne addition yielded the 1,2-addition species as the sole product in quantitative yield.

1.2.4 Other photo-induced reactions

Similar with photo-induced tetrazole–ene reactions, light-induced azirine–ene cycloaddition reaction was developed by Lin and co-workers.^[95] By photolysis of *2H*-azirines under UV irradiation, highly reactive nitrile ylides could be generated and then react with alkene dipolarophiles spontaneously to produce Δ^1 -pyrrolines (Figure 1.16). The reaction rate constants increase with decreasing electron density of the olefinic compound and with increasing electron density of the nitrile ylide.^[96] To achieve an efficient click reaction, highly electron-deficient dipolarophiles, such as methyl methacrylate, are requested. Selective modification of azirine-containing lysozyme with PEGylation via light-induced azirine ligation in PBS buffer is also possible.

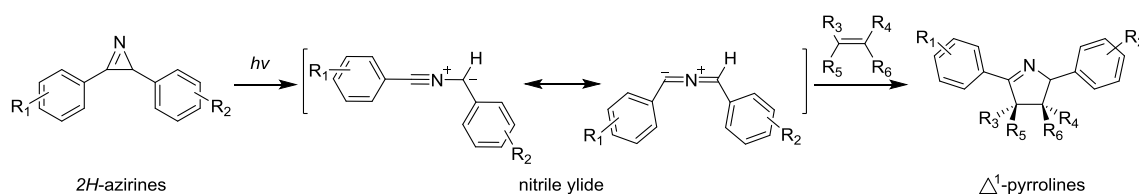


Figure 1.16. Scheme for photo-induced formation of the nitrile ylide intermediate from photolysis of *2H*-azirines and subsequent 1,3-dipolar cycloaddition of azirines with dipolarophiles.

(Hetero-)Diels-Alder [4+2] cycloadditions between an electron-rich diene and an electron-poor dienophile are recognized as another kind of click reactions. Diels-Alder click reactions offer several advantages such as: 1) these reactions usually do not require catalysts although Lewis acids could be used as a catalyst to increase the region-selectivity and the rate of the reaction in some cases; 2) these reactions are simple and with high yields under mild conditions even in water; 3) these reactions don't produce any by-products. In most cases, the (Hetero-)Diels-Alder [4+2] cycloaddition is initiated thermally and does not require activation by light.^[97] Photochemical generation diene is one strategy to control the Diels-Alder cycloaddition reactions by light. Popik and co-workers utilized a 3-(hydroxymethyl)-2-naphthol to react with polarized alkene in an aqueous solution under UV light.^[98] 3-(hydroxymethyl)-2-naphthol is photodehydrated efficiently and produces 2-naphthoquinone-3-methides, which in turn undergoes hetero-Diels-Alder addition to the polarized alkene yielding benzochroman products in quantitative yield (Figure 1.17A). The residual 2-naphthoquinone-3-methides are again hydrated to regenerate the starting diol. Figure 1.17B shows the surface patterning via this kind of photo-induced Hetero-Diels-Alder reactions.^[99, 100]

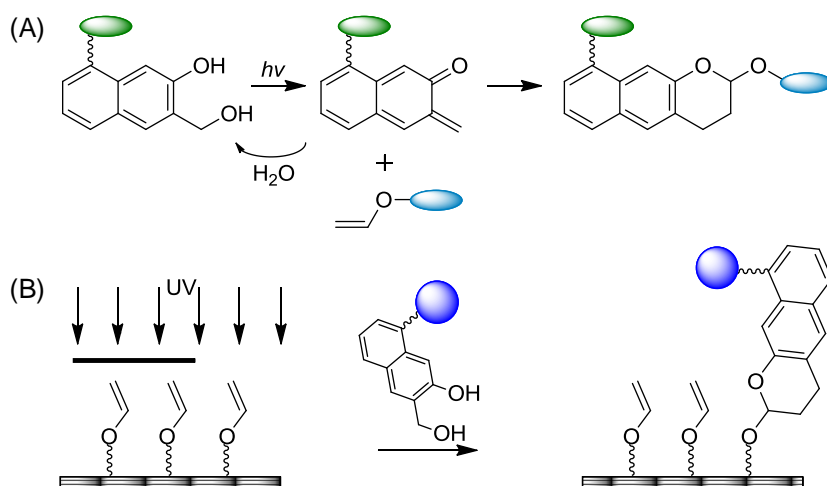


Figure 1.17. (A) Scheme for light-induced hetero-Diels-Alder click reactions based on 3-hydroxy-2-naphthalenemethanol. (B) Scheme for surface patterning via light-induced hetero-Diels-Alder reactions.

Barner-Kowollik and co-workers introduced another kind of light-induced (Hetero-)Diels-Alder [4+2] cycloaddition in solution for polymer-polymer conjugation^[101] or on

solid substrates for surface modification.^[102] In these reactions, ortho-alkyl-substituted aromatic ketones^[103] (Figure 1.18A) or aldehydes^[102] (Figure 1.18B) are used to generate reactive cis-dienes, photoenols, *in situ* under UV irradiating. These photoenols could induce efficient Diels-Alder conjugation with electron-deficient alkenes such as the substituted maleimides.^[104, 105] It's also possible to couple a non-activated dithioester, a chain transfer agent used in reversible addition-fragmentation chain transfer (RAFT) polymerization, with reactive photoenols by using Diels-Alder reactions at ambient temperature (Figure 1.18C).^[106] In this case the dithioester serves as the chain-transfer agent mediates polymerization and meanwhile acts as dienophile (C=S bond) for Hetero-Diels-Alder conjugation, facilitating for the synthesis of block copolymers. In these light-induced (Hetero) Diels-Alder [4+2] cycloaddition reactions, the photochemically formed photoenol is also reversible. The residual reactive diene would rearrange to the starting ketones or aldehydes which retain their reactivity when the light is turned on again.

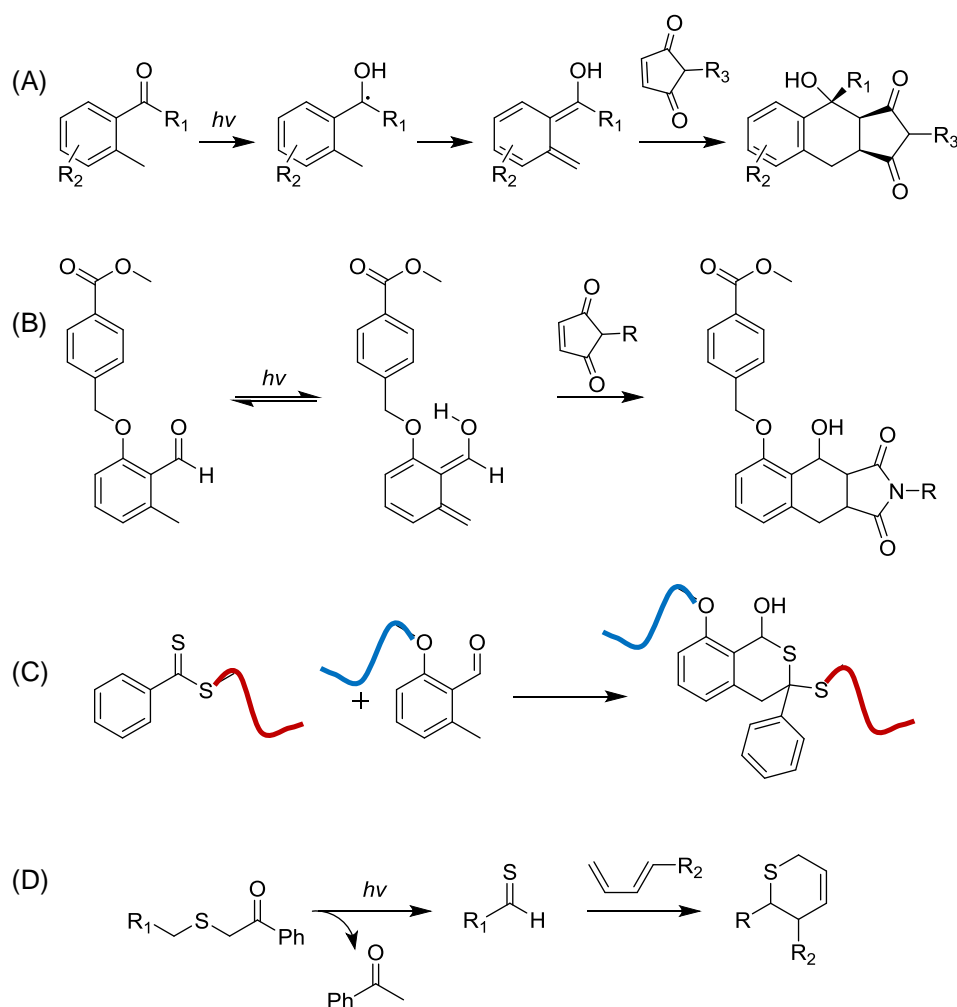


Figure 1.18. Scheme for light-induced (hetero-)Diels-Alder click reaction based on (A) photo-excitation of *o*-methylphenyl ketones to a reactive *o*-xylylene intermediate that could react with electron-deficient dienophiles such as maleimides via Diels-Alder [4+2] cycloaddition. (B) Photoinduced isomerization of a 2-formyl-3-methylphenoxy to a reactive diene and subsequent Diels–Alder [4+2] cycloaddition with a dienophile. (C) Synthesis of block copolymers via a light-induced hetero-Diels-Alder cycloaddition reaction between dithiobenzoate end-capped polymer and photoenol-functionalized polymer. (D) Photolytic cleavage of phenacyl sulfides yielding thioaldehydes that can react with a diene via hetero-Diels-Alder [4+2] cycloaddition.

Instead of photo-generating dienes, photo-generating dienophiles is another strategy to control the (hetero-)Diels-Alder [4+2] cycloaddition reactions by light. For example, photolytic cleavage of phenacyl sulfides yields reactive thioaldehydes which can act as dienophile (C=S bond) to react with a diene via hetero-Diels-Alder [4+2] cycloaddition (Figure 1.18D).^[107] Even the dienes bearing electron-withdrawing groups could react with the resulting thioaldehydes in a quantitative way without any observable side products.

Photo-induced oxime ligation based on the reaction between of an aldehyde/ketone and an alkoxyamine is another form of photo-induced click chemistry. This ligation occurs in two steps: 1) photo-deprotection of an aldehyde/ketone or an alkoxyamine; and 2) oxime bond formation with the counterpart. As an example, Figure 1.19A shows the low-energy photo-deprotection of a 2-[(4,5-dimethoxy-2-nitro-benzyl)oxy]tetrahydro-2*H*-pyran derivative to generate aldehyde and subsequent oxime ligation with alkoxyamine moieties.^[108] As another example, a nitroveratryloxycarbonyl-protected alkoxyamine group was deprotected under UV irradiation,^[109] and subsequently reacted with ketone or aldehyde tethered ligands to form oxime bond (Figure 1.19B).^[110]

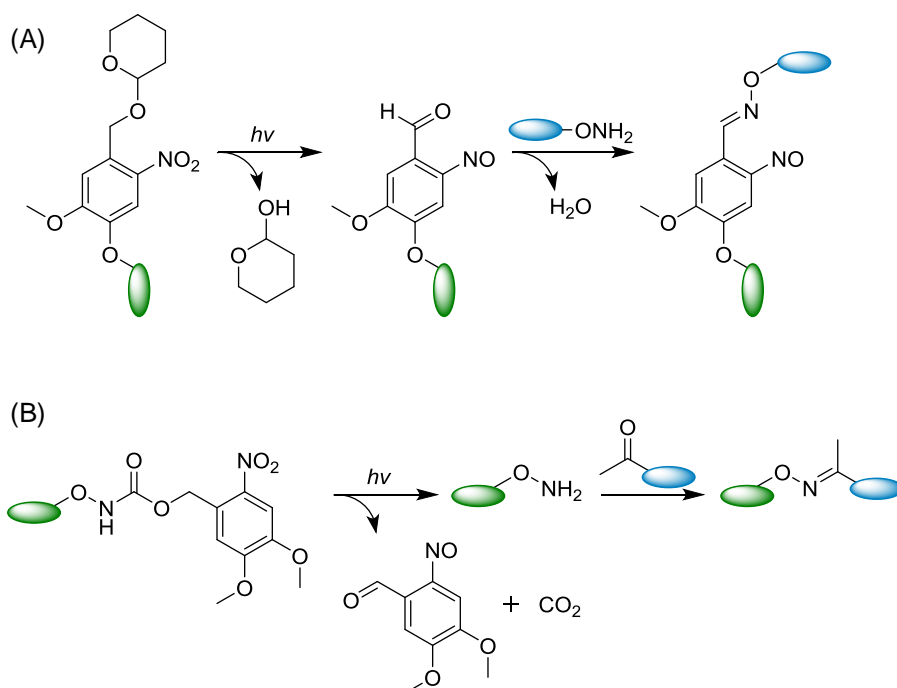


Figure 1.19. (A) Photoinduced cleavage of a 2-[(4,5-dimethoxy-2-nitrobenzyl)oxy]tetrahydro-2*H*-pyran derivative and subsequent oxime ligation with alkoxyamine derivatives. (B) Photoinduced cleavage of a nitroveratryloxycarbonyl-protected alkoxyamine group and subsequent oxime ligation with ketone derivatives.

Parts of light-induced covalent immobilizations of nucleophiles also possess some classical advantages of click reactions. A kind of hetero-Diels-Alder [4+2] addition of the photochemically generated 2-naphthoquinone-3-methides with polarized alkene is mentioned above in Figure 1.17. Instead of alkene, thiol group also could react with the photochemically generated 2-naphthoquinone-3-methides as a nucleophile (Figure 1.20).^[111] Importantly, the resulting thioether linkage is stable under ambient conditions; but it also can be cleaved to regenerate the free thiol after photolysis under UV light. The reversible nature of this reaction allows the surface functionalization to be carried out by “write and erase” procedure.

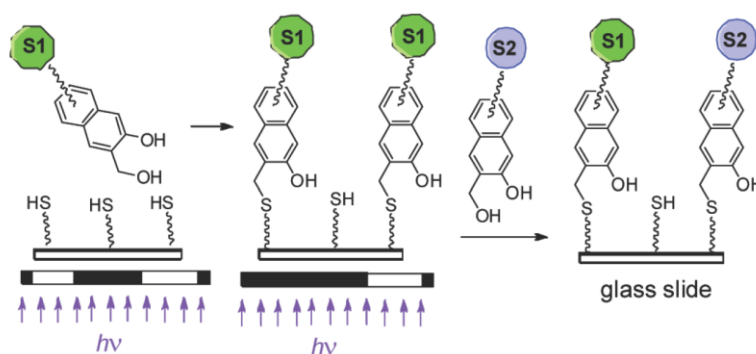


Figure 1.20. Scheme for spatial immobilization and replacement of 3-hydroxymethyl-2-naphthol derivatives on a thiol-functionalized surface under UV irradiation. Adapted from Ref.^[111].

Another photochemical strategy to provide spatial control for the direct covalent immobilization of nucleophiles is based on photogenerated thioaldehydes.^[112] Under UV light (355 nm) phenacyl sulfides can be cleaved to form acetophenone and reactive thioaldehydes which can be efficiently trapped by nucleophiles such as amines, hydroxylamines, and thiols at ambient temperature (Figure 1.21). The reaction of thioaldehyde with amines affords imines, but which are partially susceptible to oxidation by sulfur species to form thioamide fragments.^[113] The reaction with hydroxylamines affords oximes, and the reaction with thiols affords disulfide bridges in quantitative yields.^[112] The intermediate thioaldehyde shows extreme reactivity that it could react with different nucleophiles at the same time. Although the thioaldehydes reactions are not considered as click reactions because of the limited selectivity and orthogonality, they can be utilized as a facile coupling tool to pattern mono-functional substrate with small molecules or polymers.^[114]

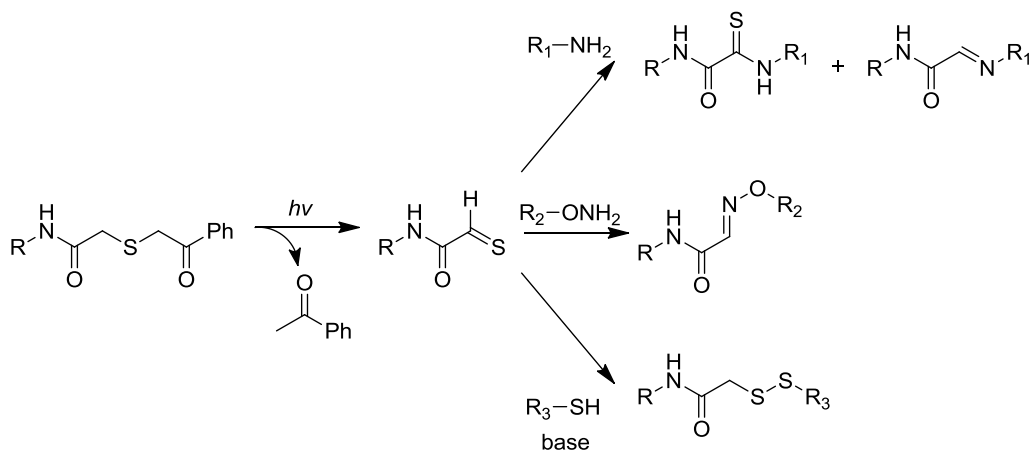


Figure 1.21. Scheme for the immobilization of amine derivatives, alkoxyamine derivatives, and thiol derivatives to the photo-generated thioaldehydes.

Although it has been over a century since ketenes were discovered by Staudinger in 1907^[115] and widely used in complex small-molecule syntheses, recently ketene chemistry is re-recognized as a promising route for the modification of macromolecular structures with significant yields. Ketene is a very reactive intermediate which can be produced thermally from dialkyl Medrum's acid^[116] or produced photochemically from benzodioxinone.^[117, 118] In the latter case, benzodioxinones under UV irradiation concomitantly generates the corresponding ketone and the reactive ketene. This intermediate would directly react with nucleophiles such as alcohols^[119] or amines^[118] present in the reaction media (Figure 1.22). Since the hydroxyl group is one of the most common surface functionalities, the light-induced ketene reactions offer a great chance to directly modify surface under mild conditions and without any catalyst or any additional reagent.

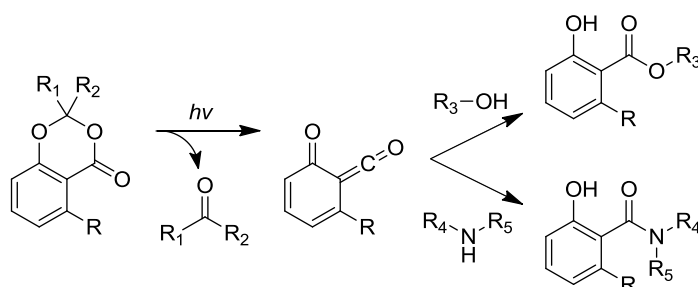


Figure 1.22. Photoinduced cleavage of benzodioxinone, and the resulting ketene reacting with alcohols and amines to produce esters and amides, respectively.

Another light-induced reaction that can be used to directly modify hydroxyl group on surface is named as thiol-ol chemistry.^[120] Unlike the UV-initiated thiol radical additions (such as thiol-ene/yne chemistry) or Michael additions, this approach is based on an oxidative conjugation of thiols to hydroxyl groups (Figure 1.23). In most cases UV light is capable to trigger or accelerate oxidation via the formation of reactive oxygen species (ROS).^[121] In this reaction the thiol group is firstly oxidized by oxygen in air during UV irradiation and reacts with hydroxyl group in situ to generate sulfonic and sulfinic esters. Although the yield of the thiol-ol reaction is not high enough to fill the criterion of click reaction, this simple, initiator-free and oxygen-tolerant reaction could be used for convenient surface modifications.

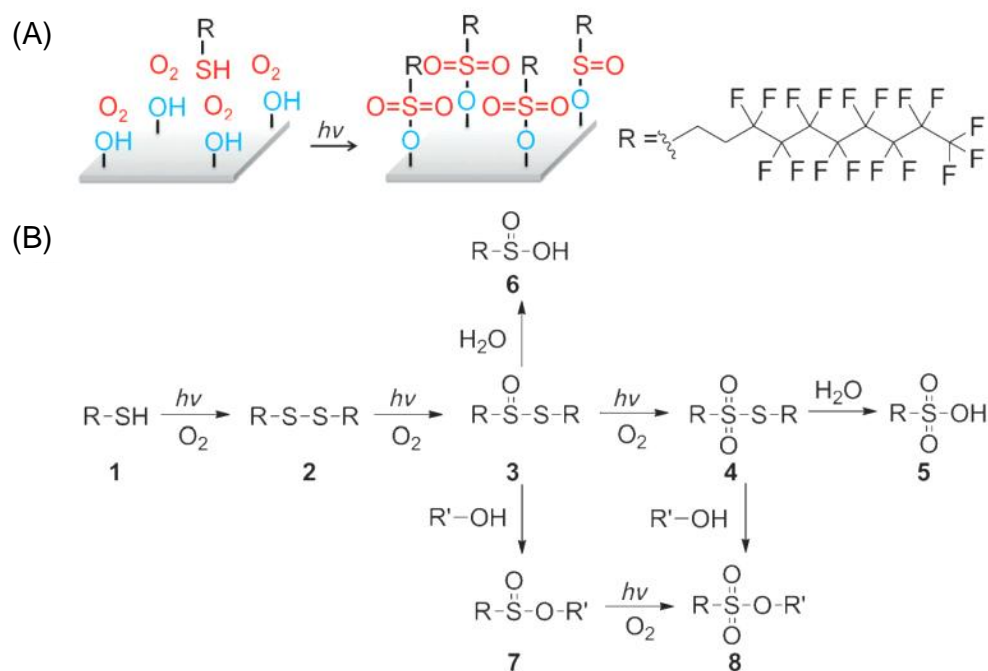


Figure 1.23. (A) Scheme for the surface modification by thiol-ol chemistry under UV irradiation. (B) Possible mechanism of the functionalization of surface hydroxyl groups by thiol-ol chemistry mediated by oxygen and UV irradiation. Adapted from Ref.^[120].

The last powerful photo-induced chemistry introduced in this chapter is based on nitrene (R-N:), a very reactive intermediate involved in many chemical reactions including C=C addition or even C-H insertion.^[122] Generation of nitrenes by photolytic decomposition of azides would provide an opportunity for modifying substrates in a

spatially controlled manner.^[123] Perfluorophenylazides, a popular light-sensitive compound, has been widely used as versatile surface coupling agents. Perfluorophenylazide in Figure 1.24 has two distinct and synthetically distinguishable reactive centers: 1) the carboxyl group through which a variety of functionality can be attached via standard coupling reactions, and 2) the fluorinated phenylazide group. Upon activation by light, the fluorinated phenylazide moiety decomposes to an electron deficient perfluorophenyl nitrene which is capable of forming stable covalent adducts with solid materials. Because of the ultrahigh reactivity of the nitrene intermediate which could react with CH, NH and C=C bonds, this coupling reaction lacks of the functional-group specificity. Nevertheless, this general and versatile coupling chemistry could be applicable to a wide range of materials that lack reactive functional groups such as polyolefins and carbon materials.

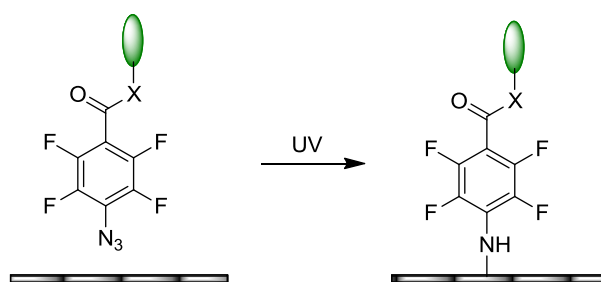


Figure 1.24. Modification of multiwalled carbon nanotube forests through light-induced perfluorophenylazide chemistry.^[123]

1.3 Superhydrophobic surfaces

1.3.1 Theoretical background

Water contact angle (CA) θ is an important measurement used to determine the wettability of the surface. Two types of CA values are used in practice: static CA, advancing CA and receding CA. Static CA (θ_{st}) is an equilibrium CA obtained by a goniometer when a water drop is deposited on the surface (Figure 1.25A). Advancing and receding CAs are non-equilibrium CAs which are measured during the water droplet growth (advancing CA, θ_{adv} , Figure 1.25B) and shrinkage (receding CA, θ_{rec} , Figure

1.25C). The difference between advancing CA and receding CA is defined as CA hysteresis.

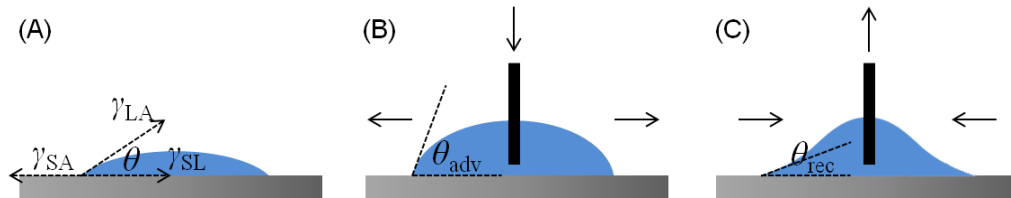


Figure 1.25. Scheme for the static CA (A), advancing CA (B) and receding CA (C) measurements on a smooth surface.

The wettability of a smooth surface is given by Young's equation (Equation 1.1),

$$\cos \theta_Y = \frac{\gamma_{SA} - \gamma_{SL}}{\gamma_{LA}} \quad (1.1)$$

where γ_{SA} is the surface tension between the surface and air, γ_{SL} is the surface tension between the surface and water, and γ_{LA} is the surface tension between water and air (Figure 1.25A).^[124] Young's angle θ_Y arises from the consideration of a thermodynamic equilibrium of the free energy at the solid-liquid-vapor interphase. Thus, static contact angle of a flat surface is very close to Young's angle.

Water on a rough hydrophobic surface can be in either Wenzel state^[125] or Cassie-Baxter state^[126], and CAs on the rough surfaces could be predicted using either the Wenzel model or Cassie-Baxter model.

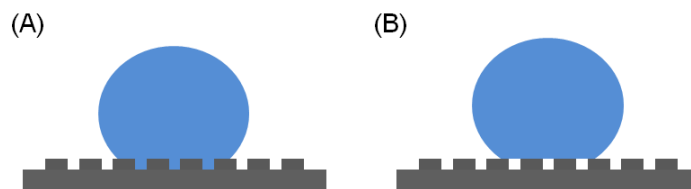


Figure 1.26. Behavior of a liquid drop on a rough surface. (A) liquid penetrates into the asperities (Wenzel state); (B) liquid suspends on the asperities (Cassie–Baxter state).

In Wenzel state, water penetrates the asperities of a surface as shown in Figure 1.26A. At thermodynamic equilibrium, the apparent CA θ_w is calculated with equation 1.2:

$$\cos\theta_w = r * \cos\theta_Y \quad (1.2)$$

where r is the surface roughness defined as the ratio of the actual surface area to the projected area. For a rough surface, this ratio is larger than 1. That means for a hydrophobic surface $\theta_w > \theta_Y > 90^\circ$ and for a hydrophilic surface $\theta_w < \theta_Y < 90^\circ$. Roughness enhances both hydrophobicity and hydrophilicity depending on the intrinsic property of the corresponding flat surface. When r is above 1.7, the contact angle hysteresis of a hydrophobic surface doesn't increase with the roughness factor anymore and starts to decrease^[127], which is attributed to the switching from the Wenzel state to the Cassie–Baxter state.

In Cassie–Baxter state, water doesn't penetrate the asperities but suspends above the asperities (Figure 1.26B). Air is trapped inside the asperities leading to a composite air–solid interface between the water droplet and the surface. For a rough surface containing only one type of asperities, the resulting CA (θ_{CB}) can be calculated by using equation (1.3) according to the Cassie–Baxter model:

$$\cos\theta_{CB} = f_s * (1 + \cos\theta_Y) - 1 \quad (1.3)$$

where f_s is the fraction of the solid on the surface.

In the Wenzel state, the liquid penetrates the asperities and is in complete contact with the surface. A droplet in the Wenzel state would be pinned to the surface. However, in the Cassie–Baxter state, due to the air trapped between the liquid and the asperities of the rough surface, the fraction of solid that is in contact with liquid decreases dramatically. A droplet in the Cassie–Baxter state is prone to bounce or roll off the surface.^[128]

1.3.2 Superhydrophobic surfaces

Superhydrophobic surfaces are characterized by extreme water repellency with water contact angles (CA) greater than 150° , and a water CA hysteresis of less than 10° .^[1, 128–130] Water on the superhydrophobic surfaces forms spherical droplets that roll off the surface when the surface is tilted at a low angle ($<10^\circ$). Nature also utilizes the extreme water repellent properties in many plants and animals. The most well-known examples of superhydrophobic surface are the lotus leaf^[131] and water strider's legs^[132] (Figure 1.27).

Due to the extreme water repellent, self-clean and anti-fouling properties, superhydrophobic surfaces have attracted much interest for both fundamental research and industrial applications in the last decade.^[130, 133]

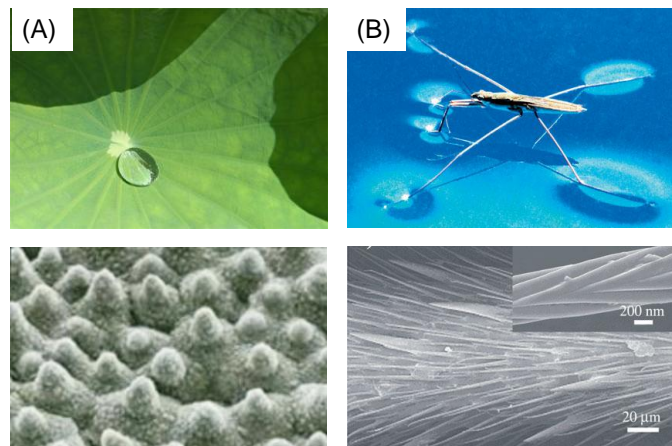


Figure 1.27. (A) Optical images of a water droplet on a lotus leaf (top) and a SEM image of the lotus leaf surface (bottom). Adapted from Ref.^[131]. (B) Optical images of a water strider standing on water surface (top) and a SEM image of a leg showing numerous oriented spindly microsetae and the fine nanoscale grooved structures on a seta (bottom). Adapted from Ref.^[132].

To obtain a surface with both high CA and low CA, a water droplet on the surface has to behave in the Cassie-Baxter state. According to the Cassie-Baxter model (Equation 1.3), the resulting θ_{CB} is actually inversely proportional to the f_s , and is in proportion to the θ_Y of the solid surface. In another word, to obtain a superhydrophobic surface, the substrate should be rough enough (contribution of the solid part f_s approaches zero) and the solid material should be hydrophobic enough to have a high CA. SEM image in Figure 1.27 A shows the hierarchical micro- and nano-structures of a lotus leaf. The structure of a lotus leaf consists of a combination of two scale roughness: one around 10 μm and one around 100 nm.^[131] Meanwhile, lotus leaf secretes epicuticular wax itself (water CA equals 110°). The superhydrophobicity of lotus leaf is the result of a combination of high surface roughness with the hydrophobicity of the wax.^[134]

Jiang et al. demonstrated that surface roughness with hierarchical micro- and nano-structures could make a hydrophilic surface ($\theta < 65^\circ$) more hydrophilic, and hydrophobic surface ($\theta > 65^\circ$) more hydrophobic and ultimately superhydrophobic (Figure 1.28).^{[135,}

^{136]} Generally, surface properties could be determined as hydrophobic ($\theta \geq 90^\circ$) or hydrophilic ($\theta < 90^\circ$). However, in this case, the number, 65° , is more suitable to be defined as the boundary between hydrophilicity and hydrophobicity.^[137]

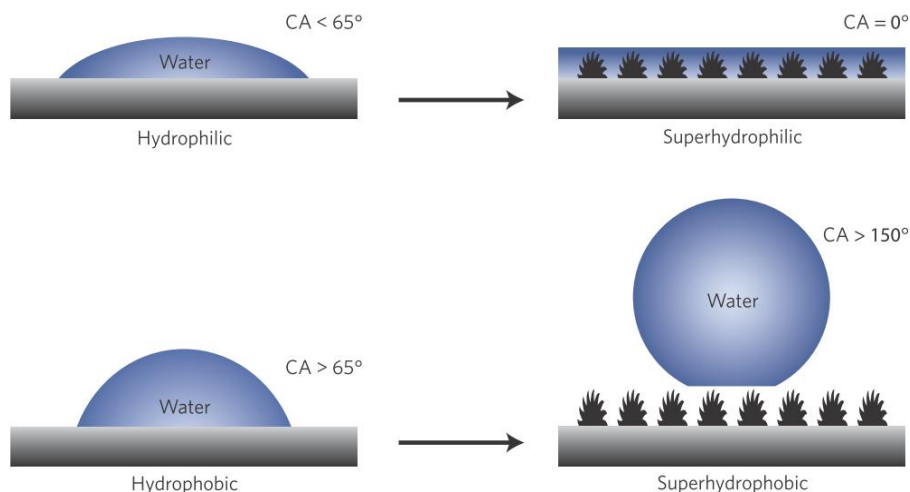


Figure 1.28. Surface wettability can be enhanced by structured roughness. Adapted from Ref.^[135].

Approaches for superhydrophobic surface preparation have been covered in depth in several good reviews,^[130, 134, 138-140] and therefore are not described herein.

1.3.3 Porous polymethacrylate monoliths

Due to the combination of advantages of porous materials and polymeric materials, porous polymethacrylate monoliths have attracted much research interest and are widely used in separation science and chromatography applications.^[141, 142] The polymethacrylate monoliths could be prepared using free radical polymerization of monomers in different models (Figure 1.29A). Thermal initiators, redox initiators and photoinitiators are commonly used to initiate the free radical polymerization. Comparatively photo-initiated free radical polymerization has a great advantage that it can take place under room temperature, and can be spatially and temporally controlled. Free radicals are only produced from photoinitiators under irradiation (Figure 1.29B), inducing the polymerization taking place only in the irradiated areas.

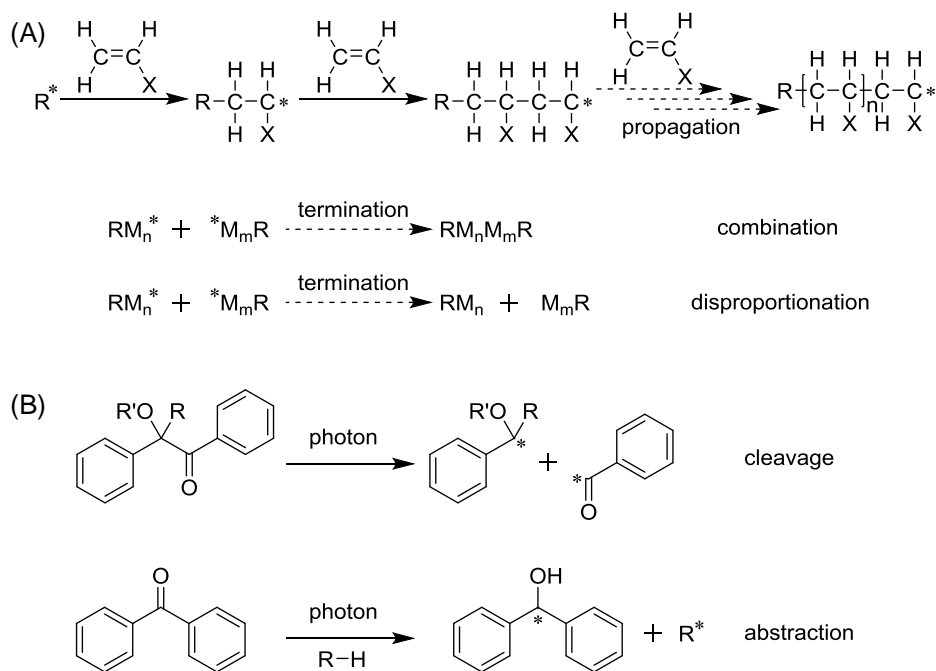


Figure 1.29. (A) Scheme showing the propagation and termination of free radical polymerization of vinyl monomers. During the free radical polymerization, reactive centers are generated from the excited initiator and polymerization proceeds by the propagation of the reactive center by successive additions of monomer molecules. The growth of the polymer is terminated by elimination of the reactive center. The termination reaction usually proceeds through combination where two chain radicals are joined together, or through disproportionation. (B) Scheme showing the production of the free radicals from photoinitiators through cleavage or abstraction of a hydrogen atom from a donor compound such as alcohols, ethers, amines and thiols.

During the polymerization the polymer phase starts to separate from the porogens due to its limited solubility (phase separation), resulting in a porous structure.^[143] The physical properties of porous polymethacrylate monoliths can be tailored by adjusting the composition of the polymerization mixture. Firstly, the morphology of the porous structure can be controlled by varying the porogens in the polymerization mixture.^[144] Polymer monoliths with smaller pores could be obtained if the porogens are good solvents for the monomer/crosslinker, while polymerization in the porogens which are poor solvents for the monomer and crosslinker generates monoliths with larger pores (Figure 1.30A). Secondly, this morphological change also makes a significant impact on the transparency^[145] (Figure 1.30B) as well as the rigidity of the polymer layers.

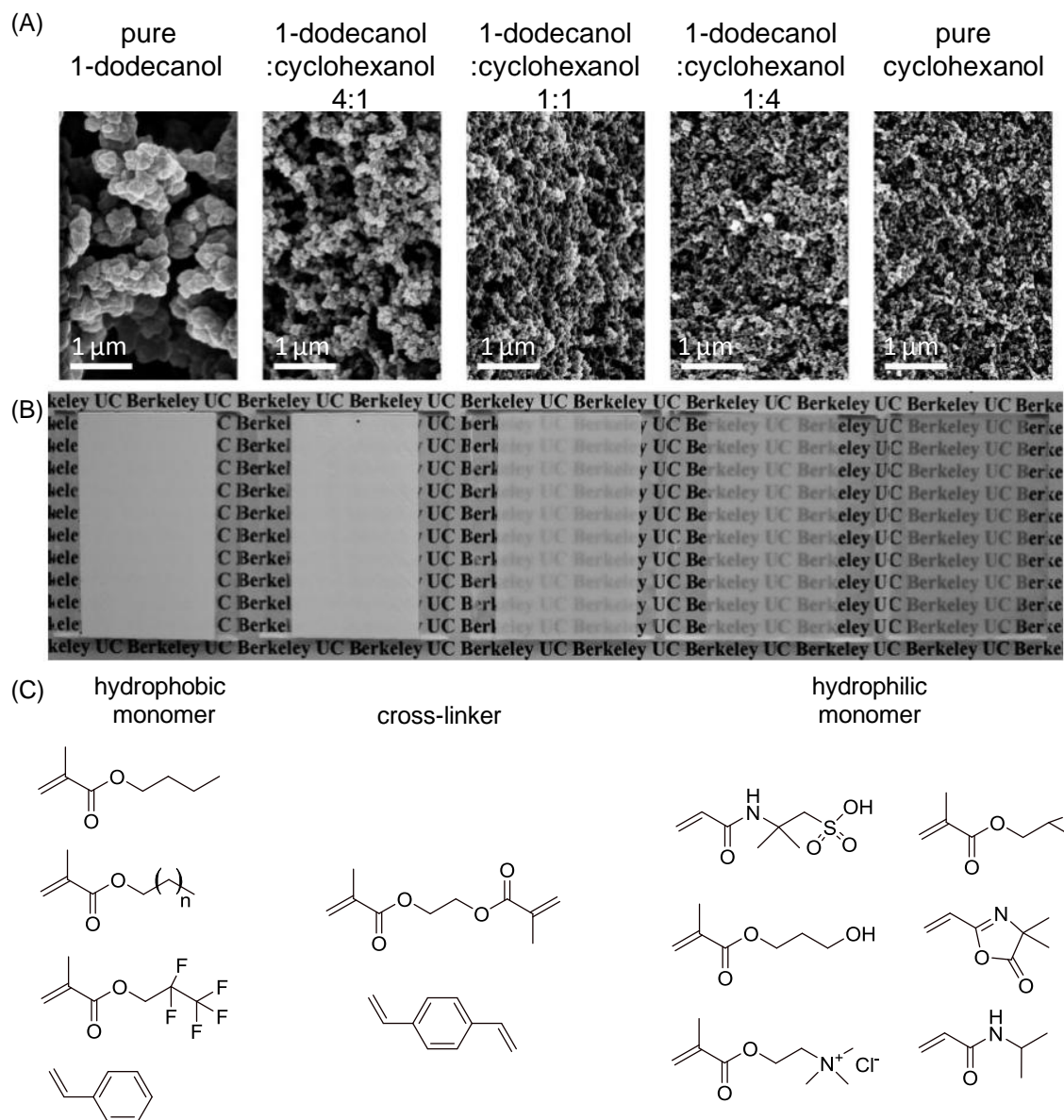


Figure 1.30. (A) SEM images of 50 μm thick porous poly(butyl methacrylate-co-ethylene dimethacrylate) layers prepared using different porogens. (B) Photographs of these porous poly(butyl methacrylate-co-ethylene dimethacrylate) layers, showing the relative transparency of the layers. Adapted from Ref.^[145]. (C) Different monomers with different functional groups and crosslinkers used in the fabrication of porous polymethacrylate monoliths.

In addition, chemical properties of porous polymethacrylate monoliths can also be well controlled. A variety of monomers and crosslinkers with different functional groups (Figure 1.30C) is available for the preparation of porous polymethacrylate monoliths with

different chemical properties.^[19, 47, 146] Besides, reactive groups excitant on the porous polymethacrylate monoliths, such as vinyl group, hydroxyl group or epoxy group, can also be post-modified with desired molecules after the monolith is prepared.

Importantly, highly porous structures of the polymethacrylate monoliths could offer both micro- and nano-scale roughness which is essential to fabricate superhydrophobic or superhydrophilic surfaces (Figure 1.31). One-step fabrication of superhydrophobic film poly(butyl methacrylate-co-ethylene dimethacrylate) (BMA-EDMA)^[19, 145], superhydrophilic film poly(2-hydroxyethyl methacrylate-co-ethylene dimethacrylate) (HEMA-EDMA)^[47] and thiol/amine-reactive superhydrophilic poly(glycidyl methacrylate-co-ethylene dimethacrylate) (GMA-EDMA)^[147] were already reported.

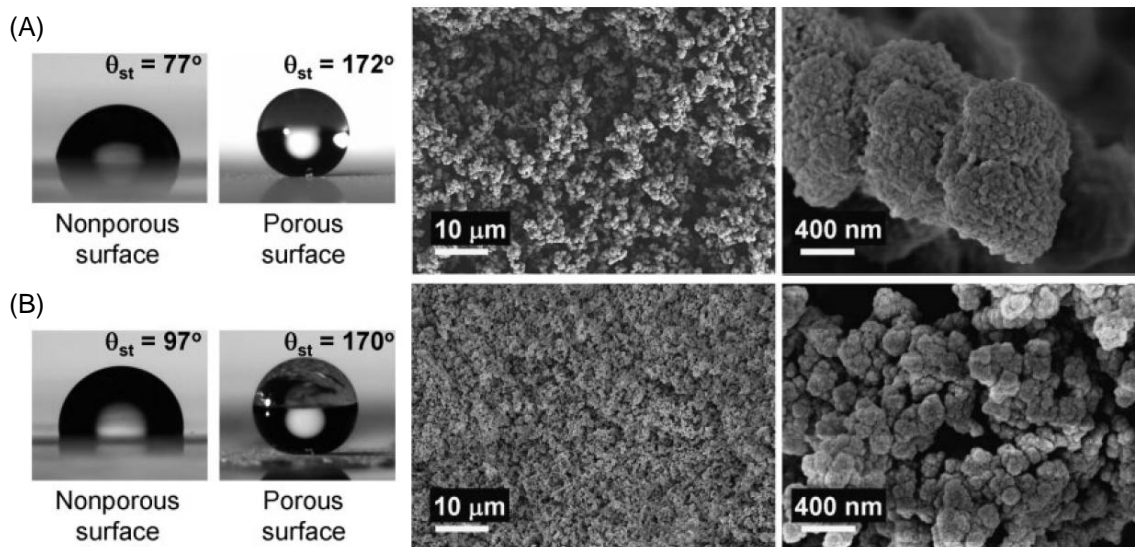


Figure 1.31. Photographs of water droplets formed on porous and nonporous (A) poly(butyl methacrylate-co-ethylene dimethacrylate) layer and (B) poly(styrene-co-divinylbenzene) layer. SEM images of the corresponding porous polymers are inserted, showing the micro- and nano-scale roughness. Adapted from Ref.^[145].

**Chapter 2. Surface Patterning via Thiol-Yne Click
Chemistry: A Fast and Versatile Approach to
Superhydrophilic-Superhydrophobic Micropatterns**

2.1 Introduction

Superhydrophobic surfaces are characterized by extreme water repellency with water contact angles (WCA) greater than 150° , and a WCA hysteresis of less than 10° .^[1, 128-130, 132] On the contrary, water spreads immediately on superhydrophilic surfaces leading to WCAs less than 10° .^[14, 148] Both superhydrophobicity and superhydrophilicity are the result of a combination of high surface roughness with either hydrophobic or hydrophilic material, respectively.^[1, 128, 132] Combining these two extreme properties on the same surface in precise two-dimensional micropatterns opens exciting new functionalities and possibilities in a wide variety of applications from cell,^[47, 149, 150] droplet,^[149, 151-153] and hydrogel microarrays^[149, 154] for screening to surface tension-confined microfluidic channels for separation and diagnostic devices.^[155, 156] A number of methods for making superhydrophobic-superhydrophilic micropatterns have been introduced over the past decade. For example, methods based on UV-induced decomposition of hydrophobic coatings on different substrates (alumina, TiO₂ film or SiO₂ etc.) were reported.^[49, 50, 157] Photoinduced modification of carbon nanotubes with hydrophilic azides,^[123] plasma treatment,^[158-160] microprinting,^[41, 161, 162] or mussel-mimetic deposition of dopamine in combination with soft-lithography^[163] have been described. A method based on UV-initiated photografting for making superhydrophobic-superhydrophilic micropatterns on porous polymer films was introduced by our group.^[19, 47] Manna et al. reported an amine reactive superhydrophobic surface that permits post-fabrication by amine-functionalized molecules.^[164] Most of the described methods, however, proceed slowly (e.g. 15 min irradiation time in the case of photografting), lack the ability to easily tailor or modify the properties by different target functional groups, or require harsh conditions (e.g. plasma treatment or UV-induced decomposition), organic solvents (i.e. incompatible with aqueous conditions) and, therefore, cannot be directly applied to make patterns of biomolecules. These limitations restrict the range and number of possible practical applications of produced superhydrophobic-superhydrophilic micropatterns. Developing a universal method that is facile, versatile, as well as provides good optical and chemical surface properties remains a big challenge.

To meet this challenge, here I present an extremely fast (<15 s), initiator-free surface modification method compatible with aqueous conditions for creating superhydrophobic-superhydrophilic micropatterns using thiol-yne “click” chemistry.^[91, 165, 166]

Phototriggered thiol-yne reactions have been explored as a viable approach to surface modifications, such as using different thiols to modify “yne”-containing polymer brushes,^[53] immobilizing gold nanoparticles on a polymer surface site-specifically,^[167] and creating micropatterns on a monolayer by microcontact printing.^[168] To our knowledge, however, this type of functionalization strategy has never been applied to create superhydrophobic-superhydrophilic micropatterns. Here I show that an alkyne functionalized porous polymethacrylate surface could be easily transformed into either a superhydrophobic or superhydrophilic surface under UV irradiation. I show that the reaction is extremely fast and requires as little as 0.5 s of UV irradiation in the presence of an initiator and only 5 s without any initiator. The functionalization can be performed in various solvents including water allowing patterning biomolecules. In this way, superhydrophobic-superhydrophilic micropatterns incorporating different orthogonal reactive functional groups (e.g. OH, NH₂, or COOH) could be created using this method. An application of the produced superhydrophobic-superhydrophilic structures to pattern cells as well as the use of the thiol-yne photo-click method to pattern cysteine-containing peptides are presented.

2.2 Results and discussions

2.2.1 Fabrication of alkyne surface

To fabricate a nanoporous polymer layer modified with alkyne groups (Figure 2.1), I firstly used a 12.5 μm -thin nanoporous polymer layer of poly(2-hydroxyethyl methacrylate-*co*-ethylene dimethacrylate) (HEMA-EDMA) prepared on a glass substrate according to previously published procedure.^[47] The resulting HEMA-EDMA polymer layer has high surface roughness (50% porosity and 80-250 nm pores based on SEM, Figure 2.2) and is highly wettable with static (θ_{st}), advancing (θ_{adv}) and receding (θ_{rec}) WCAs close to $\sim 4.2^\circ$, 7.1° and 0° , respectively (Figure 2.2).

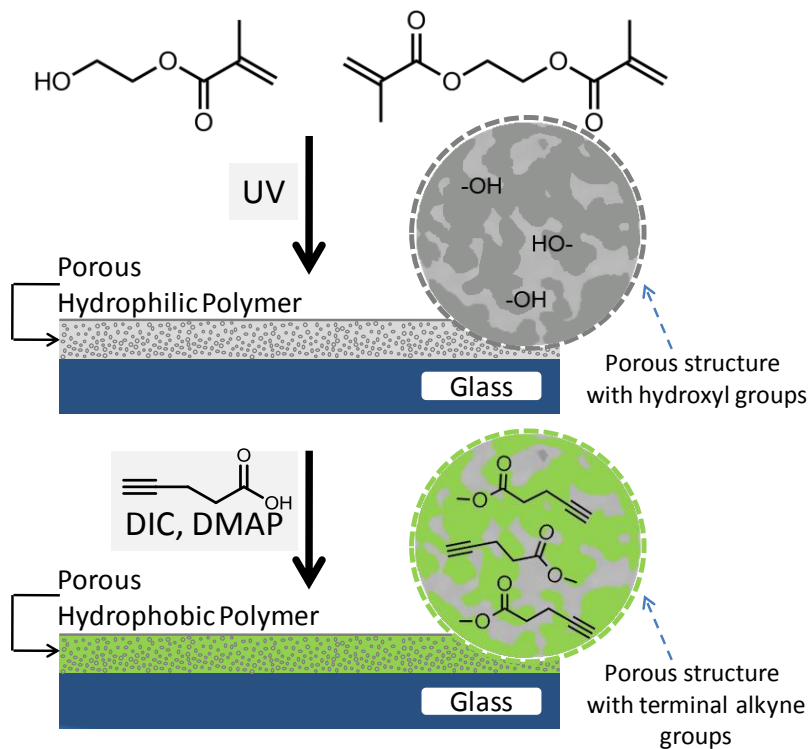


Figure 2.1. Schematic description of the alkyne surface fabrication. Firstly, a 12.5 μm thin, hydrophilic porous polymer film was prepared on a glass substrate. After immersing in a dichloromethane solution containing 4-pentynoic acid, coupling reagent *N,N'*-diisopropylcarbodiimide (DIC), and catalyst 4-(dimethylamino)pyridine (DMAP) and stirring at RT for 4 h, the polymer film underwent esterification to form a porous surface functionalized with alkyne groups.

The HEMA-EDMA surface was modified with 4-pentynoic acid by an esterification procedure. The esterification progress was characterized by measuring the static WCA on the polymer layer during the esterification. The analysis of the WCA variation over time verified that the modification proceeded completely after 4 h of the reaction time (Figure 2.3A). To characterize the esterification within the porous polymer, the superficial surface layer (esterification for 4 h) was removed by attaching conventional pressure-sensitive tape (Scotch tape) to the polymer layer and then peeling it off layer by layer. After each layer was removed with the tape, static WCA was measured at the same spot on the polymer film (Figure 2.3B). After taping 11 times, the polymer layer shows the same static WCAs as a bare glass substrate, indicating that the esterification reaction takes place throughout the whole thickness of the polymer layer. The θ_{st} of the polymer surface increased from 4.2° to 124° after the esterification. After surface modification, the

polymer layer maintained its nanoporous structure and did not show significant changes of the morphology (SEM in Figure 2.2). The intense peak at 2120 cm^{-1} in the Raman spectrum (Figure 2.4) also confirmed the presence of terminal alkyne groups at the polymer surface.^[169] Due to the small size of the pores,^[145] the light scattering on the wetted polymer layer is reduced leading to more than 90% transmittance of visible light (Figure 2.5).

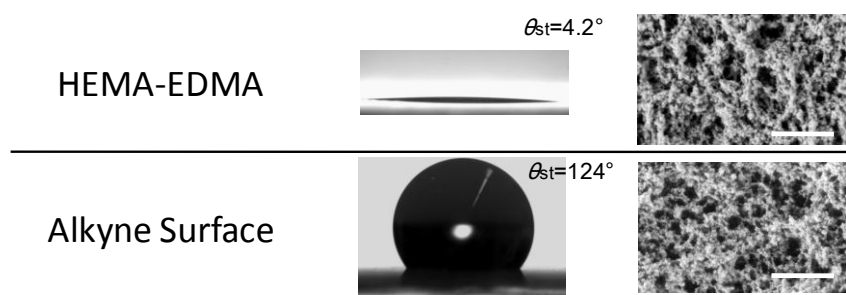


Figure 2.2. Water droplets on HEMA-EDMA and alkyne surface as well as the corresponding SEM images. Scale bars $1\text{ }\mu\text{m}$.

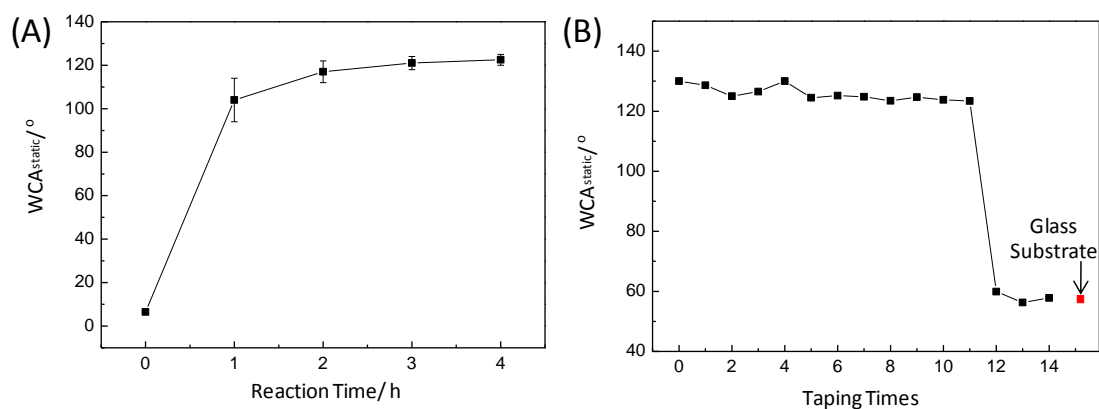


Figure 2.3. (A) Static WCA on the polymer layer as a function of the reaction time during the esterification. The static WCA on the surface is still about 124° after 24h of the reaction time. (B) Static WCA at the same spot on the polymer film after different taping times. The red spot shows the static WCA of a bare glass substrate. Five different spots were measured and all results showed the same trend.

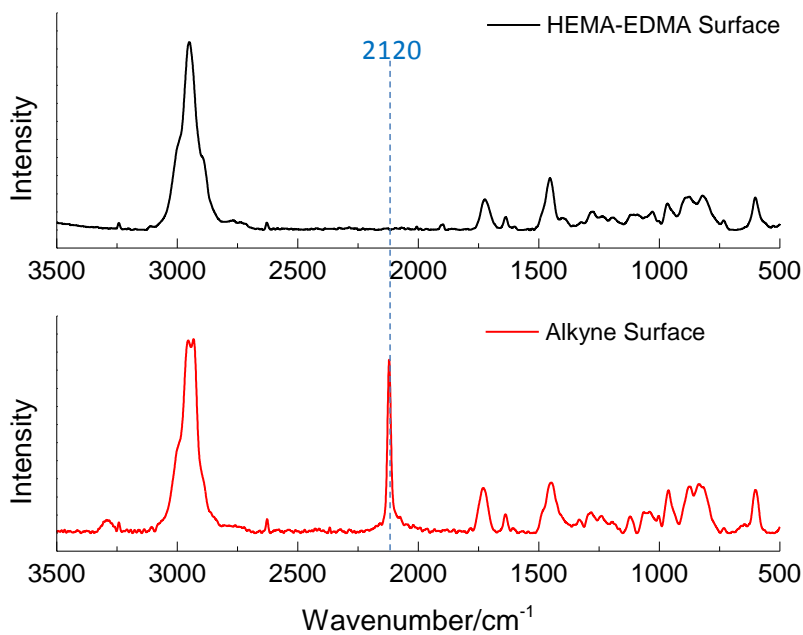


Figure 2.4. Raman spectra of the HEMA-EDMA polymer surface (top, black) and a 4-pentynoic acid-functionalized alkyne polymer surface (bottom, red). The intense band at $\sim 2120\text{ cm}^{-1}$ supports the presence of $-\text{C}\equiv\text{C}-\text{H}$ units on the alkyne surface.

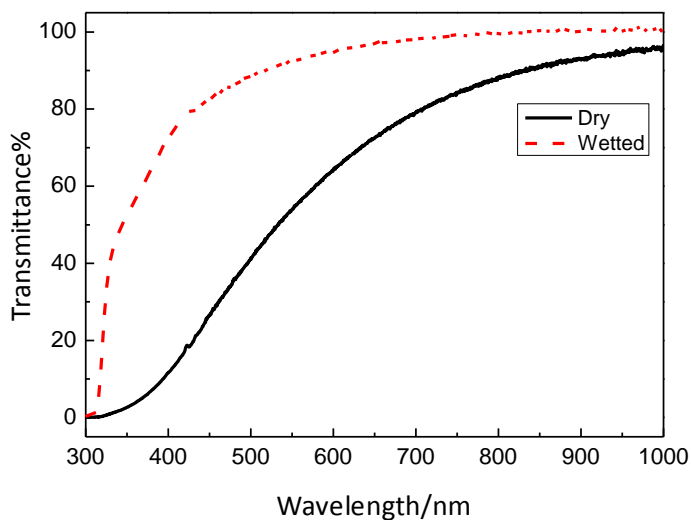


Figure 2.5. UV-Vis-NIR transmittance spectra of wetted and dry porous HEMA-EDMA.

2.2.2 Kinetics of the thiol-yne reactions on alkyne surface

The resulting alkyne porous polymer can be functionalized via the thiol-yne click reaction to transform the surface either into a superhydrophobic or superhydrophilic surface depending on whether a hydrophobic or hydrophilic thiol being used (Figures 2.6A-C). As a general procedure, the porous alkyne surface is wetted with a thiol solution, covered with a quartz slide and irradiated with 260 nm UV light (12 mW cm^{-2}) at room temperature.

In general, long UV irradiation times can lead to oxidation and degradation of the substrate as well as to the damage of biomolecules used for functionalization. Most of the existing UV-based techniques for the formation of superhydrophobic-superhydrophilic patterns require irradiation times ranging from several minutes to several hours, which limits possible applications of such methods. On the other hand, functionalization of the alkyne-surface with cysteamine using the thiol-yne reaction required as little as 0.5 s of UV irradiation in the presence of 2,2-dimethoxy-2-phenylacetophenone (DMPAP) as a photoinitiator to completely transform the hydrophobic alkyne polymer ($\theta_{st}=124^\circ$) into a superhydrophilic surface ($\theta_{st}=4.4^\circ$) (Figure 2.6D). The same reaction without the photoinitiator required only 5 s for the functionalization and no reaction happened without UV light. The thiol-ene reaction without a photoinitiator was reported previously by Cramer et al.^[85] Without UV irradiation, however, the WCAs of the surface did not change at all even in the presence of the photoinitiator, indicating that there was no physisorption of the thiols on the surface.

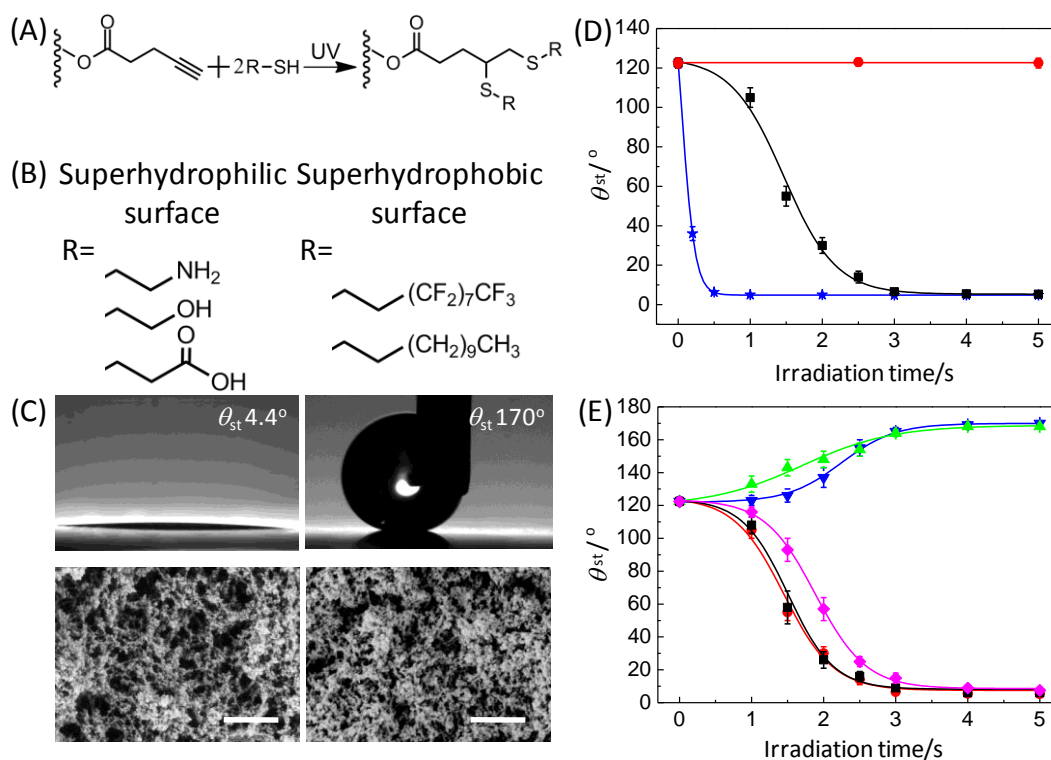


Figure 2.6. (A) Schematic representation of the alkyne surface modification via UV-induced thiol-yne click chemistry. (B) Examples of thiols used for the formation of either superhydrophilic or superhydrophobic surfaces. (C) Water droplet on a cysteamine-modified superhydrophilic surface (left) and on a 1H,1H,2H,2H-perfluorodecanethiol modified superhydrophobic surface (right), and SEM images of the corresponding porous polymers. (D, E) Kinetics of the alkyne surface modification using the thiol-yne click chemistry. The θ_{st} of the polymer layer modified using: (D) cysteamine with (★) or without (■) photoinitiator 2,2-dimethoxy-2-phenylacetophenone (DMPAP) and with DMPAP but without UV irradiation (●); (E) cysteamine (■), 3-mercaptopropionic acid (●), 2-mercaptoethanol (◆), 1H,1H,2H,2H-perfluorodecanethiol (▼), and 1-dodecanethiol (▲) without DMPAP upon UV irradiation. Scale bars: 1 μm .

Figure 2.6E shows the fast kinetics of the initiator-free surface modification as well as the ability to use different thiols to create either superhydrophobic or superhydrophilic surfaces. Modification of the surface with hydrophobic 1-dodecanethiol or 1H,1H,2H,2H-perfluorodecanethiol endows the porous surface with superhydrophobicity (θ_{adv} , θ_{st} and θ_{rec} are as high as 171°, 169° and 162°, or 173°, 170°, and 164°, respectively). In the

Raman spectra, sharp decline of the alkyne bands ($\sim 2120\text{ cm}^{-1}$) was observed (Figure 2.7). Some alkyne groups are buried inside the polymer and not accessible, thus the alkyne signal ($\sim 2120\text{ cm}^{-1}$) would not disappear even after long UV irradiation. No sign of the vinyl sulfide species ($\sim 1657\text{ cm}^{-1}$) was detected (Figure 2.8), indicating full conversion of the alkyne groups to the 1,2-dithioether adduct.

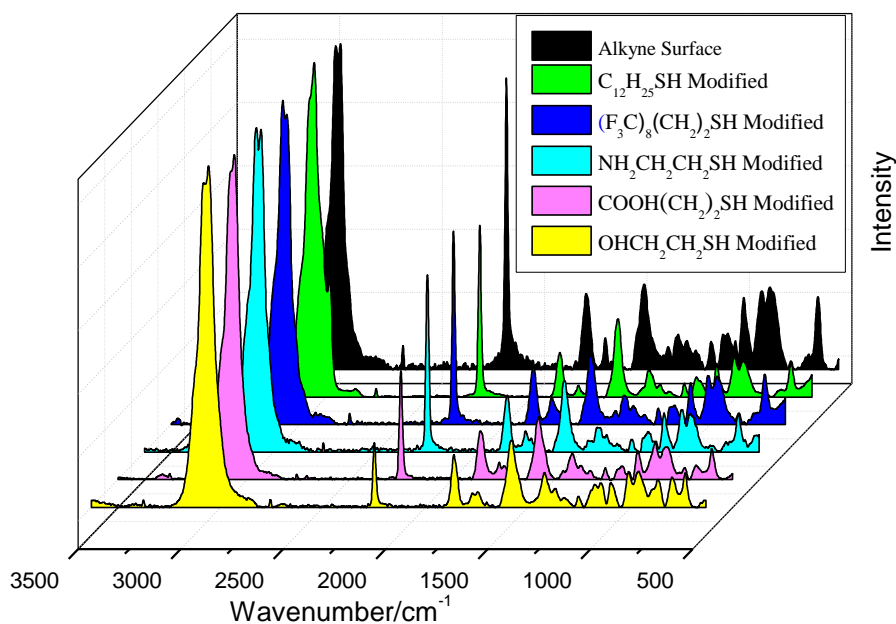


Figure 2.7. The Raman spectra of a non-modified alkyne surface (black), as well as alkyne surfaces modified with 1-dodecanethiol (green), *1H,1H,2H,2H*-perfluorodecanethiol (dark blue), cysteamine (light blue), 3-mercaptopropionic acid (pink), and 2-mercaptoethanol (yellow). The decline of the band ratios of $\sim 2940\text{ cm}^{-1}$ (C-H alkyl free vibrations) to $\sim 2120\text{ cm}^{-1}$ ($\text{C}\equiv\text{C}$ triple bond stretch) illustrates that the alkyne groups react with several kinds of thiols.

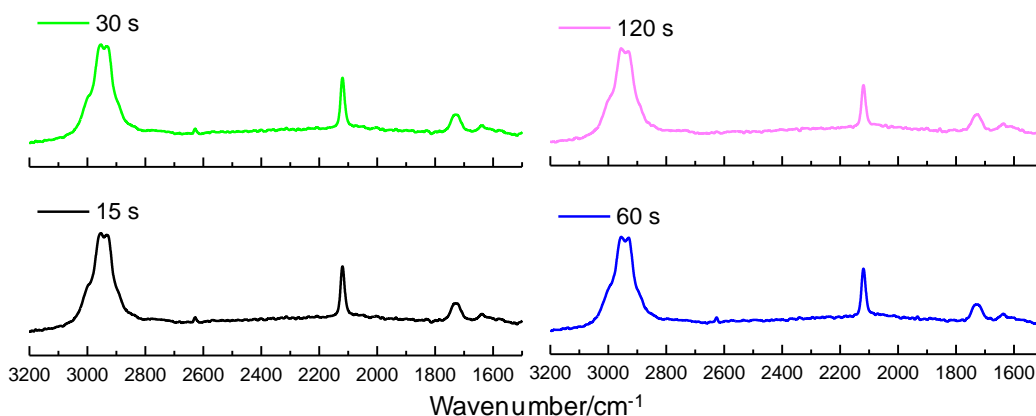


Figure 2.8. The Raman spectra of cysteamine-modified alkyne surfaces at different UV irradiation times. The band ratio of $\sim 2940\text{ cm}^{-2}$ (C-H alkyl free vibrations) to $\sim 2120\text{ cm}^{-2}$ (C \equiv C triple bond stretch) remains the same, illustrating that 15 s is enough for the alkyne complete functionalization of the alkyne groups with thiols.

2.2.3 Thiol-yne reactions in different solvents

The ability to perform the thiol-yne surface functionalization in different both apolar and polar solvents including water can increase the number of possible thiols applicable for the functionalization. Water is especially interesting in terms of its environmental impact, low cost and the compatibility with thiol-containing biomolecules, such as proteins or peptides. To test the ability to use the thiol-yne-based surface functionalization in different solvents, I modified the alkyne HEMA-EDMA surface with 3-mercaptopropionic acid dissolved in several common solvents (Figure 2.9A). Based on the water contact angle measurements, the reaction proceeded extremely fast in ethanol, acetone, ethyl acetate, DCM, THF and water. The hydrophobic alkyne-modified polymer could be transformed into the superhydrophilic surface after only 5 s of irradiation. The reaction in DMF and DMSO required 15 s of the irradiation to make the surface superhydrophilic.

The fact that the reaction proceeds well in water and without an initiator can be important for the rapid functionalization of such surfaces with biomolecules. This was shown by patterning a fluorescein- β -Ala-GGGGC peptide containing a terminal cysteine residue on the alkyne functionalized HEMA-EDMA surface (Figure 2.9B). The pattern

was prepared by irradiating the alkyne surface wetted with an aqueous solution of the peptide (0.25 mg/L) during 15 s.

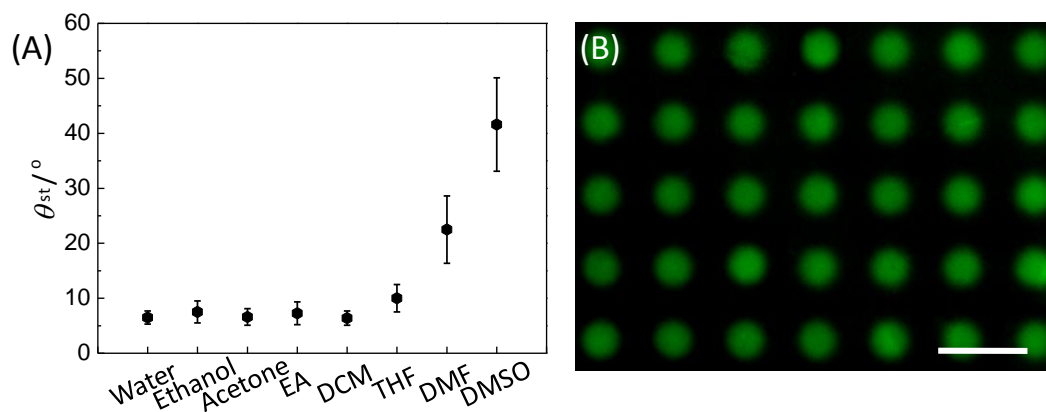


Figure 2.9. (A) θ_{st} of the alkyne surfaces functionalized using 3-mercaptopropionic acid dissolved in different solvents; no photoinitiator; 5 s UV irradiation. I got the results from 3 different samples and took two measurements on every sample. (B) Fluorescence microscope image of a fluorescein- β -Ala-GGGGC peptide pattern prepared by the thiol-yne reaction on the alkyne porous surface carried out in aqueous solution. Scale bars: 500 μm .

2.2.4 Stability of the superhydrophobic surface

Figure 2.10 shows the stability test of superhydrophobic surfaces in air, PBS buffer, DMEM solution with 10% FBS (often used in cell culture) and both acetic and basic water solutions (pH=5 and 10) environments for 120 h. The static WCAs of the surfaces in air, PBS buffer, and acetic and basic water solutions (pH=5 and 10) remained above 160° after 120 h incubation. Due to the protein adsorption, the static WCA of the surface decreased in DMEM solution containing 10 vol% FBS.

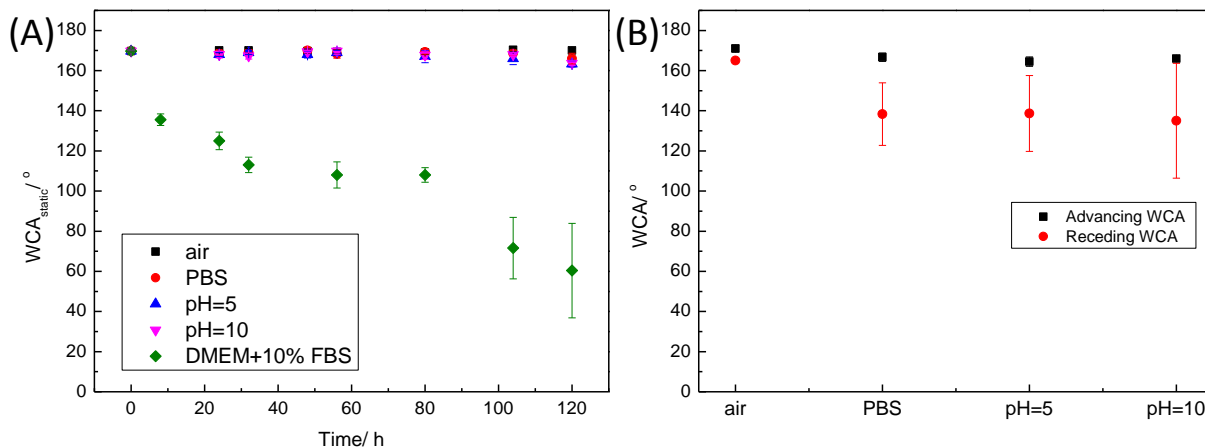


Figure 2.10. The stability test of superhydrophobic surfaces. A) Static WCAs of superhydrophobic surfaces as a function of the incubation time in different environments. B) The advancing and receding WCAs of the surfaces after incubation for 120 h in different environments. The advancing WCAs almost remained the same after incubation. The receding WCAs of the surface in PBS buffer, acetic and basic water solutions decreased slightly.

2.2.5 Superhydrophobic-superhydrophilic micropatterns on alkyne surface

An advantage of using the thiol-reactive alkyne surface for patterning is that the non-irradiated areas remain reactive after the first step of patterning and can be subsequently modified to create patterns of a secondary functionality. Importantly, the second step of modification does not require a photomask as a reactive alkyne pattern is generated during the first step of irradiation through a photomask. Figure 2.11A shows schematically the process for creating superhydrophobic-superhydrophilic micropatterns. First, the alkyne porous layer was wetted with an acetone solution containing 5 vol% 1*H*,1*H*,2*H*,2*H*-perfluorodecanethiol and irradiated with UV light through a photomask yielding a pattern of superhydrophobic as well as reactive alkyne areas. After removing the photomask and washing with acetone, the whole surface was subjected to a second thiol-yne reaction with cysteamine hydrochloride (15 wt% ethanol solution), leading to the modification of unreacted alkyne groups and the formation of a superhydrophobic-superhydrophilic pattern. It is worth noting that θ_{rec} on the superhydrophobic areas decreased by only 2° after the second modification step.

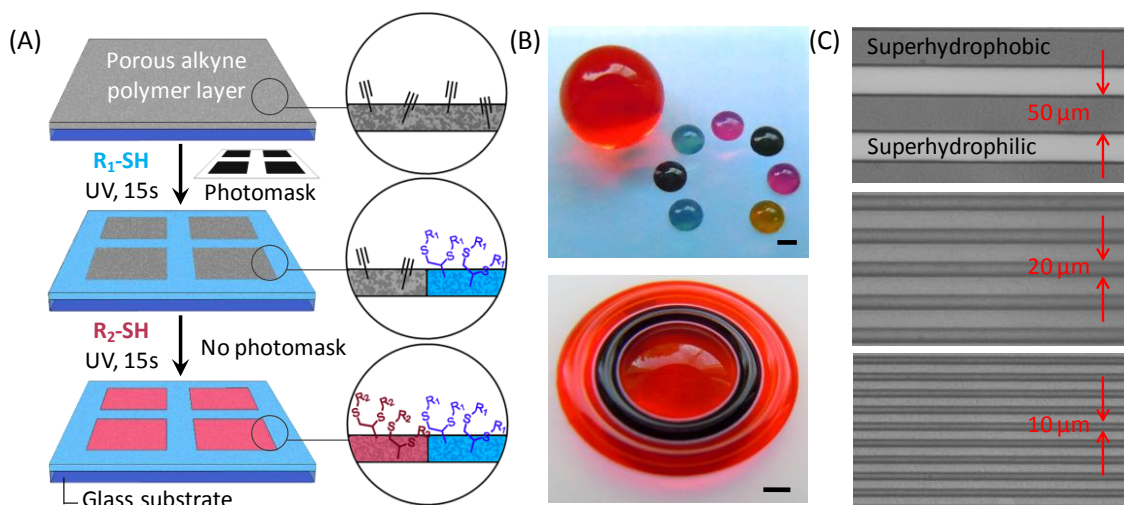


Figure 2.11. (A) Schematic representation of the thiol-yne photo-click reaction for creating superhydrophobic-superhydrophilic micropatterns using the alkyne-modified porous polymer layer as a substrate. Optical images of (B) superhydrophilic-superhydrophobic patterns filled with dye water solutions; superhydrophobic gap between the two rings is 100 μm . (C) Superhydrophilic regions (light areas) separated by superhydrophobic gaps (dark areas) of different widths. Scale bars are 1 mm.

Figure 2.11B shows examples of well-defined superhydrophobic-superhydrophilic patterns of different sizes and geometries prepared by this method. Multicomponent patterns with feature sizes as small as 10 μm (Figure 2.11C) could be produced. Using the method from Ueda et al.,^[149] it is possible to create high-density arrays of completely separated microdroplets (DropletMicroarray approach) on the produced superhydrophobic-superhydrophilic patterns (Figure 2.12). Due to the reduced light scattering, the superhydrophilic nanoporous polymer layer becomes transparent when wetted with water, allowing easier discrimination of spots and facilitating the use of inverted microscopes.

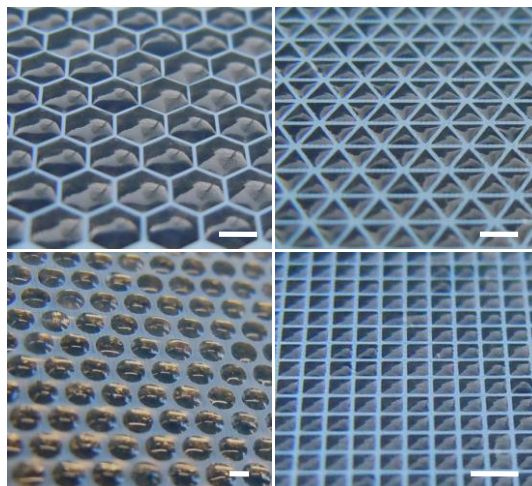


Figure 2.12. DropletMicroarrays formed by dipping the superhydrophobic-superhydrophilic arrays with different geometries into water. The wetted parts become transparent (dark). Scale bars are 1 mm.

2.2.5 Inverse micropatterns

To further improve this method and to avoid possible modification of the residual alkyne groups remaining after the first irradiation step, I used an ethanol-water (1:1) solution instead of pure ethanol to dissolve cysteamine. In this case, the contact angle (θ_{st}) of the ethanol-water solution on the alkyne-functionalized and the fluorinated surfaces was 0° and $135 \pm 3^\circ$, respectively. Thus, the cysteamine solution could only wet the alkyne-functionalized areas ($\theta_{st}=0^\circ$), while the fluorinated areas remained dry (Figure 2.13). This simple method completely prevents immobilization of the thiol on the superhydrophobic areas during the second functionalization step. This was confirmed by time-of-flight secondary ion mass spectrometry (ToF-SIMS) (Figure 2.14A).

Another advantage of this sequential surface modification method is that inverse patterns can be obtained simply by switching the order of the two chemicals in the patterning procedure. Inverse patterns produced using the same photomask by switching the order in which the hydrophobic and hydrophilic regions were created (Figure 2.14B-C).

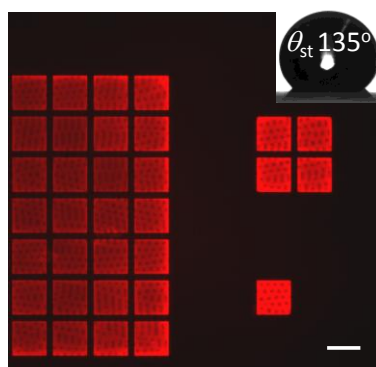


Figure 2.13. Superhydrophobic micropattern, with alkyne-functionalized squares and superhydrophobic *1H,1H,2H,2H*-perfluorodecanethiol-modified barriers. The alkyne spots are wetted with ethanol-water solution containing Rhodamine B. The dye solution can only wet the alkyne spots and is repelled by the superhydrophobic barrier. No leaking occurs outside of the single spot containing the dye solution. The static water contact angle is 135° . Scale bar 1 mm.

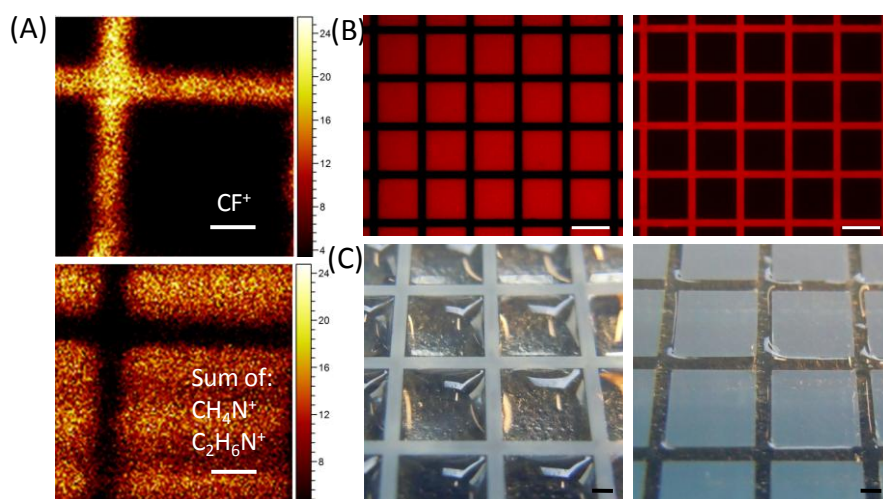


Figure 2.14. (A) ToF-SIMS 2D graphs of positive CF^+ -ion and the sum of CH_4N^+ -ion and $\text{C}_2\text{H}_6\text{N}^+$ -ion, showing the patterning of *1H,1H,2H,2H*-perfluorodecanethiol and cysteamine, respectively. (B) Fluorescence microscope images showing the inverse superhydrophobic-superhydrophilic patterns filled with aqueous solution of Rhodamine B; (C) The superhydrophilic regions of inverse superhydrophobic-superhydrophilic patterns filled with water. Scale bars are $100\ \mu\text{m}$ (A), $300\ \mu\text{m}$ (B) and $1\ \text{mm}$ (C).

2.2.6 HeLa-GFP cells array on superhydrophobic-superhydrophilic micropatterns

The produced superhydrophobic micropatterns also show excellent cell repellent properties superior to those produced by a previously described photografting technique.^[47, 170] To visualize this, HeLa-GFP cells were seeded on an array of superhydrophilic spots and superhydrophobic barriers and incubated for 2 days. Figure 2.15 shows that cells adhered well to the superhydrophilic microspots, demonstrating the biocompatibility and nontoxicity of the surface; however, less than 1% of cells occupied the superhydrophobic regions separating the microspot areas after 2 days of culture.

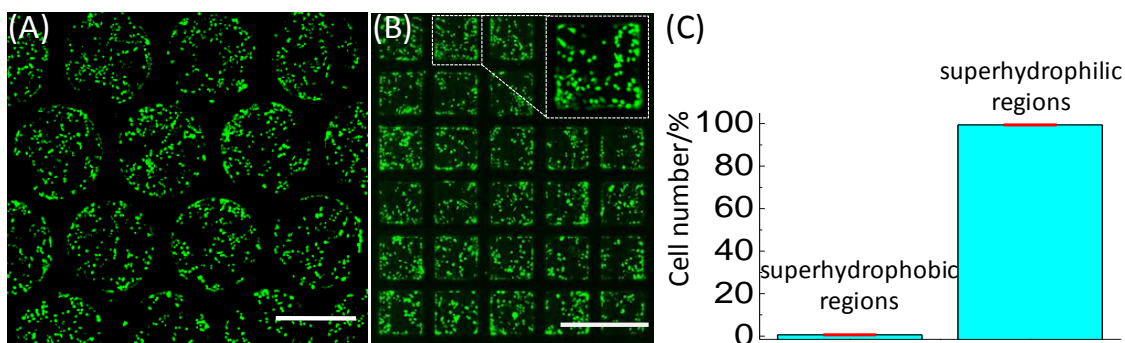


Figure 2.15. Fluorescence microscope images of HeLa-GFP cells after growing for 48 h on superhydrophobic-superhydrophilic arrays in circle (A) and square (B) shapes, showing the preferential adherence of cells on superhydrophilic spots and less than 1% occupation on the superhydrophobic barriers (C). Scale bars are 1 mm.

2.3 Conclusions

An extremely fast initiator-free method based on the thiol-yne click chemistry was developed for the rapid fabrication of superhydrophobic-superhydrophilic micropatterns. The method can be applied to a variety of different functional molecules, containing, for example, unprotected OH, NH₂ or COOH groups, as long as a terminal thiol group is present. Thus, functional and/or reactive superhydrophobic and superhydrophilic micropatterns can be created. The patterning could be performed in aqueous conditions, making this method useful for biological applications, where rapid transformation and benign aqueous conditions are crucial. Given the swiftness, versatility, mild reaction conditions, and compatibility with various chemistries and solvents, I believe that this

method will find numerous applications for creating multifunctional superhydrophobic-superhydrophilic micropatterns.

2.4 Experimental details

2.4.1 Materials

2-Hydroxyethyl methacrylate (HEMA) and ethylene dimethacrylate (EDMA) were purchased from Sigma-Aldrich (Germany) and purified using a short column filled with basic aluminum oxide to get rid of the inhibitors. The food dyes used in Figure 2.11 were obtained from August Thomsen Corp. (USA). All the other chemicals were purchased from Sigma-Aldrich (Germany) and used without further purification. HeLa-GFP cells were purchased from Biocat (Germany). The GFP-peptide containing thiol group (fluorescein- β -Ala-GGGGC) was obtained from Dr. Cornelia Lee-Thedieck at the Institute of Functional Interfaces at Karlsruhe Institute of Technology. Schott (Germany) Nexterion Glass B UV transparent glass plates were used as substrates for polymer layers. The polymerizations and photografting were carried out on an OAI Model 30 deep-UV collimated light source (San Jose, CA) fitted with an USHIO 500 W Hg-xenon lamp (Japan).

2.4.2 Preparation of 12.5 μ m-thin porous HEMA-EDMA films

Here I employed a recently published procedure developed in our group to make nanoporous HEMA-EDMA polymer layers.^[47] Briefly, two 12.5 μ m-thin strips of Teflon film (American Durafilm Co.) were placed at the edges of one 3-(trimethoxysilyl)propyl methacrylate modified glass-plate (25 \times 75 \times 1 mm, width \times length \times thickness) and one fluorinated glass slide was clamped on top of it. 70 μ L of polymerization mixture of HEMA (24 wt%), ethylene dimethacrylate (EDMA) (16 wt%), 1-decanol (12 wt%), cyclohexanol (48 wt%) and 2,2-dimethoxy-2-phenylacetophenone (DMPAP) (photoinitiator, 1 wt% with respect to monomers) was injected in the mold between the glass slides and irradiated for 15 min with 12.0 mW cm⁻² 260 nm UV-light. The mold was then carefully opened using a scalpel.

The resulting non-porous superficial surface was removed by applying and rapidly removing adhesive film (“Scotch tape”) after separating the plates while the layer was still wetted. A homogeneous porous surface was formed. The plate was washed extensively with ethanol and kept in ethanol for some minutes.

2.4.3 Preparation of alkyne modified HEMA-EDMA

Two glass plates coated with a HEMA-EDMA layer were immersed into 50 mL of dichloromethane solution containing 4-pentynoic acid (111.6 mg, 1.14 mmol) and catalyst 4-(dimethylamino)pyridine (DMAP) (56 mg, 0.46 mmol). Then, the coupling reagent *N,N'*-diisopropylcarbodiimide (DIC) (176.5 μ L, 1.14 mmol) was added to the solution cooled to about 0 $^{\circ}$ C, followed by stirring the solution at RT for 4 h. The plates were then washed extensively with acetone and kept in ethanol for several minutes, followed by drying.

2.4.4 Thiol-yne “click” reactions on the porous polymer layer

According to the solubility of a thiol, 1-dodecanethiol (5 vol%) and 1*H*,1*H*,2*H*,2*H*-perfluorodecanethiol (5 vol%) were dissolved in acetone, while 2-mercaptoethanol (15 vol%), cysteamine hydrochloride (15 wt%), and 3-mercaptopropionic acid (15 vol%) were dissolved in ethanol. These thiol solutions were not degassed prior to use.

The alkyne polymer layer was wetted with the respective thiol solution and covered with a fluorinated quartz slide (25 \times 75 \times 1 mm, width \times length \times thickness). All of the fabrications of superhydrophobic or superhydrophilic layers using thiol-yne reactions were performed by UV irradiation (12.0 mW cm⁻², 260 nm) without photoinitiator under ambient laboratory conditions. After the reactions, the samples were washed extensively with acetone and dried with a nitrogen gun.

To study the kinetics of the thiol-yne reactions on the alkyne polymer layer, polymer layers were wetted with a respective thiol solution, covered with a fluorinated quartz slide and irradiated with UV light for different times. Time exposures of UV light were controlled by a time-controller (OAI 150 Exposure Timer). The minimum exposure time is 0.1 s. After the reaction, the samples were washed extensively with acetone and dried with a nitrogen gun. Then static WCAs of the polymer surfaces were measured.

2.4.5 Preparation of superhydrophobic-superhydrophilic micropatterns via thiol-yne click photopatterning

A typical example for the preparation of superhydrophobic-superhydrophilic micropatterns using subsequent thiol-yne reactions is presented. First, the alkyne porous layer was wetted with acetone solution containing 5 vol% 1*H*,1*H*,2*H*,2*H*-perfluorodecanethiol, covered by a fluorinated quartz slide, and irradiated by UV light through a photomask for 15 s. After removing the photomask, washing with acetone and drying, the polymer layer was wetted with an ethanol solution containing 15 wt% cysteamine hydrochloride and irradiated by UV light for another 15 s. Finally, the plate was washed extensively with acetone and dried with a nitrogen gun.

After the first reaction, the exposed fluoro-surface showed superhydrophobicity with θ_{st} , θ_{adv} and θ_{rec} as high as 170°, 173°, and 164°, respectively, while the θ_{st} of unexposed alkyne functionalized areas were maintained at 124°. After the second reaction with cysteamine, the θ_{st} on the alkyne areas reduced to 4.4°. As for the fluorinated areas, the receding WCA decreased by only 2°, while the advancing WCA did not change at all and the surface maintained superhydrophobicity, confirming almost completeness of the reaction of the first step.

2.4.6 Preparation of inverse patterns

Patterns with superhydrophobic spots and superhydrophilic barriers can be created by switching the order of the thiols used for functionalization and using the same method and the same photomask.

2.4.7 Using the thiol-yne patterning method for creating peptide patterns

The alkyne HEMA-EDMA porous layer was first wetted with a 9/1 water/ethanol solution. Then, the plate was washed extensively with pure water to replace the ethanol-water solution with water. Excess of water was removed from the surface and 10 μ L of

the aqueous peptide solution (fluorescein- β -Ala-GGGGC, 0.25 mg/mL) was dropped on the surface. The substrate was covered with a fluorinated quartz slide and a photomask. The polymer layer was then irradiated with UV light through a photomask for 15 s (6 mW/cm², 260 nm). Then, the plate was washed extensively with ethanol and dried with a nitrogen gun.

2.4.8 Fabrication of cell microarray

Hela-GFP cells were cultured in DMEM containing 10% of fetal bovine serum (FBS). A cell suspension was obtained by trypsinizing a confluent (80% monolayer) culture grown in a Petri dish in an incubator (37 °C, 5% CO₂) for 2-3 days. For sterilization, the glass substrate with a superhydrophobic-superhydrophilic pattern was kept in ethanol for 20 min, dried in air, and placed in a 10 mL Petri dish. Then, 5 mL of cell-suspension was added so that the plate was fully covered (seeding density: 12100 cells cm⁻²). The seeded array was cultured in the incubator for 2 d.

Chapter 3. Single-Step Fabrication of High-Density Microdroplet Arrays of Low Surface Tension Liquids

3.1 Introduction

Discontinuous dewetting is a powerful method enabling the generation of thousands of microdroplets with a specific geometry, volume and at predefined locations on a patterned substrate.^[149, 152, 171, 172] During the discontinuous dewetting process, liquid is moved along a surface possessing strong dewettability with a pattern of highly wettable spots to create an array of pinned droplets from picoliter up to microliter volumes.^[173] The advantages of this procedure are that it is a single-step method, permits massive parallelization, is compatible with high-throughput screening (HTS) experiments^[18, 174] but does not depend on expensive robotics and automation, thereby minimizing experimental costs. These advantages make this method attractive for HTS of cells including single cell screenings, diagnostic or personalized medicine applications.

Recently several biological applications requiring both miniaturization and multiplexing have been realized via discontinuous dewetting. Superhydrophobic-superhydrophilic microarrays were used to create droplet-microarrays for high-throughput screening of living cells^[18, 47, 175, 176], to create arrays of hydrogel micropads^[149] and for single cell screenings^[177] Driven by surface tension, cell-laden hydrogels were assembled on a glass surface patterned with hydrophobic and hydrophilic regions.^[178]

However, most of the patterns developed thus far only apply to fabricating microdroplet arrays of high surface tension liquids such as water (surface tension $\gamma_{lv} = 72.2 \text{ mN m}^{-1}$), while the method often fails when most of the organic solvents with lower surface tensions (e.g., ethanol, $\gamma_{lv} = 22.1 \text{ mN m}^{-1}$ or *n*-hexane, $\gamma_{lv} = 18.4 \text{ mN m}^{-1}$) are involved. There are very few methods compatible with low surface tension liquids. Thus, Whitesides and co-workers utilized a two-phase system consisting of water and an immiscible hydrocarbon fluid to generate microdroplet arrays of hydrocarbons on patterned SAMs.^[179] However, their approach is incompatible with water-miscible organic solvents. Droplet-microarrays were also generated using discontinuous dewetting on arrays of microwells produced in poly(dimethylsiloxane) (PDMS).^[171] Tuteja et al. fabricated superomniphobic surface by electro-spinning solutions of *1H,1H,2H,2H*-heptadecafluorodecyl polyhedral oligomeric silsequioxane (fluoro-decyl POSS) and poly(methyl methacrylate), and patterned this surface with superomniphilic spots by spatial O₂ plasma treatment.^[152] Fuchs et al. patterned superamphiphilic areas on a superamphiphobic background via site-selective decomposition of *1H,1H,2H,2H*-

perfluorodecyltriethoxysilane on TiO₂ nanostructure films under UV light.^[51] These superomniphobic surfaces have been applied to form microdroplets of organic liquids by discontinuous dewetting. To fabricate superoleophobic surfaces, however, special designs of surface topography such as overhang^[180] or pinecone-like structures^[51] are needed, and in many cases the surfaces obtain this complex topography at the expense of their laborious preparation, sacrificing mechanical strength and transparency.^[181, 182]

In this chapter, I describe a straightforward two-step approach for surface patterning that enables the fabrication of high-density arrays of microdroplets by discontinuous dewetting compatible with organic liquids with surface tension as low as $\gamma_{lv}=18.4 \text{ mN m}^{-1}$. The method is based on the chemical modification of a chloro(dimethyl)vinylsilane-coated flat glass surface with *1H,1H,2H,2H*-perfluorodecanethiol (PFDT) via the UV-induced thiol-ene click reaction. Since the method does not involve superoleophobic or superhydrophobic surfaces, it eliminates the problems of low transparency and complex fabrication, and makes substrates with excellent mechanical stability possible. Thanks to the feasibility of using organic solvents to prepare high-density droplet microarrays, this approach enables the formation of homogeneous arrays of hydrophobic nanoparticles, polymer micropads of controlled shapes, as well as polymer microlens arrays. Organic microdroplet arrays prepared on flexible polymeric substrates have been also realized.

3.2 Results and discussions

3.2.1 Glass surface modification via silanation and UV-induced thiol-ene click reactions

The general surface modification and patterning procedure is shown in Figure 3.1. First, a microscope glass slide was immersed in a dichloromethane solution containing triethylamine (1.6 vol%), 4-(dimethylamino)pyridine (1 mg/mL) as well as chloro(dimethyl)vinylsilane (0.4 vol%) for 2 min under room temperature. The silanization reaction endowed the glass substrate with a thiol-reactive monolayer of vinyl groups^[183] (Figure 3.2).

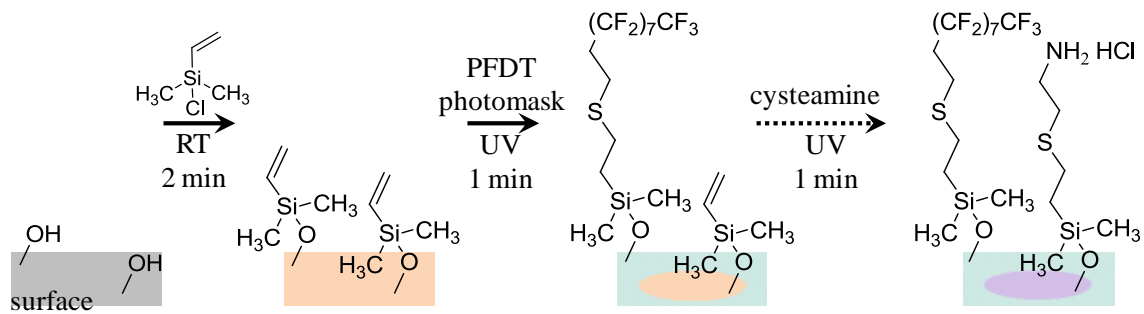


Figure 3.1. Schematic representation of the silanization reaction and UV-induced thiolene photo-click reactions for creating the wetting-dewetting micropatterns.

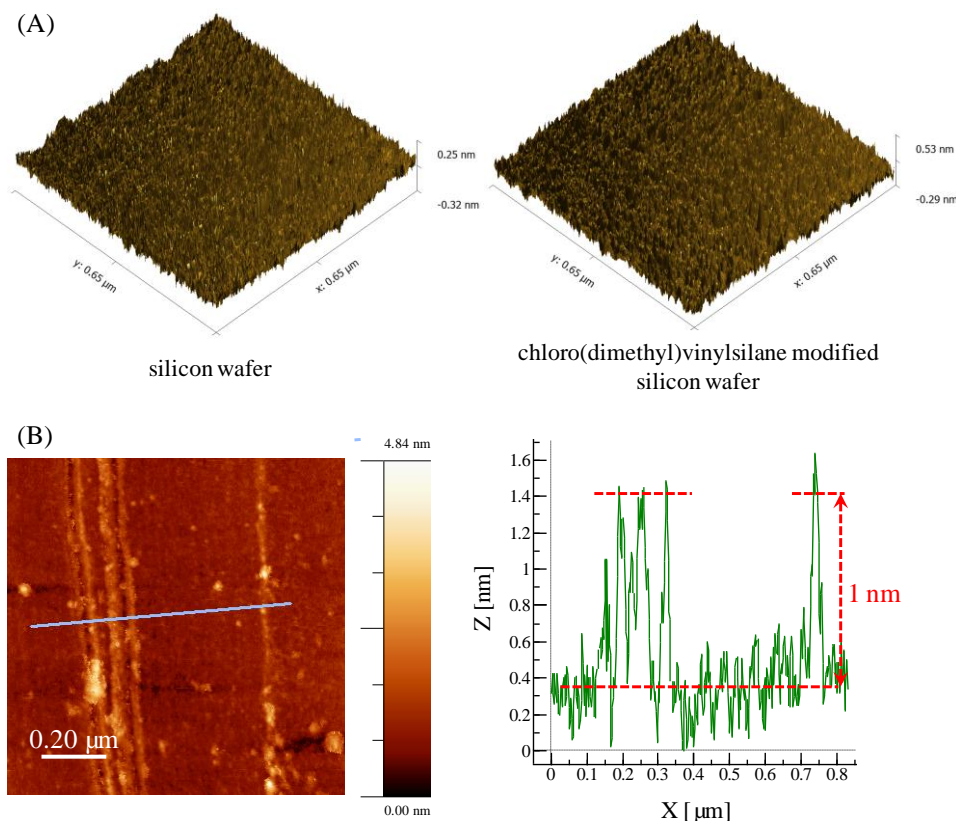


Figure 3.2. (A) Atomic force microscopy (AFM) image of a silicon wafer before (top) and after (bottom) chloro(dimethyl)vinylsilane modification. (B) AFM image of a chloro(dimethyl)vinylsilane modified silicon wafer scratched by tweezers (left) and the height change along the blue line shown in A (right). The calculated thickness of the chloro(dimethyl)vinylsilane layer is around 1 nm and is similar to the ellipsometry result (0.97 ± 0.08 nm), illustrating that the chloro(dimethyl)vinylsilane coating on silicon wafer is a monolayer. Furthermore, unlike di- or trichloro-functional silanes, the chloro(dimethyl)vinylsilane can only dimerize and not polymerize.^[183] Hence, I could

infer that the chloro(dimethyl)vinylsilane coating on glass, a silica-like substrate, is also a monolayer.

In the second step, a pattern of fluorinated areas was prepared by site-selective immobilization of *1H,1H,2H,2H*-perfluorodecanethiol (PFDT) on the vinyl-modified glass surface under UV irradiation (1 min, 260 nm, 5 mW/cm²) through a quartz photomask. The remaining surface vinyl groups were then further modified by cysteamine hydrochloride using the thiol-ene reaction. The well-delineated chemical pattern with sharp edges was confirmed via time-of-flight secondary ion mass spectrometry (ToF-SIMS) (Figure 3.3). Surface modification was also confirmed by measuring water and hexadecane static contact angles (θ_{st}) (Figure 3.4). Thus, PFDT- and cysteamine-modified surfaces possessed 38° and 5° hexadecane θ_{st} , respectively. In addition to the functionalization of vinyl-modified surfaces by cysteamine, I also confirmed site-selective immobilization of thiol-containing biomolecules, such as biotin-PEG-SH (Figure 3.5).

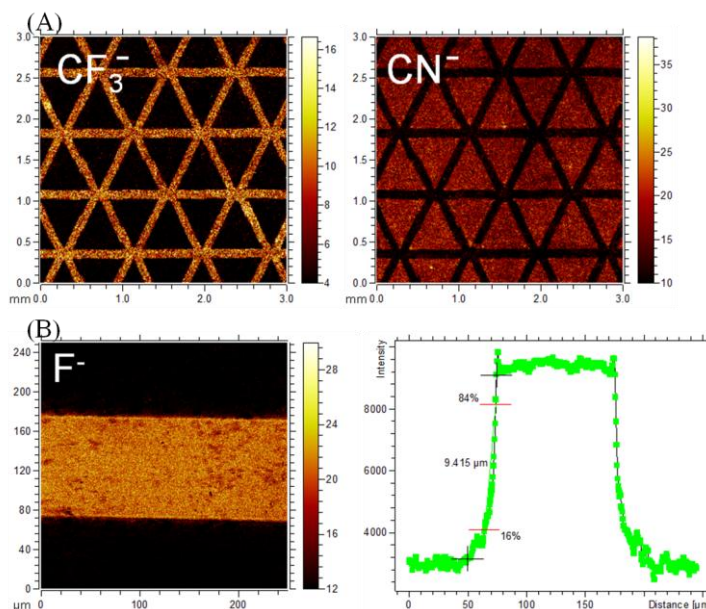


Figure 3.3. (A) ToF-SIMS 2D graphs of negative CF_3^- and the CN^- secondary ions, showing the patterning of PFDT and cysteamine, respectively. (B) High resolution ToF-SIMS image of F^- ions, showing a sharp edge of the PFDT-modified pattern.

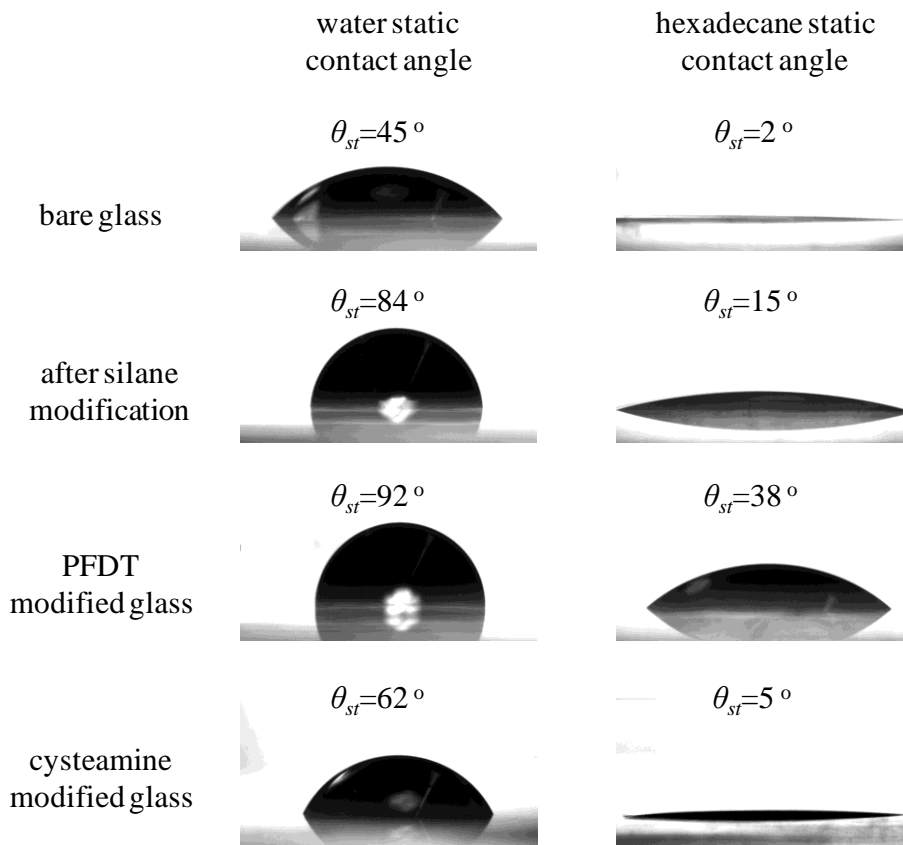


Figure 3.4. Water (left column) and *n*-hexadecane (right column) static contact angles on various surfaces.

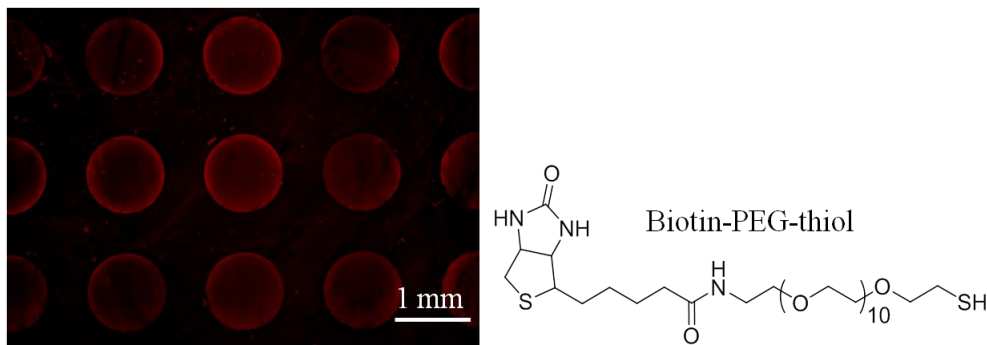


Figure 3.5. A vinyl-modified glass was site-selectively modified by *1H,1H,2H,2H*-perfluorodecanethiol. Then a microdroplets array of acetone solution containing biotin-PEG-thiol (100 mg/mL) was generated on the pre-patterned glass and irradiated under UV light, followed by washing. The pattern was visualized by incubating the substrate with a solution of Alexa Fluor 594-labeled streptavidin.

3.2.2 Dewetting ability

To characterize the PFDT-surface for its resistance to liquid droplet mobility, so important for achieving discontinuous dewetting, sliding angles with 10, 20, 30 and 40 μL droplets of liquids possessing different surface tension (see Table 3.1) were measured (Figure 3.6). All liquids with surface tensions between 47.7 and 18.4 $^\circ$ displayed sliding angles less than 10 $^\circ$ for droplets above 30 μL revealing the PFDT-modified glass's remarkable dynamic dewettability. The sliding angles of organic liquids increased upon lowering the droplet volumes from 40 to 10 μL , which can be attributed to the static friction between the droplet and substrate.^[184] The cysteamine modified surface, on the other hand, displayed ideal wettability by all organic solvents tested with a receding contact angle approaching 0 $^\circ$.

Table 3.1. Surface tension of different liquid at 20 $^\circ\text{C}$.

Liquid	σ [mN m^{-1}]
Ethylene glycol	47.7
<i>N,N</i> -Dimethylformamide	37.1
Cyclohexanol	34.4
Olive oil	32.0
n-Hexadecane	27.5
Dichloromethane	26.5
Acetone	25.2
1-butanol	24.5
Ethyl acetate	23.6
Ethanol	22.1
n-Hexane	18.4

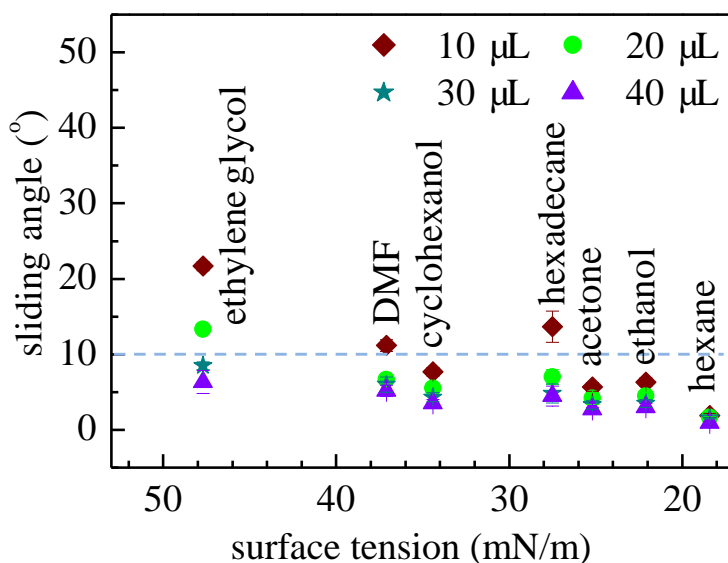


Figure 3.6. Sliding angles of low surface tension solvents on PFDT-modified glass.

3.2.3 Fabrication of microdroplet arrays via discontinuous dewetting

I utilized this surface modification strategy to create wettable cysteamine micropatterns surrounded by non-wettable PFDT areas, and studied the effect of discontinuous dewetting. The approach to fabricate microdroplet arrays is schematically presented in Figure 3.7A. When liquid is moved along a PFDT-cysteamine patterned glass surface, the solvent discontinuously dewets at the PFDT barriers and spontaneously forms a high-density array of separated droplets, each located on cysteamine-modified areas (Figure 3.7B). Microdroplets with complex geometries such as squares, triangles, stars (Figure 3.7C) or even lines of 20 μm -wide channel-like droplets (Figure 3.7D), could be formed. Apart from hexadecane, many other low surface tension organic liquids, such as olive oil (32 mN m^{-1}), dimethylformamide (DMF, 37.1 mN m^{-1}), dichloromethane (DCM, 26.5 mN m^{-1}), ethyl acetate (EtOAc, 23.6 mN m^{-1}), acetone (25.2 mN m^{-1}), ethanol (22.1 mN m^{-1}), and *n*-hexane (18.4 mN m^{-1}), can be used to form corresponding microdroplet arrays (Figure 3.8). Finally, the diameter and height of hexadecane droplets formed on cysteamine circles of 1000 μm diameter measured $1000 \pm 7 \mu\text{m}$ and $54 \pm 2 \mu\text{m}$, respectively (Figure 3.7E), illustrating good uniformity of the droplets produced via discontinuous dewetting method.

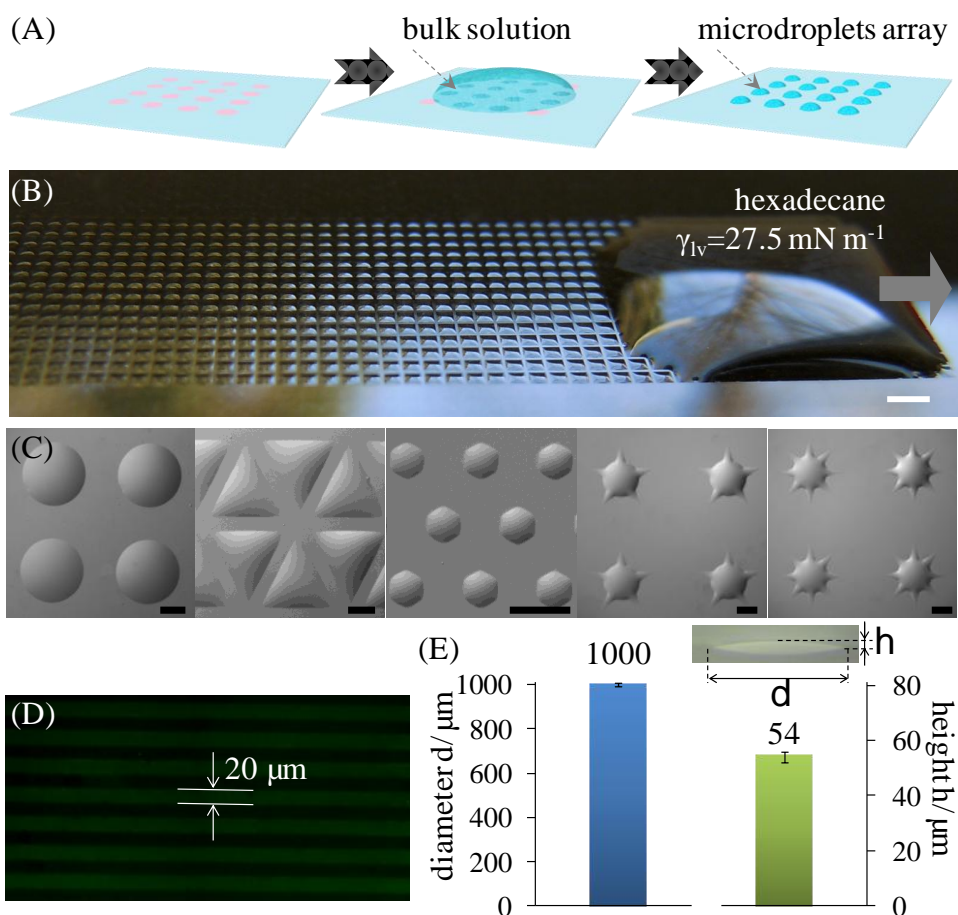


Figure 3.7. (A) Schematic representation of the fabrication of a microdroplet array of low surface tension liquid via discontinuous dewetting. (B) Formation of an array of hexadecane microdroplets on a PFDT-cysteamine patterned glass slide. (C) Brightfield microscopy images of hexadecane microdroplets of different geometries. (D) Fluorescence microscopy image of an array of microchannels formed by rolling an acetone solution of fluorescein along a glass slide patterned with 20- μm cysteamine-modified stripes. (E) Quantification of diameters and heights of hexadecane droplets formed on a 1 mm circular pattern.

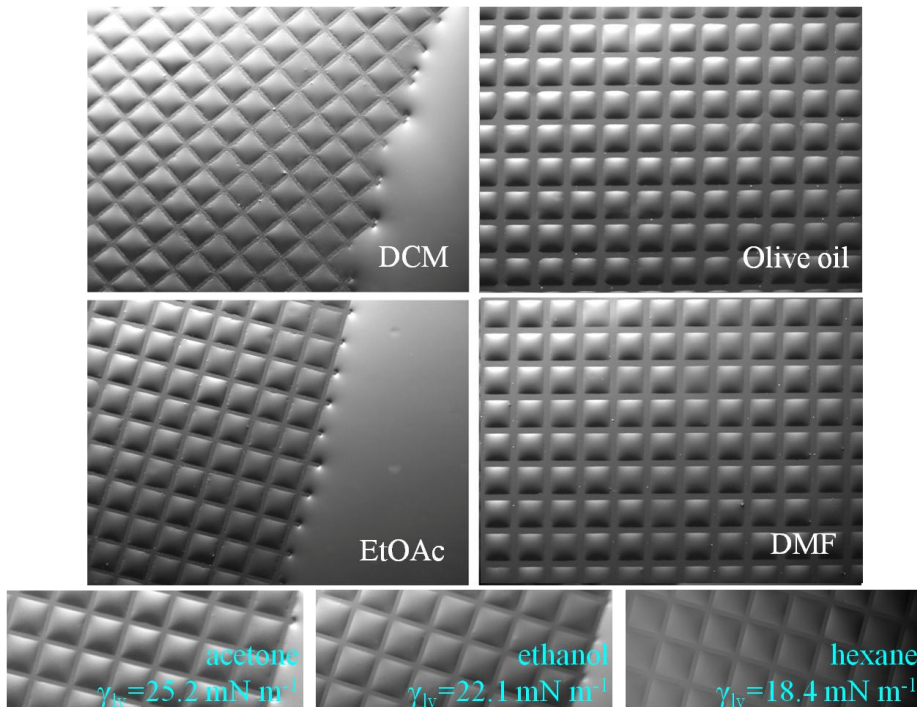


Figure 3.8. Brightfield microscopy images of DCM, olive oil, EtOAc, DMF, acetone, ethanol and hexane microdroplet arrays prepared by discontinuous dewetting method on a prepatterned glass. The side length of the square spots is 500 μm .

3.2.4 Smooth and rough surfaces

To achieve the effect of discontinuous dewetting, one needs regions with good wettability (or poor dewettability with high sliding angles) where droplets become pinned and regions with good dewettability that will be dewetted during a liquid's movement, leading to the formation of arrays of discrete droplets. There are two main means of achieving perfect dewettability. First, by combining special surface topography with low surface energy, superhydrophobicity or superoleophobicity possessing excellent dewetting properties can be achieved.^[180, 181, 185, 186] An opposite approach is based on creating a perfectly smooth and defect-free surface with low surface energy, which can also lead to a surface with a very low sliding angle and excellent dewetting properties.^[187-191] Any substrate with a surface roughness between these two extreme cases, i.e. either with surface defects or with sub-optimal surface topography, will either lead to liquid pinning effects on smooth surfaces or result in the Wenzel state on a rough surface, being non-compatible with good dewettability. It should be noted that this defect-sensitivity

behavior is especially pronounced in conjunction with low surface tension liquids, making it increasingly difficult to achieve both good dewettability and discontinuous dewetting using such liquids.

I tested this defect sensitivity effect by comparing a roughened PFDT-modified glass with its flat analogue. As opposed to the smooth surface, the rough surface revealed higher sliding angles for hexadecane, and it lost the ability to form droplet arrays via the discontinuous dewetting (Figure 3.9).

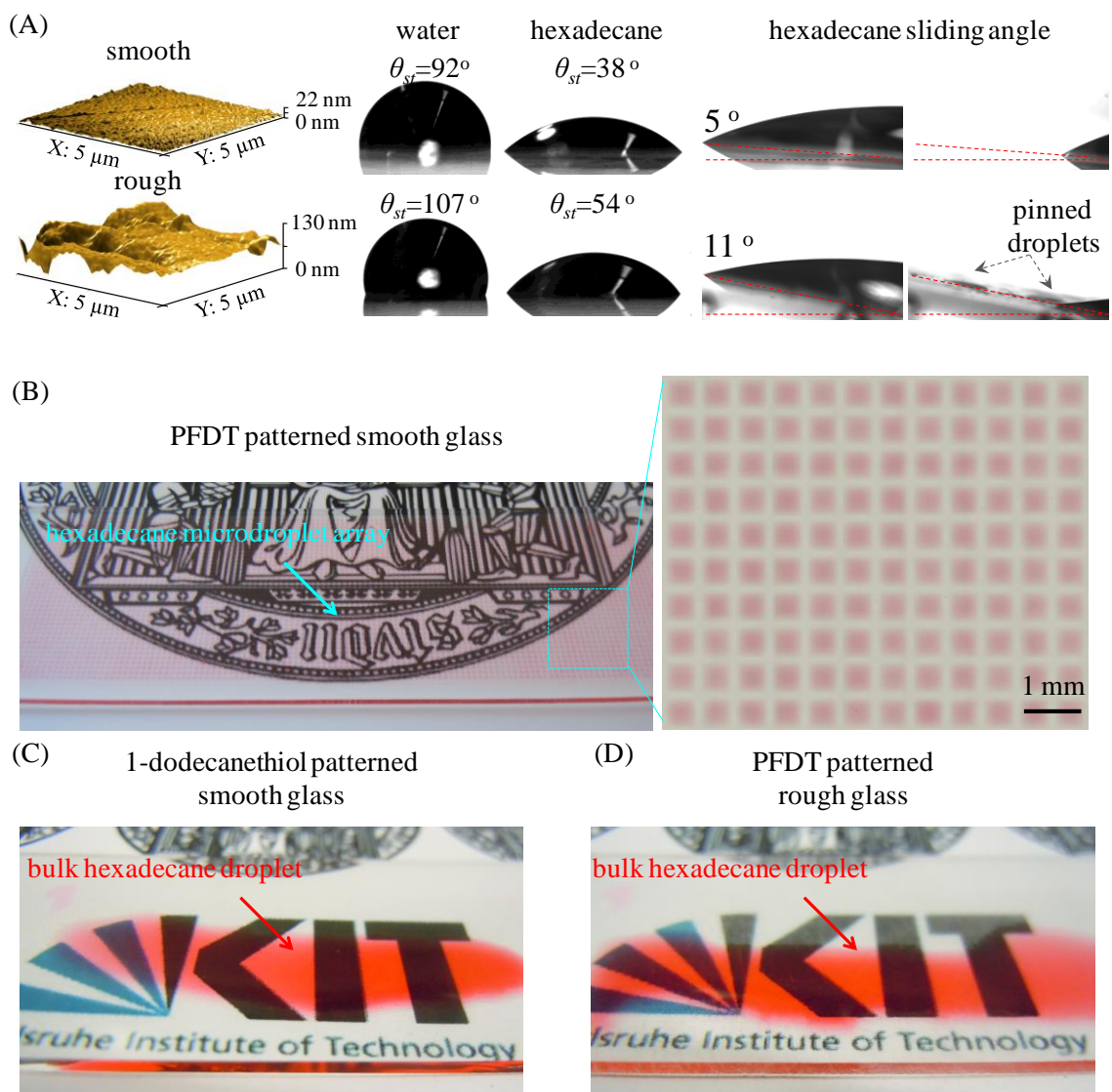


Figure 3.9. (A) AFM images of PFDT-modified smooth (top) and roughened (bottom) glass, water and hexadecane static θ_{st} and sliding angle. (B) Photograph showing the formation of an array of hexadecane microdroplets on a PFDT-prepatterned smooth glass via discontinuous dewetting. A color-mode microscopy image of the hexadecane array is

inserted. 1-dodecanethiol patterned smooth glass (C) and PFDT patterned rough glass (D) don't have the ability to form hexadecane microdroplets arrays via the discontinuous dewetting. The hexadecane liquid is dyed red (Oil Red O).

3.2.5 Transparency

The development of microdroplet array on a transparent substrate is essential for a range of applications, such as high-throughput screenings using optical detection methods, microscopy or UV-Vis absorption spectroscopy. One of the biggest drawbacks associated with superhydrophobic and superomniphobic coatings is their poor transparency due to light scattering.^[145] In contrast, the transmittance of the glass substrate employed in this investigation is not altered after the PFDT modification, remaining above 90% in the visible light range (Figure 3.10).

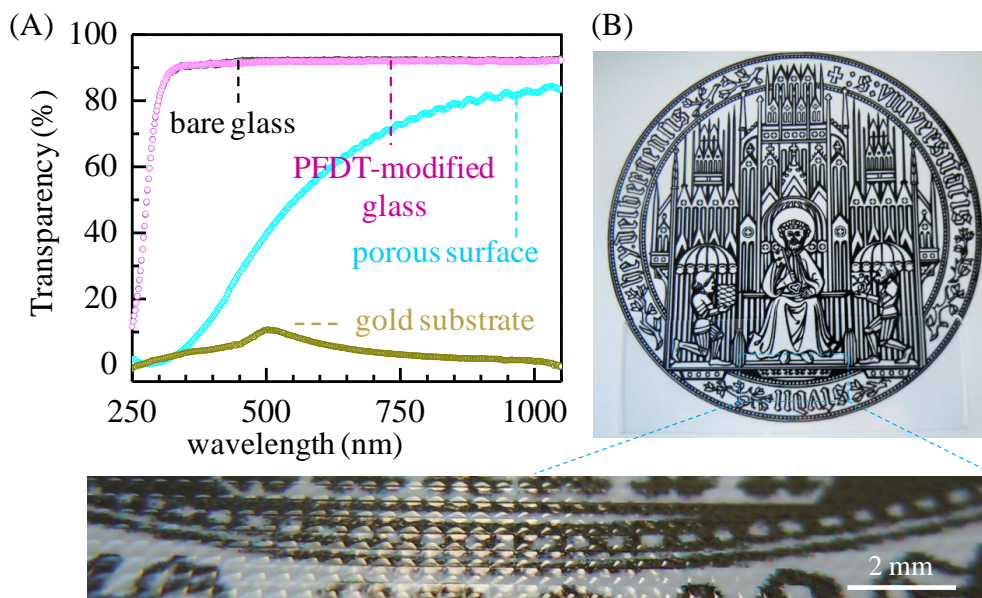


Figure 3.10. (A) Transmittance spectra of bare glass, PFDT-modified glass, porous polymer layer coated glass, and gold coated glass (100 nm Au/5 nm Ti evaporated on glass slide). Compared with bare glass, the transparency of a PFDT-modified glass is unchanged and above 90% in the visible light range. (B) Photograph showing the relative transparency of a hexadecane microdroplets array on a patterned glass. The resulting hexadecane microdroplets array is highly transparent and the background photo is clearly visible through the sample.

3.2.6 Mechanical stability

Another challenge all superwettable surfaces share is their low mechanical stability resulting from their porous or hierarchical surface topography. The advantage of non-porous solid surfaces is that they are mechanically more stable. Here I show the PFDT-modified glass retained its dewetting behavior after subjection to different mechanical treatments, such as scrubbing with a tissue paper, pressing or performing multiple adhesive tape peel tests. Thus, the sliding angle of PFDT-modified glass did not significantly increase even after 25 tape peel tests, while the patterned glass could still be used to create microdroplets arrays even after 100 tape peel tests (Figure 3.11). In contrast, a superhydrophobic fluorinated porous poly(2-hydroxyethyl methacrylate-*co*-ethylene dimethacrylate) lost its superhydrophobicity after 10 tape peel tests.

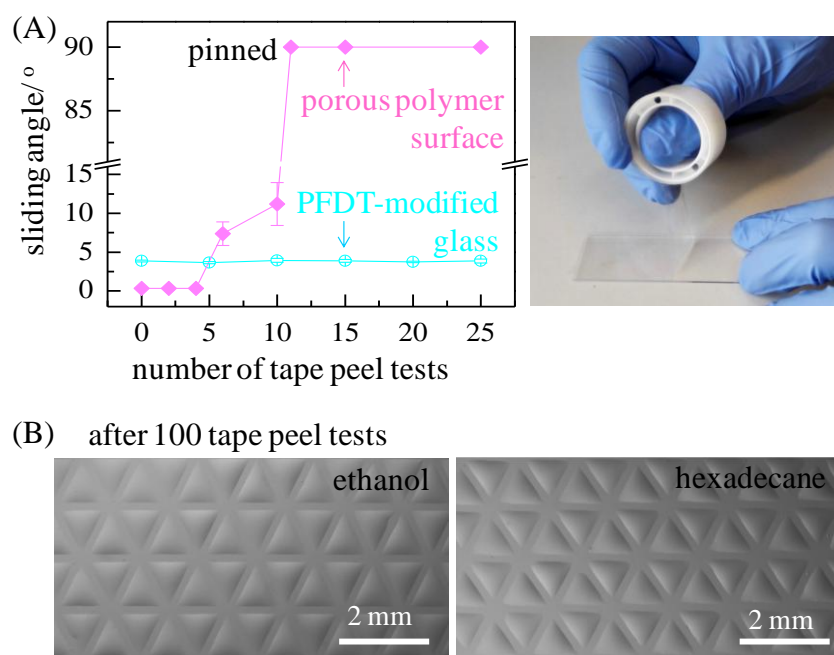


Figure 3.11. (A) Sliding angles of 20 μL ethanol droplets on a PFDT-modified glass (\circ) as well as 8 μL water droplet on a superhydrophobic porous polymer layer (\blacklozenge) after tape peel test (sticking and removing the adhesive “Scotch tape”) for different times. After 10 times of tape peel tests, the porous polymer layer lost its superhydrophobicity, indicating the polymer was removed layer by layer. However, the sliding angle of PFDT-modified glass remains unchanged during 25 times of the tape peel tests, showing good mechanical durability. A photograph showing the tape peel test is inserted. (B) The brightfield image of ethanol and hexadecane microdroplet arrays on a pre-patterned glass. This prepatterned

glass can be used as a template for generating liquid microdroplets array even after the tape peel tests for 100 times.

3.2.7 High-throughput screening

The main potential of microarray platforms consists in the possibility of high-throughput screening (HTS) applications. However, it is usually difficult to add libraries of different chemicals simultaneously into individual liquid microreservoirs. Here I employed the “sandwiching” approach^[18] to enable the parallel single-step addition of different chemicals into individual organic solvent microdroplets formed via the discontinuous dewetting approach. A schematic representation of the organic droplet-array sandwich platform is shown in Figure 3.12A. To demonstrate a proof-of-principle, a library-microarray (LMA) slide (Figure 3.12B) was prepared by printing two different dyes onto a fluorinated glass slide. In the second step, an array of 1-butanol microdroplets (1000 μm square pattern) was sandwiched with the LMA slide leading to the dissolution of the chemicals in the individual microdroplets without cross-contamination between adjacent droplets (Figure 3.12C). This method sets the stage for performing miniaturized and parallel high-throughput chemical reactions in organic solvents without multiple pipetting steps. In addition, water–oil interfaces in microdroplets could be formed by sandwiching an oil microdroplet array with an aqueous microdroplet array formed on a superhydrophobic-superhydrophilic pattern (Figure 3.12D-F), thereby enabling miniaturized parallel liquid-liquid microextractions or heterophasic organic reactions.

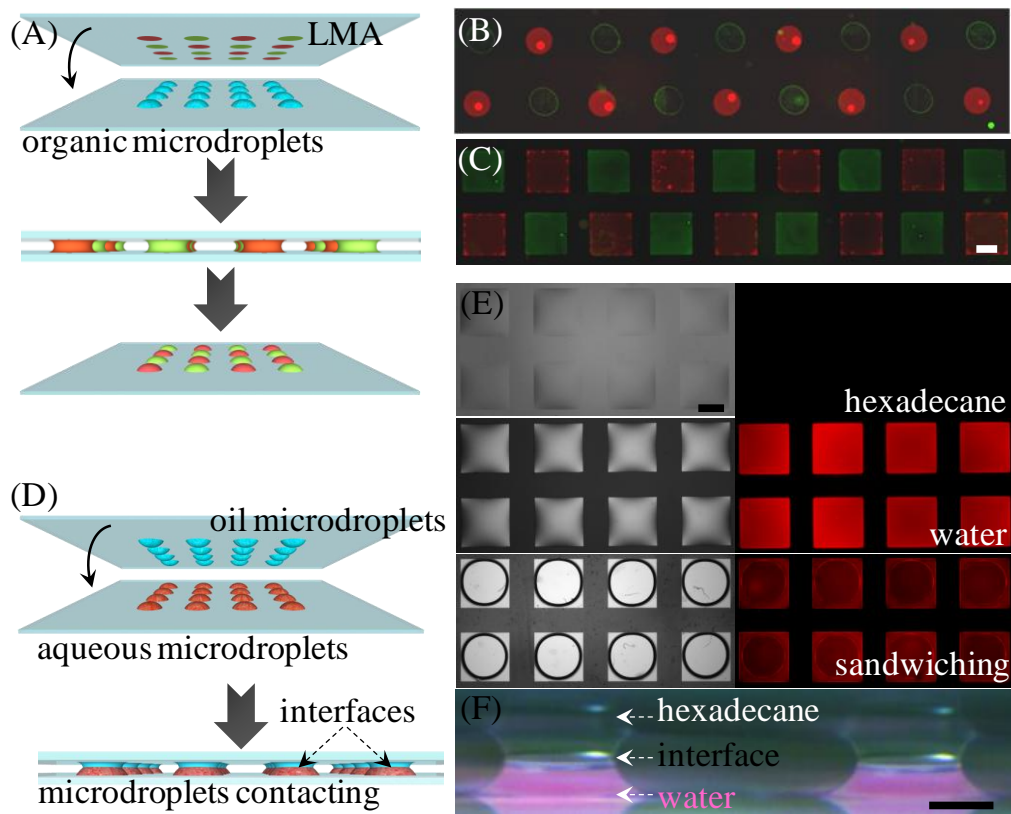


Figure 3.12. (A) Schematics representation of simultaneous addition of chemicals from a library-microarray (LMA) slide into each individual organic microdroplet by using a droplet-array sandwiching technology. (B) Fluorescence microscopy image of a LMA slide. Rhodamine 6G and FITC were printed onto a PFDT-modified glass by using a noncontact ultralow volume dispenser. (C) Fluorescence microscopy images of an array after transferring the dyes from LMA into the individual 1-butanol microdroplets using the sandwiching method. (D) Schematics representation of generation of the interfaces between oil and aqueous microdroplets by using droplet-array sandwiching technology. (E) Brightfield and fluorescence microscopy images of hexadecane droplets (top), Rhodamine B dyed water droplets (middle) and the droplets after sandwiching (bottom). A superhydrophobic-superhydrophilic polymer surface^[176] was used for fabricating water droplets. (F) Side view of the interfaces between hexadecane and water microdroplets. Scale bars: 500 μm .

3.2.8 Nanoparticles arrays

The deposition of nanoparticles on solid substrates to form precise two-dimensional arrays represents another challenge in contemporary nanoscience research.^[192-194] Here I demonstrate that organic microdroplet arrays can be applied to create two-dimensional patterns of homogeneous nanoparticle layers (Figure 3.13A). Figure 3.13B illustrates a pattern of gold nanoparticles (Au NPs) prepared by sliding an ethanol suspension of 200 nm Au NPs along a pre-patterned glass surface. Another array of oleic acid-coated iron oxide nanoparticles fabricated using the same procedure is shown in Figure 3.13C. The iron oxide nanoparticles were suspended in *n*-hexane and self-assembled into hexagon-shape homogeneous patterns. Interestingly, there is almost no “coffee ring” effect in this case, most probably because the evaporation of hexane happens much faster than the liquid flow generated by the uneven evaporation at the edge of the droplets as in the case of slow evaporation of aqueous solutions.^[195]

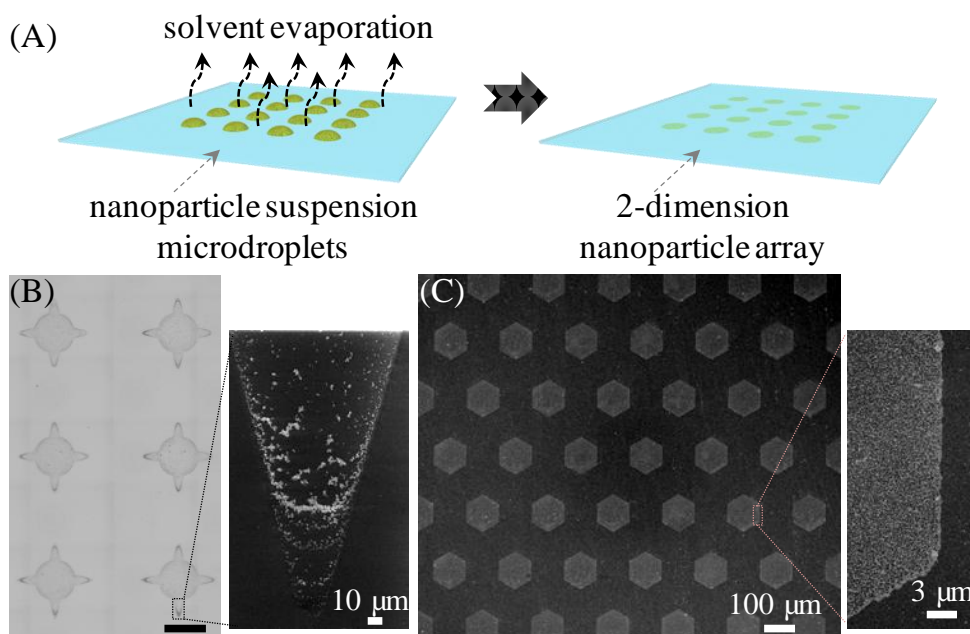


Figure 3.13. (A) Schematic representation of the fabrication of 2-dimensional nanoparticle arrays using the method of discontinuous dewetting. (B) Brightfield microscopy image of an array of Au nanoparticles formed using their ethanol dispersion. Scale bar: 500 μm. SEM image shows the formation of coffee ring structures at the corners. (C) SEM images of an array of oleic acid coated iron oxide nanoparticles formed

by the discontinuous dewetting of their hexane dispersion. High-magnification image shows the absence of the coffee ring effect due to the fast evaporation of hexane droplets.

3.2.9 Polymer micropads arrays

The potential of applying the microdroplet array strategy to create patterns of polymer micropads (PMPs) is also investigated (Figure 3.14A). I first formed an array of ethylene dimethacrylate microdroplets with the desired geometries on a pre-patterned glass, followed by photo-polymerization under N_2 atmosphere to form an array of PMPs, creating poly(ethylene dimethacrylate) micropads with features down to $30\ \mu\text{m}$ (volume $0.84\ \text{pL}$) and circular, square, triangular or more complex shapes (Figure 3.14B,C). Due to their arched shape and transparency, such arrays of transparent polymer micropads of defined shapes behave as arrays of microlenses (Figure 3.14D,E).

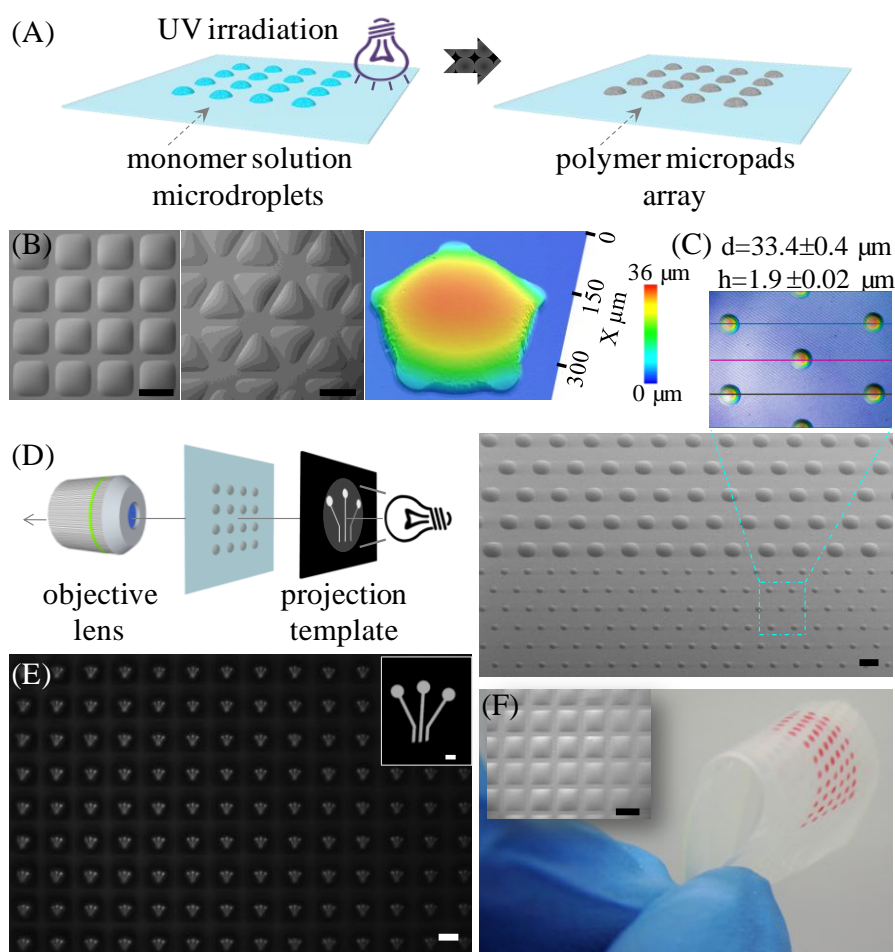


Figure 3.14. (A) Schematic showing the formation of 2.5D polymer micropad arrays. Liquid ethylene dimethacrylate monomer is first self-assembled into microdroplets with

desired geometry on a pre-patterned glass slide, and then polymerized under UV light. (B) Brightfield images of poly(ethylene dimethacrylate) micropads with square (left) and triangle (middle) geometries, and a 3D-profilometry image of a star-shaped micropad (right). (C) SEM image of poly(ethylene dimethacrylate) micropads as small as 33 μm in diameter. Diameter and heights of five polymer micropads are measured by optical profilometry. (D) Experimental setup of the projection experiment. (E) Optical micrograph of images projected through an array of microlenses. Original image is in the inset. (F) Photograph of a flexible HEMA-EDMA polymer layer with a hexadecane microdroplet array. A brightfield microscopy image of the hexadecane array on the polymer film is inserted. Scale bars: B and F, 500 μm ; C, 50 μm ; E, 300 μm .

3.2.10 Flexible polymeric substrate

Finally, I demonstrated that the same chemical modification approach can be applied to create wetting-dewetting micropatterns and corresponding organic droplet microarrays on flexible polymeric substrates bearing surface hydroxyl groups such as smooth poly(2-hydroxyethyl methacrylate-*co*-ethylene dimethacrylate) (HEMA-EDMA) membrane. Figure 3.14F shows a flexible HEMA-EDMA polymer layer with a hexadecane microdroplet array.

3.3 Conclusions

In this chapter, I demonstrated a rapid and convenient surface functionalization method to create transparent micropatterns of both highly wettable and non-wettable slippery areas on smooth glass or flexible polymer films. These patterns were used to realize a single-step approach for the fabrication of arrays of low surface tension liquid microdroplets via the discontinuous-dewetting method. A wide range of low surface tension liquids including ethanol, methanol, acetone, dichloromethane, toluene and even hexane could be used to produce arrays of separated microdroplets with square, circular, hexagon or more complex shapes. Such single step formation of thousands of organic microdroplets in precise locations in an array format and with the same volumes provides a unique solution for ultra high-throughput chemical screening applications. The possibility of the parallel addition of different chemicals into the individual organic

microdroplets was realized by applying the sandwiching method. I employed this method also to form arrays of low surface tension liquid methacrylate monomers, followed by their polymerization to create high-density arrays of polymer microlenses with specific shapes and positions of each lens. This approach is also uniquely suited to create patterns of hydrophobic nanoparticles that can be only dispersed in organic solvents. To provide examples, I created 2D patterns of both gold and magnetic iron oxide nanoparticles.

3.4 Experimental details

3.4.1 Materials

2-Hydroxyethyl methacrylate (HEMA) and ethylene dimethacrylate (EDMA) were purified using a short column filled with basic aluminum oxide to get rid of the inhibitors. Gold nanoparticles (250 nm) in PBS solution were purchased from Alfa Aesar (Germany). The gold nanoparticles were collected by centrifugation and re-suspended into ethanol. Oleic acid coated iron oxide nanoparticles were synthesized according to the literature.^[196] All other chemicals were purchased from Sigma-Aldrich (Germany) and used without further purification. Schott (Germany) Nexterion Glass B UV transparent glass plates were used in this work.

3.4.2 Characterization

Ellipsometric data (shown in the Figure 3.2 legend) were acquired using a SENpro ellipsometer (SENTECH Instruments, Germany) in the rotating analyzer mode in the spectral range of 370–1050 nm. SEM images were obtained using the LEO 1530 Gemini scanning electron microscope (Zeiss, Germany) at the Institute of Nanotechnology (INT), KIT. Prior to SEM measurements, samples were sputtered with a 10 nm gold layer using a Cressington 108 auto sputter coater (INT, KIT). The distribution of cysteamine and PFDT fragments on the surface was confirmed by ToF-SIMS (ION TOF Inc., Münster, Germany), IFG, KIT. The brightfield images were taken using a Leica DFC360 microscope (Germany). The fluorescence images were captured by a Keyence BZ-9000 fluorescent microscope (Japan). A UK 1115 digital camera from EHD imaging (Germany) was used to take images of water and hexadecane droplets on the surface under ambient conditions. ImageJ software with a Dropsnake plugin was used to measure the contact

angle. UV-Vis spectroscopy was performed with a HR2000+ high resolution spectrometer (Ocean Optics Inc., USA) equipped with DH-2000-BAL light source (Mikropack GmbH, Germany).

3.4.3 Preparation of dewetting-wetting pattern on bare glass

Two bare glass plates were immersed into 49 mL of dichloromethane containing triethylamine (TEA) (0.8 mL), chloro(dimethyl)vinylsilane (0.2 mL) and 4-(dimethylamino) pyridine (DMAP) (50 mg, 0.46 mmol) serving as a catalyst. Then, the solution was stirred at RT for 2 min. The plates were washed with ethanol and dried.

Chloro(dimethyl)vinylsilane modified glass plates were then wetted with ethyl acetate solution of 20 vol% of *1H,1H,2H,2H*-perfluorodecanethiol, covered by a quartz chromium photomask, and irradiated by 5.0 mW cm⁻² 260 nm UV light for 60 s. After removing the photomask, the glass was washed with acetone and dried.

The resulting glass was wetted again with ethanol-water (1:1) solution containing 10 wt% of cysteamine hydrochloride, covered by a quartz slide, and irradiated by UV light for 60 s. The plate was washed extensively with ethanol and dried.

3.4.4 Preparation of superhydrophobic porous polymer surface

A recently published procedure developed in our group was employed to make superhydrophobic surface and superhydrophobic-superhydrophilic micropatterns on nanoporous HEMA-EDMA polymer layers.^[176]

3.4.5 Preparation of poly(ethylene dimethacrylate) micropad arrays

First, 30 μ L of a mixture of ethylene dimethacrylate (EDMA) and 2,2-dimethoxy-2-phenylacetophenone (photoinitiator, 1 wt. %) was drained off a pre-patterned PFDT-cysteamine glass plate to form an array of monomer microdroplets. Then the glass substrate was placed into a flask filled with N₂ and irradiated with UV (312 nm, 2.0 mW cm⁻²) for 30 min and washed with acetone.

3.4.6 Preparation of flexible and smooth HEMA-EDMA polymer layer

A piece of cellulose membrane (Whatman regenerated cellulose membrane filter, pore size 0.2 μm) was placed on a Teflon film (American Durafilm Co.) substrate and wetted by polymerization mixture of HEMA (89 wt%), EDMA (10 wt%) and 2,2-dimethoxy-2-phenylacetophenone (photoinitiator, 1 wt%). Then this cellulose membrane was covered by another Teflon film and irradiated for 15 min with 5.0 mW cm^{-2} 260 nm UV light. After removing the Teflon films, the resulting polymer layer was washed extensively with ethanol.

In order to create a PFDT-cysteamine pattern, the HEMA-EDMA polymer layer was functionalized and patterned by the same manner as described for the functionalization of glass plates (see also Figure 3.1).

Chapter 4. UV-Induced Tetrazole-Thiol Reaction for Polymer Conjugation and Surface Functionalization

4.1 Introduction

Ever since the first reported photoreaction of an organic compound, *santonin*, in 1834 by Trommsdorf,^[54] the spatially and temporally controllable photochemistry has found diverse and widespread applications,^[197-204] including surface functionalization to create patterned or gradient immobilization of various substrates.^[47, 120, 205-208] Photo-induced click reactions have been actively investigated during the last decade in attempts to combine the benefits of click reactions with the excellent spatial and temporal controllability of photochemical processes.^[46] UV-induced thiol-ene and thiol-yne reactions are the most known radical photo-click reactions.^[84, 88, 91, 209] Non-radical photoreactions have also attracted a lot of attention in recent years.^[59, 210] For instance, Lin et al,^[66, 67, 73, 81, 211] introduced a photo-click 1,3-dipolar tetrazole-ene reaction based on Huisgen's studies.^[68, 212, 213] The tetrazole-ene reaction presents several advantages: simplicity of implementation, fast reaction kinetics, high yields, it is catalyst free, yields inoffensive by-products (N₂) and, therefore, bio-compatible. This and other photo reactions have been implemented in many different applications such as dendrimers synthesis,^[86] bioconjugation,^[214] in situ bio-labeling,^[71] hydrogels formation,^[48, 215] surface functionalization^[75-77] etc. Nevertheless, the implementation of photo reactions in bio-applications is still limited, partly because unnatural functional groups have to be first introduced to a biomolecule. In addition, only a few photo reactions could be applied for polymer-polymer coupling and site-selective conjugation of biomolecules on surfaces.^[75, 106, 216] Thus, despite a progress in the field of photo-induced reactions, there is a clear need for novel efficient photo reactions that are selective to different types of functionalities, compatible with polymer-polymer conjugation and bioapplications.

50 years ago Huisgen et al. reported that thiophenol could be added to the intermediate nitrilimine generated from decomposition of 2,5-diphenyltetrazole in boiling thiophenol.^[212, 213] Photolytic decomposition of tetrazoles with release of nitrogen and nitrilimines was also described.^[68] In this work, I report a UV-induced tetrazole-thiol reaction that allows for rapid catalyst-free polymer-polymer conjugation, efficient surface functionalization and patterning as well as opens the way to direct functionalization of biomolecules bearing periphery thiol groups.

4.2 Results and discussions

4.2.1 Kinetics of the UV-induced tetrazole-thiol reaction

In order to initially examine the kinetics of the UV-induced tetrazole-thiol reaction (Figure 4.1A), a solution of methyl 4-(2-phenyl-2H-tetrazol-5-yl)benzoate **1** in ethyl acetate and 5 eq. of 2-mercaptoethanol **2** were subjected to irradiation at 260 nm UV light (Figure 4.1B). The results showed the UV-triggered rupture of the tetrazole ring evidenced by the gradual decrease in the tetrazole absorption at 278 nm. At the same time a new absorption band around 369 nm was observed only in the presence of a thiol, confirming the formation of a tetrazole-thiol adduct (Figure 4.1C). Both steps were rapid, achieving complete conversion within 10 s based on UV-Vis spectroscopy. The resulting tetrazole-thiol product, meanwhile, showed a strong fluorescent emission band at 480 nm (Figure 4.2).

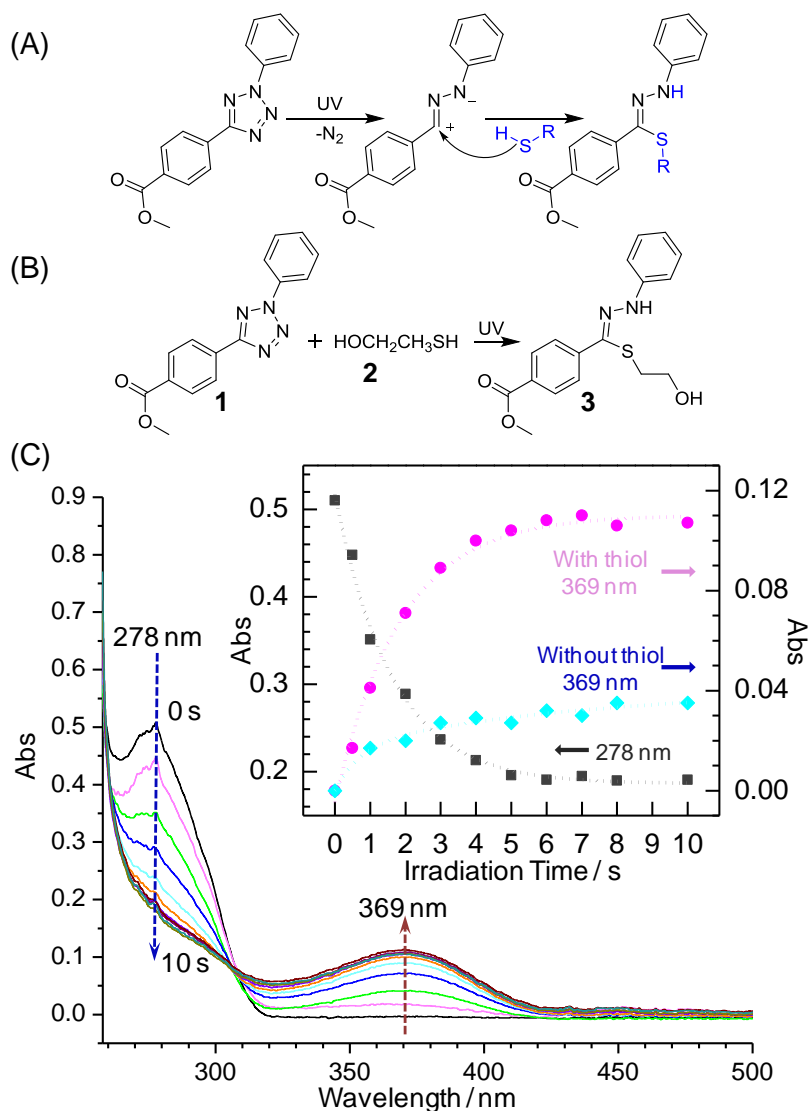


Figure 4.1. Schematic representation of (A) UV-induced formation of the nitrilimine intermediate from tetrazole **1** and subsequent nucleophilic thiol addition; (B) the UV-induced tetrazole-thiol reaction between tetrazole **1** and thiol **2**. (C) UV-Vis absorbance of the tetrazole-thiol reaction mixture as a function of UV irradiation time. The evolution of the absorbance peaks at 278 nm (■) as well as the 369 nm (●) with irradiation time (inset). The control experiments (369 nm peak is shown as ♦) were taken under the same conditions but without **2**.

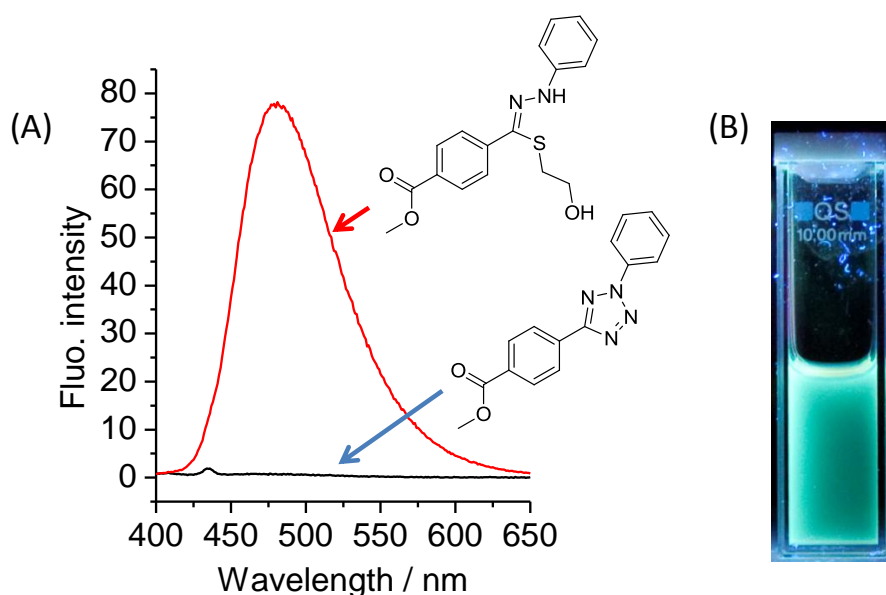


Figure 4.2. (A) The fluorescence spectra of the mixture of 20 μM **1** and 100 μM **2** in ethyl acetate before (black line) and after (red line) UV irradiation for 10 s. The photoirradiation wavelength was set at 260 nm and the excitation wavelength was set at 385 nm. The nucleophilic addition product shows an emission band at 480 nm. (B) Photograph of the thiohydrazone product (3 mg/mL in ethyl acetate) under 365-nm UV light.

The thiohydrazone structure of the product **3** was confirmed by ESI-MS (Figure 4.3) and NMR (Figure 4.4 and Figure 4.5). NMR spectra of the product of UV-induced tetrazole-thiol reaction clearly demonstrate the formation of the expected product. First, by comparing the ^1H NMR spectrum of **1** with the 1,3-dipolar nucleophilic addition product **3**, there is a clear change in the signals between $\delta=6.5$ and 8.5 ppm that are associated with the aromatic protons. The integration value for the signals arising from the aromatic protons is in perfect agreement with the number of aromatic protons expected for the product, indicating the UV-triggered rupture of the tetrazole. Moreover, the NMR signals associated with the 2-mercaptoethanol's protons shifted to lower field (from $\delta=2.68$ to $\delta=2.86$ ppm). In addition, the sextet corresponding to the HS-CH_2 -protons changes to a triplet of $-\text{S-CH}_2-$, indicating that the 2-mercaptoethanol **2** is linked now to the hydrazone. Finally, the presence of a new resonance signal at $\delta=9.24$ ppm further suggests that the thiol group reacted with the nitrilimine.^[213]

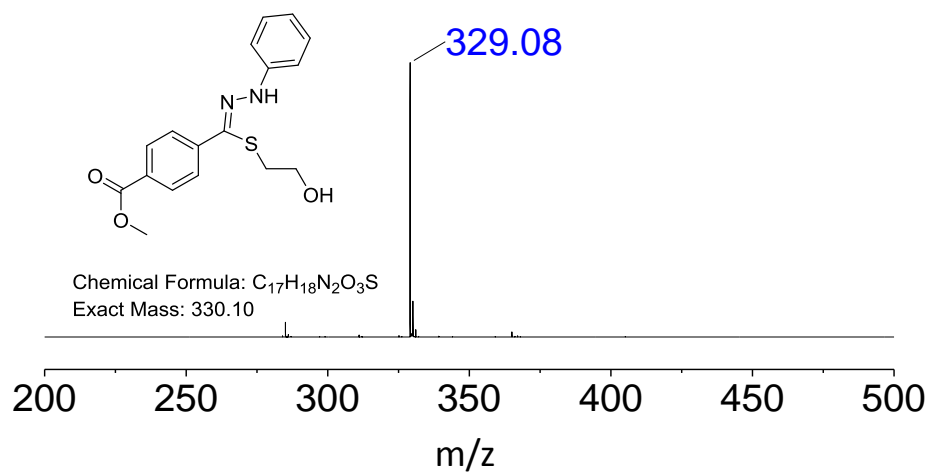
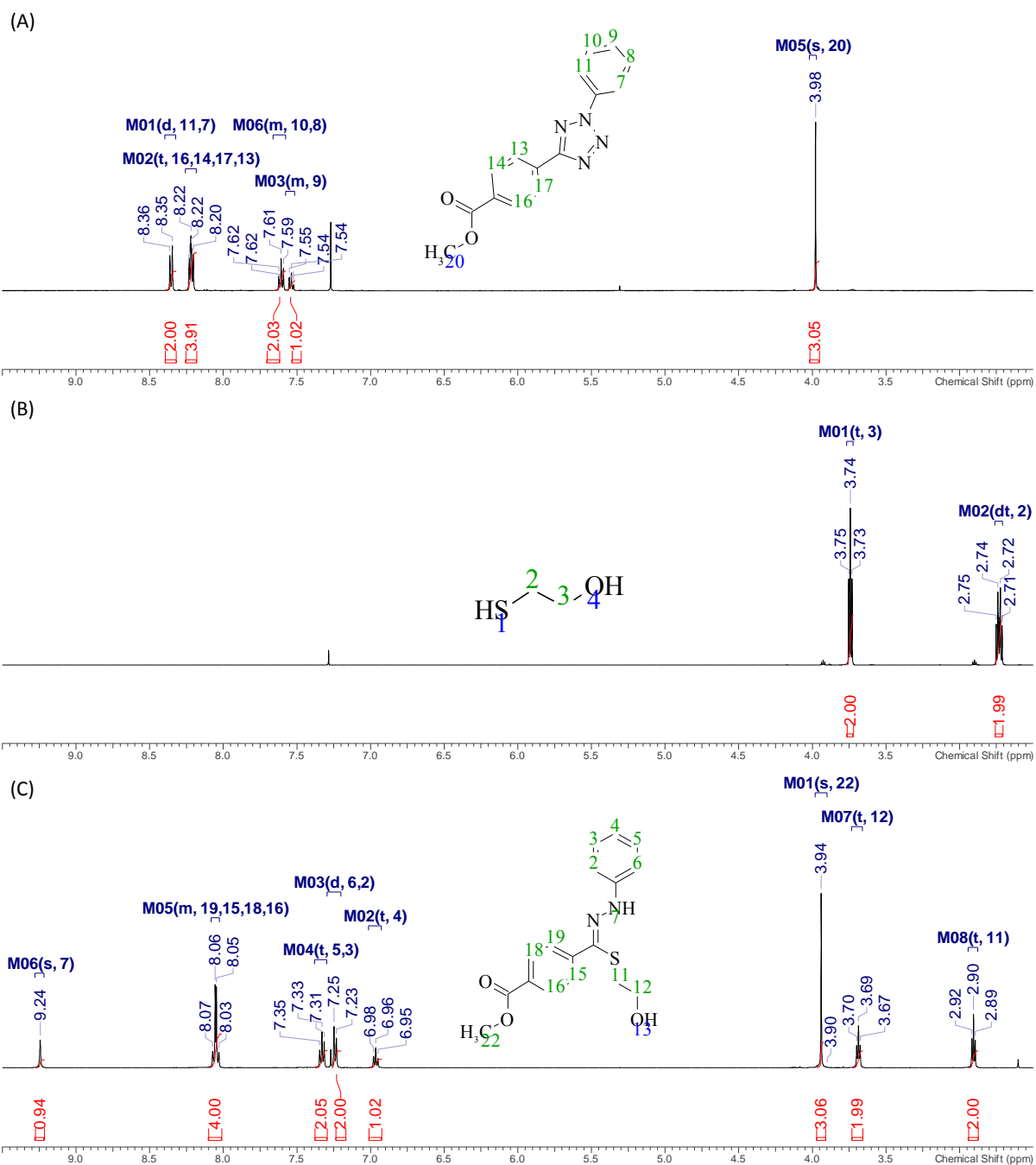


Figure 4.3. ESI-MS spectrum (negative mode) of the thiohydrazone product **3**, methyl (Z)-4-(((2-hydroxyethyl)thio)(2-phenylhydrazono)methyl)benzoate. The nucleophilic tetrazole-thiol addition product, calculated for C₁₇H₁₈N₂O₃S 330.10. [M-H]⁻, was found 329.08.

UV-Induced Tetrazole-Thiol Reaction for Polymer Conjugation and Surface Functionalization



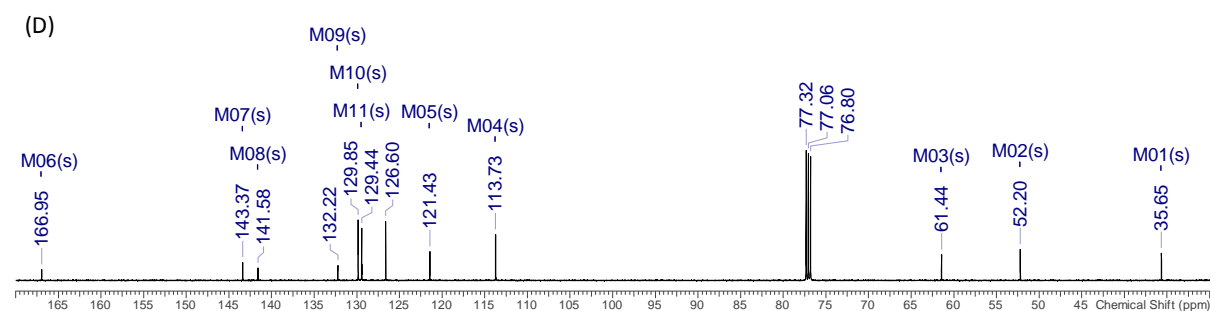


Figure 4.4. ^1H NMR spectra of the reactants (A) methyl 4-(2-phenyl-2*H*-tetrazol-5-yl)benzoate **1** and (B) 2-mercaptoethanol **2**, as well as the nucleophilic addition product **3** (C) formed after UV irradiation. (D) ^{13}C NMR spectrum of the thiohydrazone product **3**.

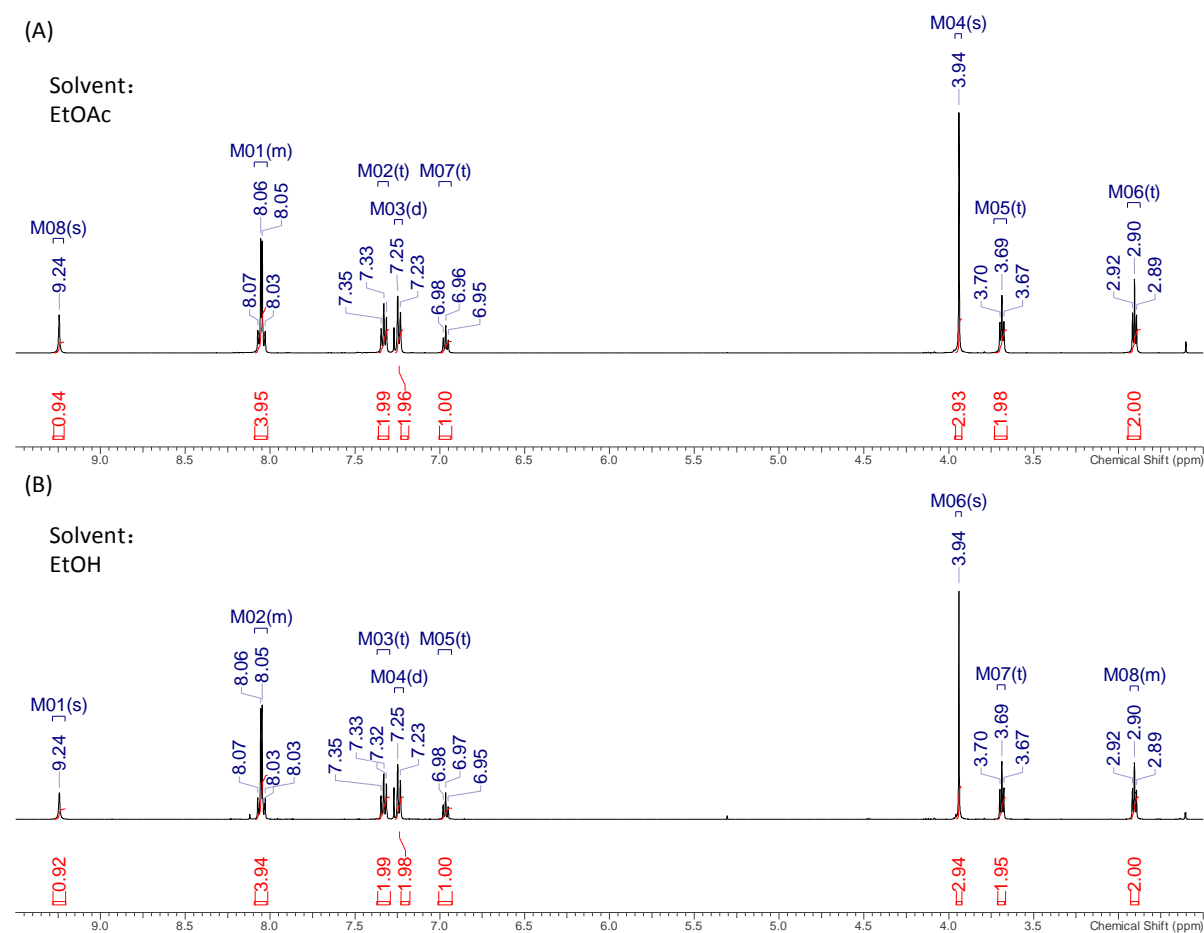


Figure 4.5. ^1H NMR spectra of the thiohydrazone product **3** formed after UV irradiation in ethyl acetate (A) and ethanol (B), respectively.

The kinetics of the UV-induced reaction was also investigated by ^1H NMR as shown in Figure 4.6. The NMR spectra clearly demonstrated fast decomposition of reactant **1** and formation of expected product **3**. This result is in agreement with the UV-Vis spectra shown in Figure 4.1C.

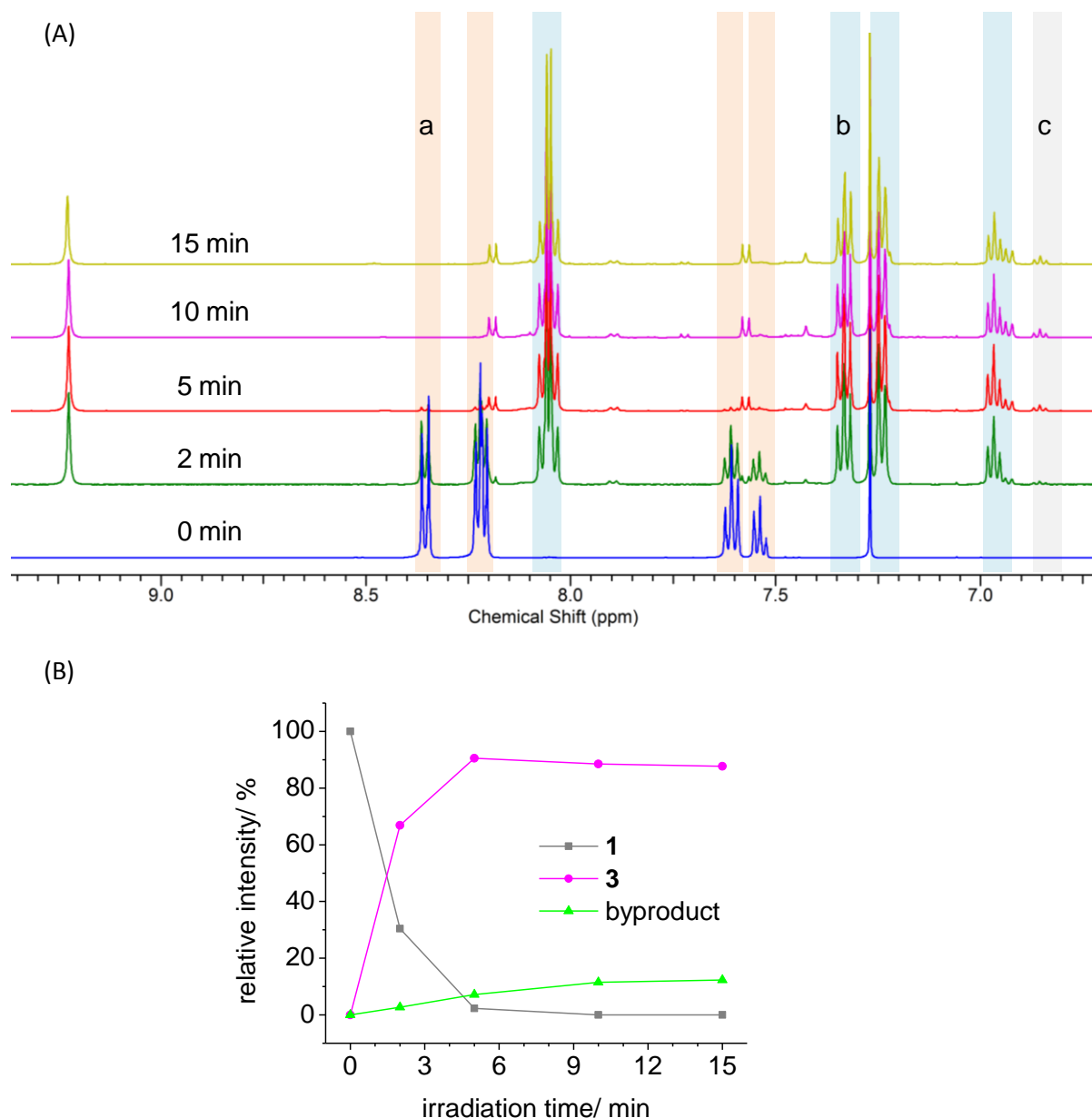


Figure 4.6. (A) ^1H NMR spectra monitoring of reaction progress between methyl 4-(2-phenyl-2*H*-tetrazol-5-yl)benzoate **1** (0.75 mg/mL) and 2-mercaptoethanol **2** (5 eq.) in ethyl acetate under 260 nm UV light (intensity 5 mW/cm²) at intervals of 0, 2, 5, 10, 15 min. (B) Evolution of the peak intensity of three major species during the UV irradiation. The NMR spectra clearly demonstrated fast decomposition of reactant **1** and formation of

expected product **3**. This result is in agreement with the UV-Vis spectra shown in Figure 4.1. Relative intensity of each species was obtained from the integration of signals a, b and c associated with **1**, **3** and a byproduct, respectively. The reactant **1** decomposed completely after 5 min irradiation and the yield of thiohydrazonate product **3** reached 91%.

4.2.2 Isolated yield of the UV-induced tetrazole-thiol reaction under different conditions.

Table 4.1 shows isolated reaction yields after UV irradiation of tetrazole **1** in the presence of thiol **2** in both polar protic (ethanol) and aprotic (ethyl acetate) solvents under 260, 312 and 365 nm UV light. Since the photoactivity of diaryltetrazoles depends on their UV absorption properties^[81, 217] and **1** absorbs strongly at shorter wavelength region ($\lambda_{\text{max}} = 278$ nm), 260 nm and 312 nm irradiation afforded highest isolated yields in the range of 75%-95%. The reaction between **1** and equimolar amount of **2** in ethanol leads to 87% of the isolated product. It is also noteworthy that the thiohydrazonate product could be observed (28% isolated yield) after irradiation at 365 nm UV light. In contrast, 365 nm photoirradiation of **1** and methyl methacrylate did not yield any observable pyrazoline cycloadduct by using tetrazole-ene click reaction.^[217]

Table 4.1. Isolated yield of the UV-induced 1,3-dipolar nucleophilic addition between **1** and **2** under different conditions.

molar ratio between 1 and 2	UV _{260nm}		UV _{312nm}		UV _{365nm}
	1:1	1:5	1:1	1:5	1:5
ethanol	87%	92%	87%	95%	12%
ethyl acetate	76%	88%	79%	94%	28%

In order to test whether UV-induced tetrazole-thiol reaction can be performed in the presence of other nucleophiles, such as amines, a mixture of **1** with **2** (2.5 eq.) and ethanolamine (2.5 eq.) in ethanol solution was irradiated with UV _{$\lambda=312$ nm} for 2 h. Although the tetrazole-amine adduct was also detected by MS (Figure 4.7), the tetrazole-

thiol adduct **3** was isolated with the yield of 70%, showing that thiols can be used in this reaction even in the presence of amines in polar protic solvents.

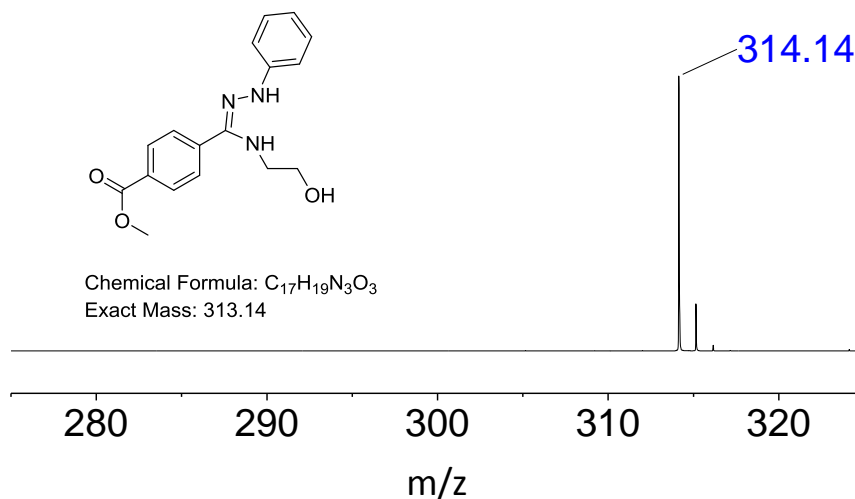


Figure 4.7. ESI-MS spectra of the nucleophilic addition product between tetrazole **1** and ethanolamine, methyl (Z)-4-(N-(2-hydroxyethyl)-N'-phenylcarbamohydrazone)benzoate. The nucleophilic tetrazole-amine addition product, calculated for C₁₇H₁₉N₃O₃ 313.14. [M+H]⁺, was found 314.14.

4.2.3 Protein modification via UV-induced tetrazole-thiol reaction in water

Most of surface immobilization or chemical modification of biomolecules require aqueous condition to avoid possible protein denaturation and loss of activity. To demonstrate that UV-induced tetrazole-thiol reaction can proceed in water, a tetrazole-bearing poly(ethylene glycol)methyl ether (MW 5000 g/mol) (PEG-tetrazole **4**, Figure 4.8) was used to react with **2** (5 eq.) in water under 312 nm UV light for 3 h. The conversion of **4** into the corresponding thiohydrazone was as high as 95% based on NMR (Figure 4.9).

In addition, bovine serum albumin (BSA), a protein containing one free peripheral thiol cysteine groups,^[218, 219] was reacted with **4** in aqueous PBS buffer under 312 nm UV light. A higher-molecular-weight band was observed in the presence of PEG-tetrazole **4** and UV irradiation after Coomassie Blue staining, suggesting the successful modification

of protein by PEG-tetrazole **4** after UV irradiation in the aqueous medium. Meanwhile, the presence of fluorescence further corroborates the successful protein functionalization. Due to the excess PEG-tetrazole **4** being used and the existence of amine groups in BSA, part of the protein could be multi-modified by the PEG-tetrazole **4** (Figure 4.10).

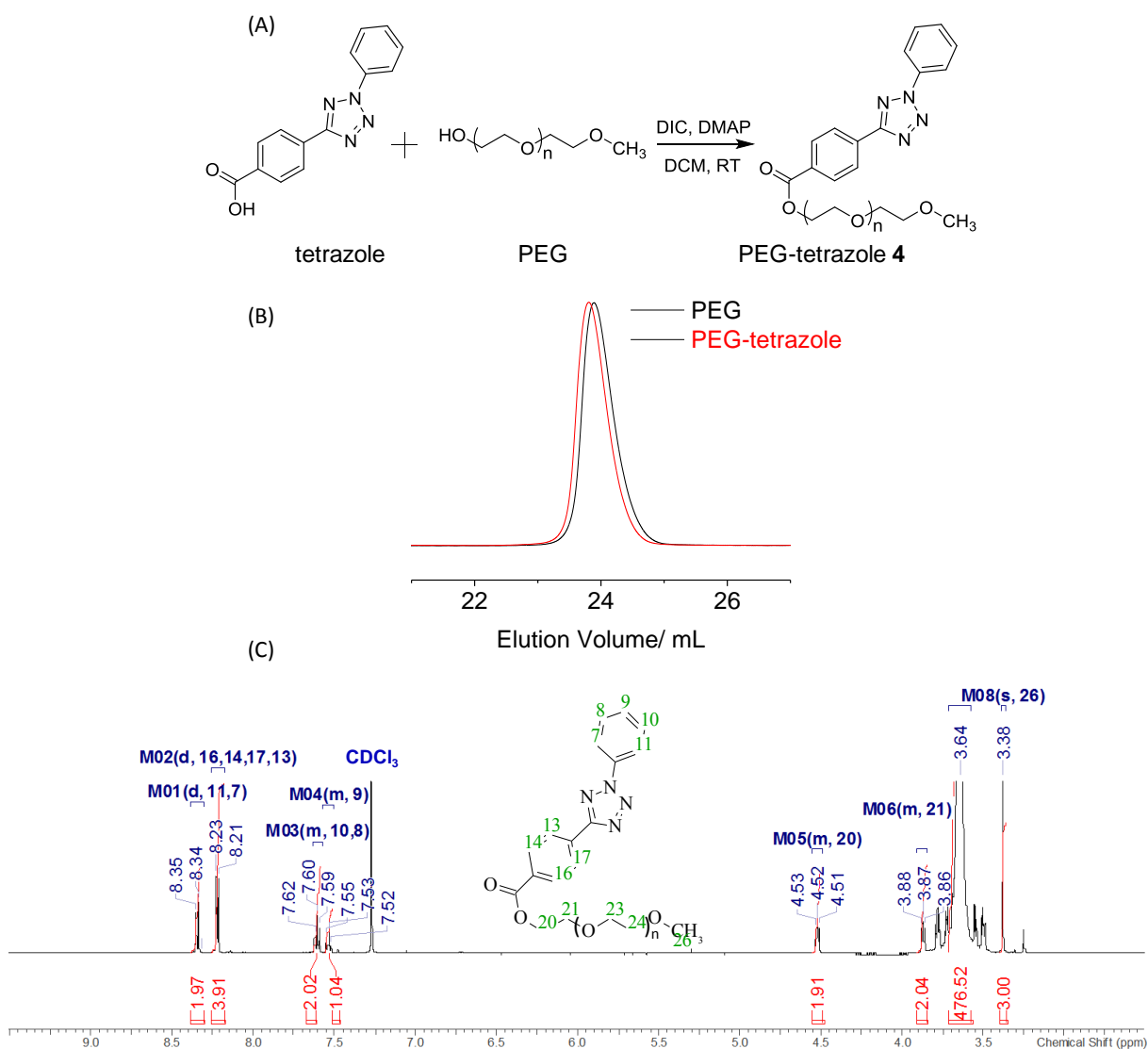


Figure 4.8. (A) Schematic representation of the formation of PEG-tetrazole **4** via esterification. (B) Overlay of GPC traces (THF) showing the formation of PEG-tetrazole **4** from PEG. The result shows that the PEG-tetrazole **4** polymer peak shifted towards lower elution volumes after the modification indicating an increased molecular weight. (C) ^1H NMR spectra of the PEG-tetrazole **4**. The presence of the resonance at 4.49 ppm (f), attributed to the PEG-tetrazole methylene protons, confirms the formation of the product. The grafting of PEG with tetrazole is calculated to be about 95% by comparing the

integrations of peaks from the methylene protons of PEG-tetrazole **4** at 4.49 ppm (f) and the methyl protons of the PEG at 3.35 ppm (i). Here the $n \approx 110$.

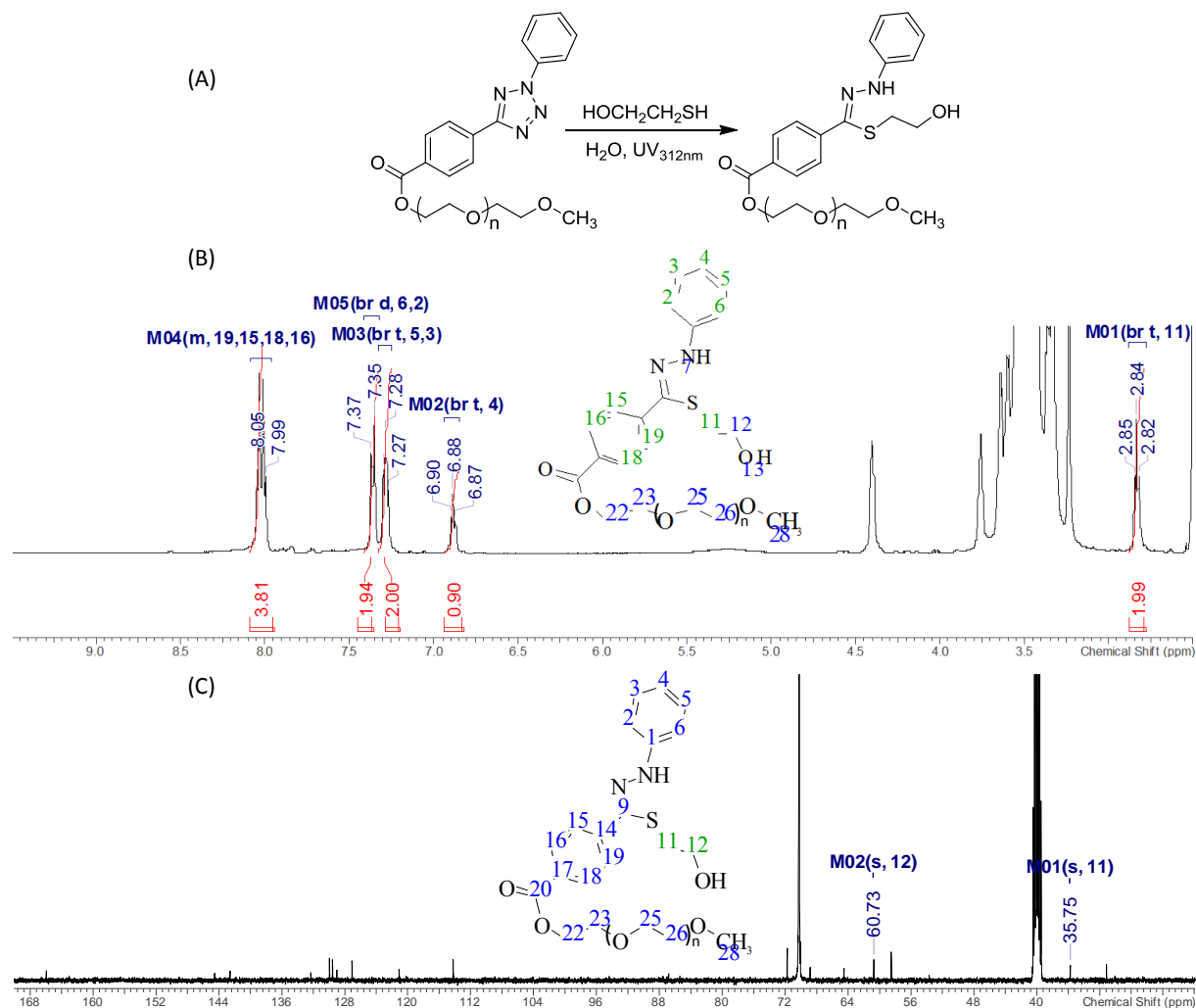


Figure 4.9. (A) Schematic representation of the UV-induced tetrazole-thiol reaction between PEG-tetrazole **4** and 2-mercaptoethanol **2** in water. (B) ^1H NMR spectra of the nucleophilic addition product formed after UV irradiation and purification. The presence of the resonance at 2.84 ppm, attributed to the methylene protons from 2-mercaptoethanol, confirms the formation of the nucleophilic addition product in water. The conversion is calculated to be about 95% by comparing the integrations of peaks from the methylene protons of nucleophilic addition product at 2.84 ppm and the aromatic protons. (C) ^{13}C NMR spectra of the nucleophilic addition product formed after UV irradiation and purification. The presence of the resonances at 35.75 ppm and 60.73 ppm, attributed to the methylene protons from 2-mercaptoethanol, confirms the formation of the nucleophilic addition product in water. Here the $n \approx 110$.

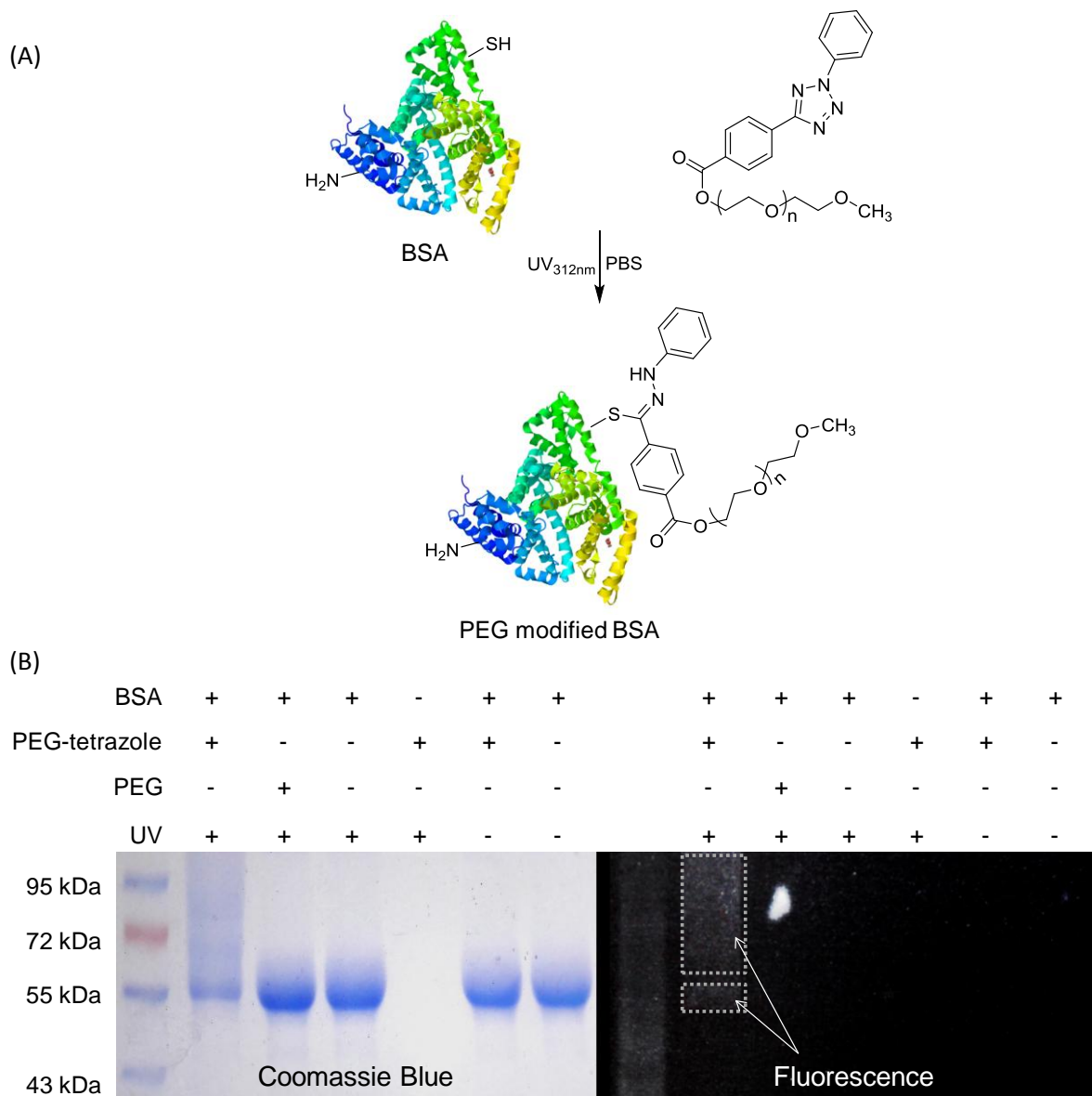


Figure 4.10. (A) Schematic representation of the bovine serum albumin (BSA) modification by PEG-tetrazole **4** using UV-induced tetrazole-thiol reaction in water. (B) Coomassie Blue staining (left) and in-gel fluorescence imaging (right, $UV_{\lambda_{ex}=365\text{ nm}}$) of various samples. Photoinduction was carried out for a duration of 5 min with UV irradiation at 312 nm and additional incubation for 2 h in PBS buffer. The experiment was repeated twice with similar results.

4.2.4 UV-induced tetrazole-thiol reaction for polymer conjugation

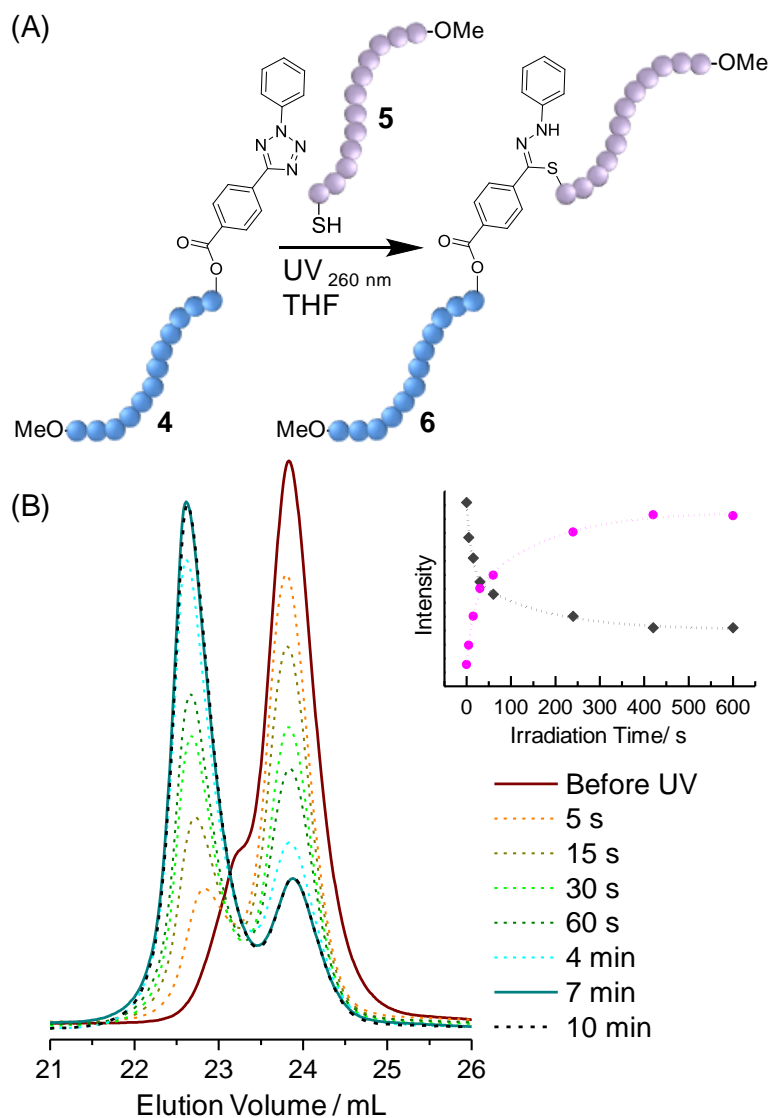


Figure 4.11. (A) UV-induced conjugation of two polymers using the tetrazole-thiol reaction to form PEG-block-PEG copolymer **6**. (B) GPC monitoring of the block-copolymer formation. Evolution of the intensity of elution volumes at 23.8 mL (\blacklozenge , gray) and 22.6 mL (\bullet , pink) with irradiation time (inset).

I further investigated the efficiency of the UV-induced tetrazole-thiol reaction for macromolecular conjugation. Figure 4.11A shows a model polymer conjugation experiment that was conducted. O-(2-mercaptoethyl)-O'-methylpolyethylene glycol **5** (MW 5000 g/mol) was utilized as the thiol-terminated polymer. Equimolar amounts of **4** and **5** were dissolved in THF (3 mg/mL) and subsequently irradiated with UV $_{\lambda=260\text{ nm}}$ light.

The reaction mixture was analyzed by GPC at different irradiation times (Figure 4.11B). A distinct shift of the GPC traces to lower elution volumes indicates successful formation of a polymer-polymer conjugate **6** already after 7 min of UV irradiation. The remaining small GPC peak corresponding to the starting material could be due to the incomplete tetrazole functionalization of the **4** as well as the non-equimolar ratio of reactant.

4.2.5 UV-induced tetrazole-thiol reaction for surface functionalization

The performance of the UV-induced tetrazole-thiol reaction for surface functionalization was also examined. A porous polymer layer functionalized with tetrazole (tetrazole surface) was applied as the substrate. To fabricate the tetrazole surface (Figure 4.12), a 12.5 μm thin, hydrophilic porous polymer film, poly(2-hydroxyethyl methacrylate-*co*-ethylene dimethacrylate) (HEMA-EDMA), was firstly prepared on a glass substrate using photo-initiated copolymerization of 2-hydroxyethyl methacrylate and ethylene dimethacrylate in the presence of porogens according to the known procedure.^[3] The hydroxyl groups were then esterified using 4-(2-phenyl-2*H*-tetrazol-5-yl)benzoic acid by incubating the surface in a dichloromethane solution of 4-(2-phenyl-2*H*-tetrazol-5-yl)benzoic acid, coupling reagent *N,N'*-diisopropylcarbodiimide (DIC) and catalyst 4-(dimethylamino)pyridine (DMAP) under stirring at room temperature for 24 hours.

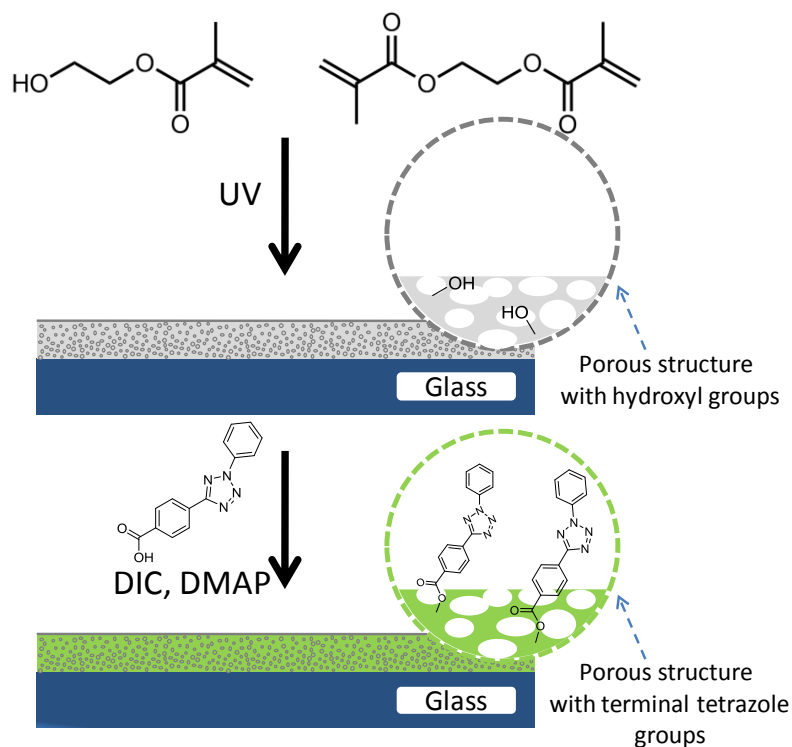


Figure 4.12. Schematic description of the fabrication of the tetrazole surface. After esterification, the hydrophilic HEMA-EDMA surface (static water contact angle θ_{st} 5°) was transformed into a hydrophobic tetrazole surface with the θ_{st} of 115° .

With the aid of a photomask, the surface was site-selective modified by 1*H*,1*H*,2*H*,2*H*-perfluorodecanethiol **7** under $UV_{\lambda=260nm}$ irradiation. The tetrazole surface was wetted with an ethyl acetate solution containing 20 vol% of 1*H*,1*H*,2*H*,2*H*-perfluorodecanethiol **7** and irradiated with $UV_{\lambda=260nm}$ through a quartz photomask for 2 min (site-selective modification, Figure 4.13A). The successful immobilization of thiol was confirmed by time-of-flight secondary ion mass spectrometry (ToF-SIMS). Both of the peaks corresponding to thiol ion **7** ($m/z=479.03$) as well as the corresponding conjugation product **8** at 716.98 were detected in the negative polarity mode (Figure 4.13B). The lateral distributions of these two signals are shown in Figure 4.13B. Figure 4.14A-C also shows clear patterns with good contrast of the F^- , S^- and $C_5H_4F_6S^-$ ions. After UV irradiation, the tetrazole ion (Figure 4.14D) only appeared on the non-irradiated areas, indicating the photolysis of tetrazole on the exposed area.

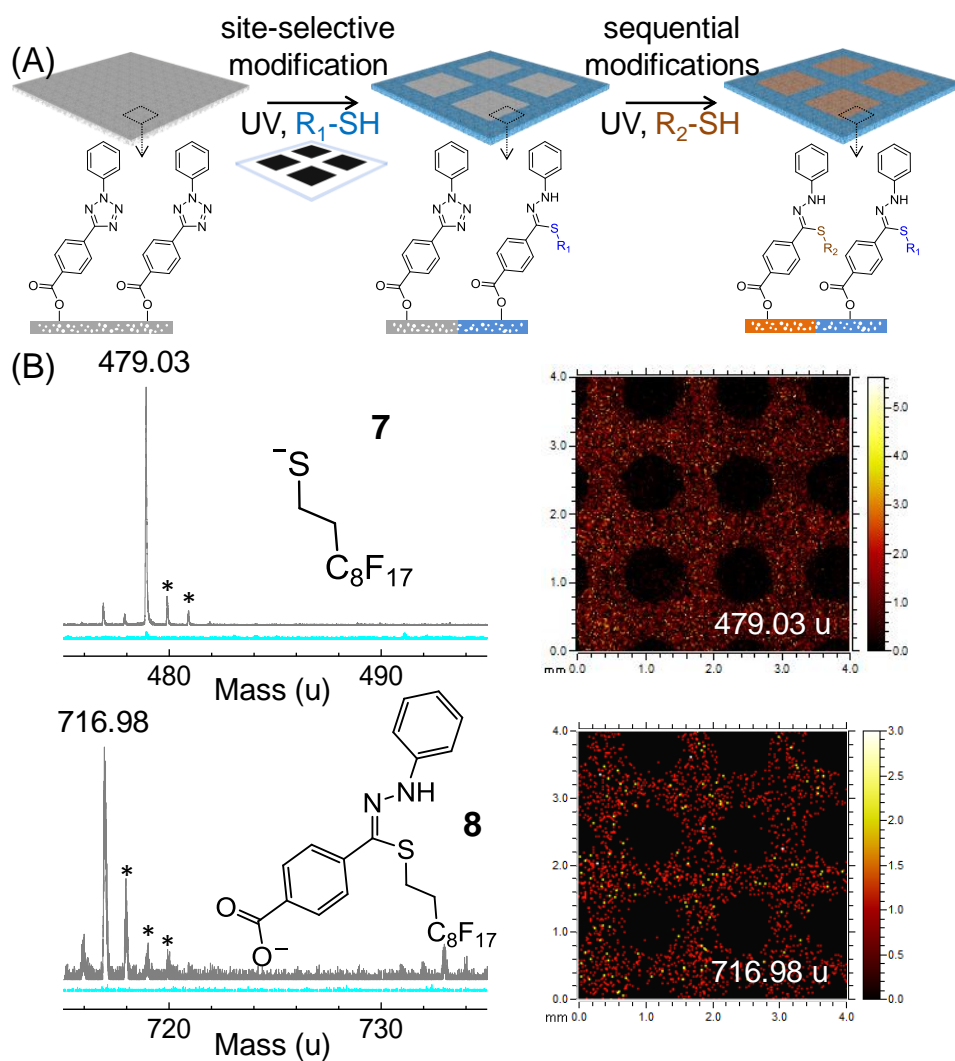


Figure 4.13. (A) Schematic showing surface micropatterning via the UV-induced tetrazole-thiol reaction. (B) ToF-SIMS (negative polarity) spectra of the tetrazole surface before (blue line) and after (dark line) functionalization with thiol **7**. Isotopic peaks are marked with asterisks. The ToF-SIMS images (fragments 479.03 u and 716.98 u, corresponding to the thiol **7** ion and the conjugation product **8**, respectively) of the polymer layer are inserted.

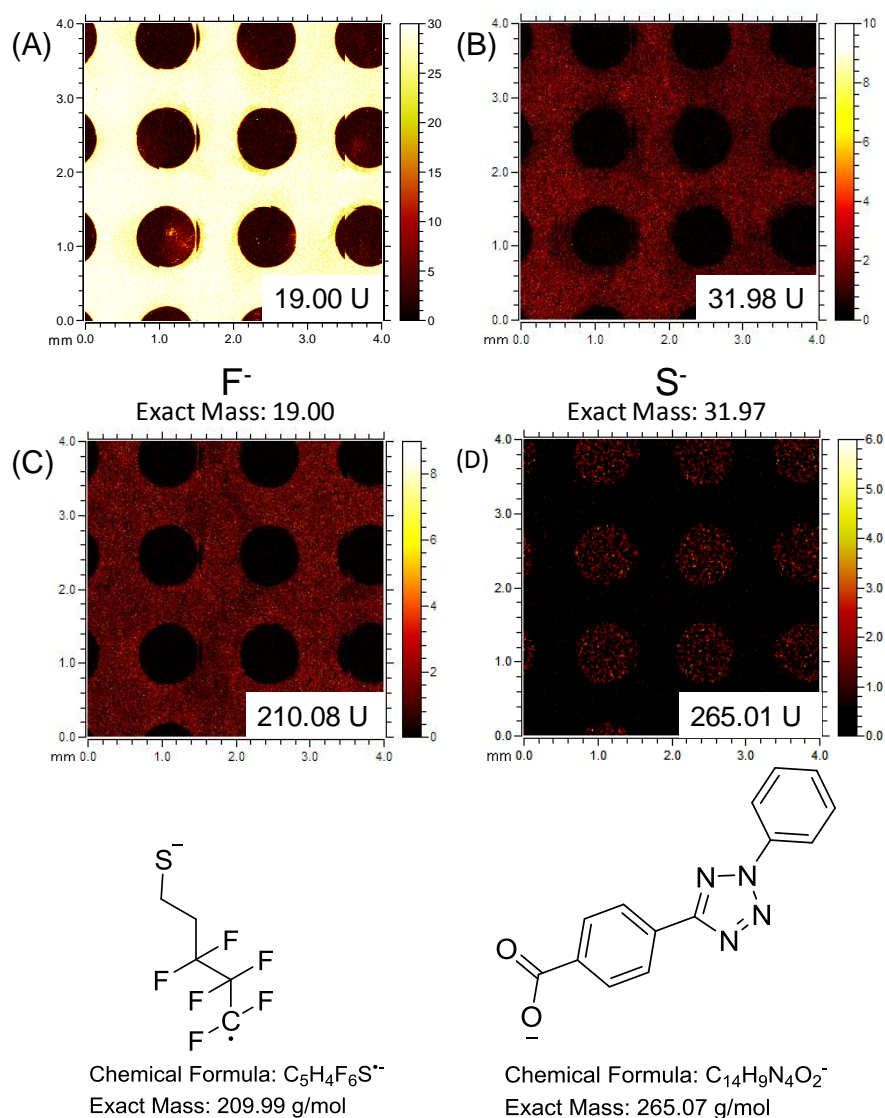


Figure 4.14. The ToF-SIMS images of the tetrazole surface after site-selective functionalization with *1H,1H,2H,2H*-perfluorodecanethiol **7**. (A) fragments 19.00 m/z, corresponding to F^- ; (B) fragments 31.98 m/z, corresponding to S^- ; (C) fragments 210.08 m/z, corresponding to the $C_5H_4F_6S^-$, part of *1H,1H,2H,2H*-perfluorodecanethiol; and (D) fragments 265.01 u, corresponding to the 4-(2-phenyl-2H-tetrazol-5-yl)benzoic acid ion.

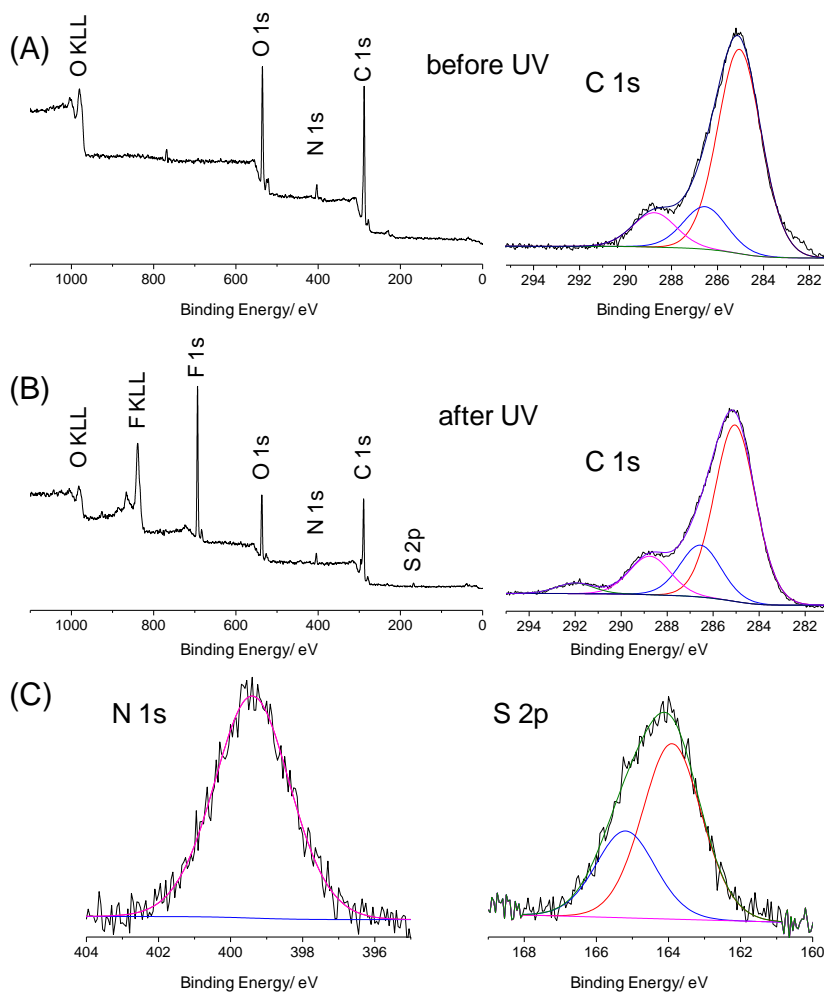
To confirm the efficiency of surface modification via UV-induced tetrazole-thiol reaction, X-ray photoelectron spectroscopy (XPS) was used. XPS revealed the presence of F1s, F KLL as well as S 2p peaks after thiol modification (Figure 4.15A and B). Furthermore, integration of N1s and S2p peak areas (Figure 4.15C and D) could be used to reveal the evolution of conversion with UV irradiation time,

$$\text{conversion} = \frac{n(\text{thiol})}{n(\text{tetrazole})} \geq \frac{n(S \text{ atom})}{n(N \text{ atom})/2} = \frac{I(S 2p) / S(S 2p)}{I(N 1s) / 2S(N 1s)}$$

where n is the number of moles, I is the peak area, and S is the surface sensitivity factor. Here, $S(S 2p)=0.37$ and $S(N 1s)=0.33$ ^[220]. The kinetic equation could be established well by using a logistic model ($R^2=0.9980$),

$$y = 0.91482 - 0.91473 / \left(1 + (t/1.11724)^{1.00521} \right)$$

where y is the conversion of the surface modification, and t is the UV irradiation time (min). The conversion reached 88% after 20 min of UV irradiation (Figure 4.15E).



(D)

Irradiation time	Area(N 1s)	Area(S 2p)
2 min	52425	17260
5 min	47223	19475
10 min	44847	20971
20 min	47210	23330
30 min	43719	21223

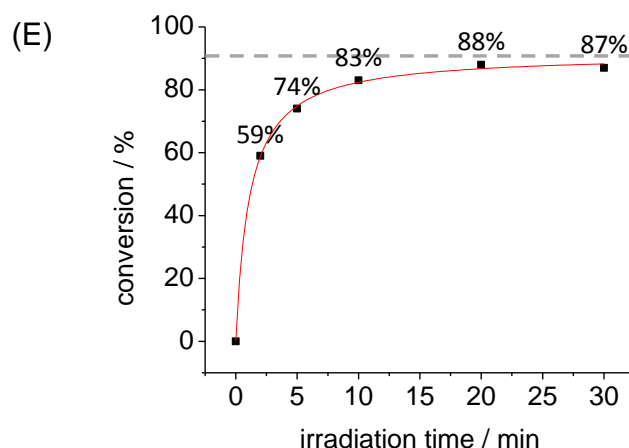


Figure 4.15. XPS survey spectra and curve-fitted high-resolution XPS C 1s spectra of the unmodified (A) and *1H,1H,2H,2H*-perfluorodecanethiol-modified (B) tetrazole surface. The new peak with binding energies at 292 eV in C1S spectra is the typical characteristics of $-CF_3$ and $-CF_2$ moieties. The main peak in the C1S spectrum at 285.0 eV is assigned to saturated carbon atoms (C–C, C–H) and is employed as a reference to compare the evolution of the different species present on the surface. (C) Curve-fitted high-resolution XPS N 1s and S 2p spectra of the thiol **7**-modified tetrazole surface. (D) Integration of N1s and S2p peak areas after UV irradiations. (E) Conversions calculated from the integration of N1s and S2p peak areas.

After tetrazole-thiol reaction, the appearance of fluorescence provides a visualization method to assess the success of surface modification (Figure 4.16A). Tetrazole surface modification with a thiol-containing fluorophore, Rhodamine-SH, was also shown in Figure 4.16B. The produced pattern shows a perfect superimposition of both red and green fluorescence. Surface micropatterns with feature sizes down to 10 μm could be obtained using an appropriate photomask (Figure 4.16C).

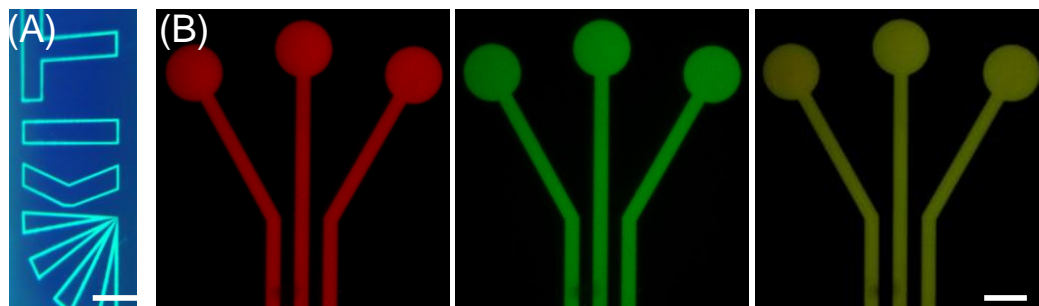


Figure 4.16. (A) Photograph of a thiol **7** patterned tetrazole surface under 365 nm UV light. The thiol modified area emits green fluorescence. Scale bar: 3 mm. (B) Red (left), green (middle) and red/green overlay (right) fluorescence microscope images of the tetrazole surface patterned by Rhodamine-SH showing both red and green fluorescence. Scale bar: 300 μm . (C) Fluorescence microscope images of Rhodamine-SH pattern on the tetrazole surface with lines of different widths.

The surface modification could be performed using different thiols in various common solvents. To assess the performance of the UV-induced tetrazole-thiol reaction under different conditions, the tetrazole surface was functionalized by both hydrophobic and hydrophilic thiols dissolved in several broadly used solvents. The tetrazole surfaces (θ_{st} 115° before thiol modification) could be functionalized by 1-dodecanethiol in ethanol (EtOH), ethyl acetate (EtOAc), acetone, dichloromethane (DCM), toluene and tetrahydrofuran (THF), which led to an increase of the θ_{st} up to ~143° independently of the solvent used (Figure 4.17). The grafting of the surface with cysteamine hydrochloride in ethanol transformed the hydrophobic tetrazole surface into hydrophilic ($\theta_{\text{st}}=22^\circ$).

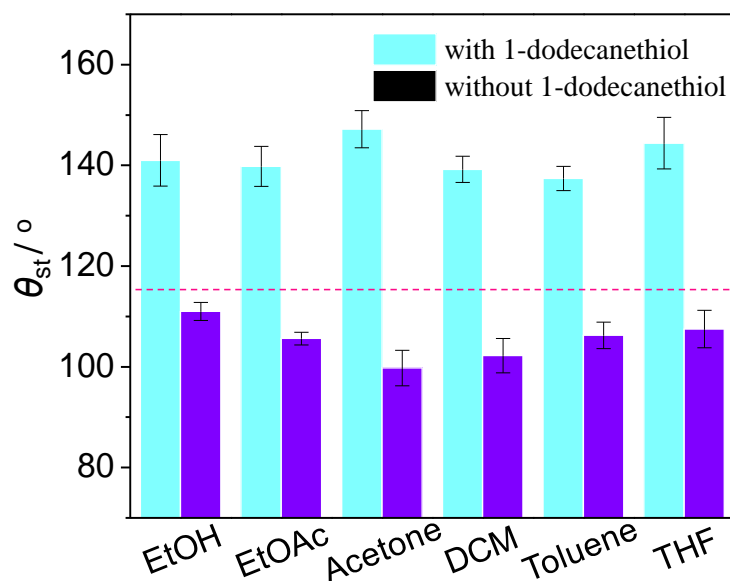


Figure 4.17. Static water contact angles (θ_{st}) of the tetrazole surfaces functionalized with 1-dodecanethiol dissolved in different solvents via the UV-induced tetrazole-thiol surface modification (cyan). The control experiments were taken under the same conditions without 1-dodecanethiol (violet). Photo modification was carried out for duration of 2 min with UV irradiation at 260 nm. The dashed pink line means the θ_{st} of the original tetrazole surface.

When fluorinated thiol *1H,1H,2H,2H*-perfluorodecanethiol **7** was employed, the hydrophobic tetrazole surface was transformed into a superhydrophobic surface exhibiting water contact angle θ_{st} , θ_{adv} and θ_{rec} as high as 167° , 170° and 161° , respectively. The SEM analysis in Figure 4.18A did not reveal any changes of the surface morphology after the thiol modification. Hence, the UV-induced tetrazole-thiol reaction could be used to create well-defined superhydrophobic-hydrophilic micropatterns of different geometries after sequential modifications (Figure 4.18B). The produced superhydrophobic barriers show good cell repellent properties and mCherry cells only adhered well to the hydrophilic areas (Figure 4.18C), which is important for a variety of different biotechnological applications ranging from sensors to cell screening microarrays.^[128]

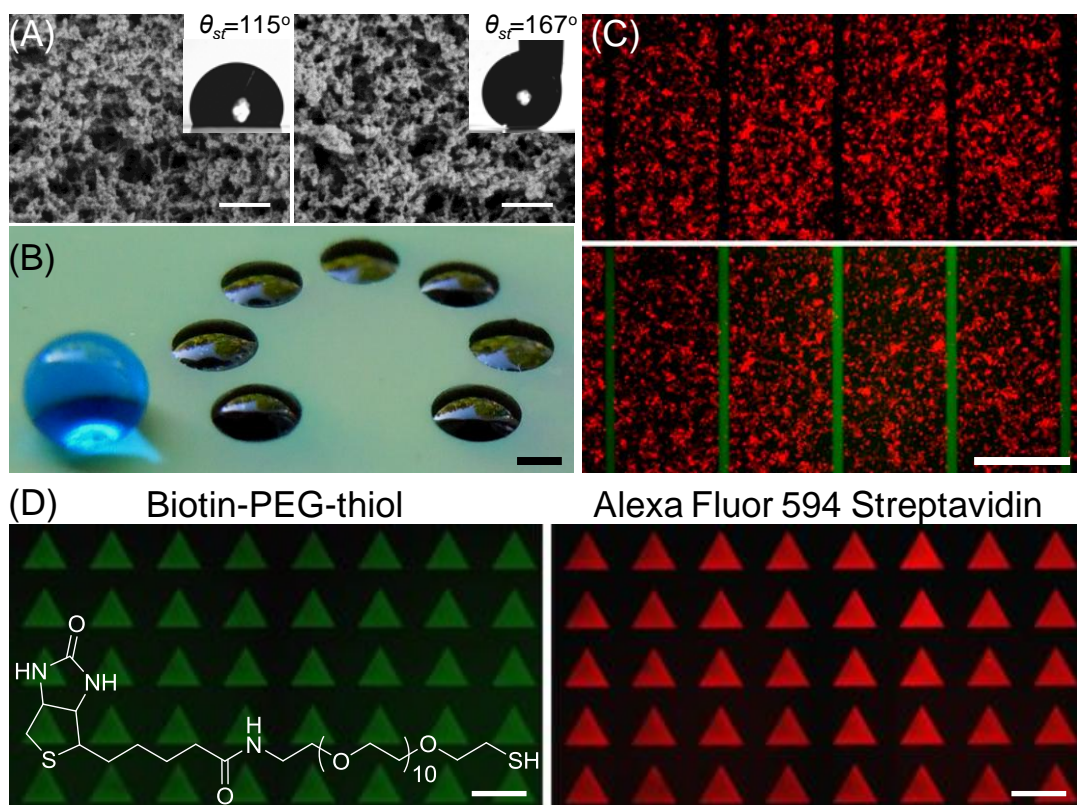


Figure 4.18. (A) SEM images of the tetrazole surface before (left) and after (right) modification with thiol **7**. The images of a water droplet on the corresponding surfaces are inserted. (B) Optical images of superhydrophobic-hydrophilic micropatterns. (C) Red (top) and red/green overlay (bottom) fluorescence microscope images of the mCherry-expressing rat mammary carcinoma cells after growing for 30 h on a thiol **7** patterned tetrazole surfaces. The **7** modified areas emit green fluorescence and show cell repellent properties. (D) Fluorescence microscopy image showing the immobilization of biotin-PEG-thiol in water under 365 nm UV light and Alexa Fluor 594 labeled-streptavidin binding. Scale bars: 500 nm (A) and 1 mm (B-D).

4.2.6 Patterning biomolecules in water under long-wavelength UV irradiation

To demonstrate that the tetrazole-thiol reaction could be used for the in-situ immobilization of biomolecules in aqueous solutions under long-wavelength UV irradiation, I patterned biotin-PEG-thiol onto the tetrazole surface in water under 365 nm UV light (Figure 4.18D). The surface was then incubated with Alexa Fluor 594 labeled-

streptavidin solution. Fluorescence microscopy revealed a two-color green-red fluorescent pattern, where green fluorescence originated from the thiohydrazone product of the tetrazole-thiol reaction, while red fluorescence originated from the Alexa Fluor 594 labeled-streptavidin bound to the biotinylated pattern.

4.3 Conclusions

A new versatile UV-induced tetrazole-thiol reaction for conjugation of polymers as well as surface functionalization is presented in this chapter. The reaction performs very rapidly at ambient temperature with high efficiency and absence of any catalyst. Furthermore, this photo-based approach can be performed in aqueous conditions, making it a promising tool for diverse biological and biotechnological applications, such as protein modification and surface biofunctionalization. The formation of a fluorescent product omits the necessity of using fluorescent labels and can be convenient for tracking the reaction or for multi-color labeling. Because of the above mentioned advantages of this method, I believe that the UV-induced tetrazole-thiol reaction will become a valuable tool for different applications.

4.4 Experimental details

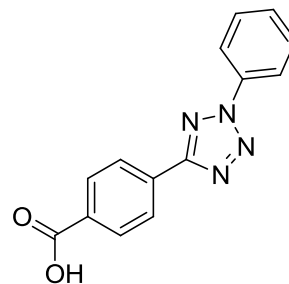
4.4.1 Materials

2-Hydroxyethyl methacrylate (HEMA) and ethylene dimethacrylate (EDMA) were purchased from Sigma-Aldrich (Germany) and purified using a short column filled with basic aluminum oxide to eliminate the inhibitors. Biotin-PEG-thiol was purchased from POLYPURE AS, Norway. Alexa Fluor 594 labeled streptavidin was purchased from Thermo Fisher Scientific Inc. All the other chemicals were purchased from Sigma-Aldrich (Germany) and used without further purification. The thiol-containing fluorophore (Rhodamine-SH) was kindly provided by Dr. Junsheng Li.^[120] Analytical thin layer chromatography (TLC) was performed on TLC aluminum oxide 60 F₂₅₄ neutral (Merck) and column chromatography was performed with aluminum oxide neutral (HPLC Flash Grade, 32-63 micron APS Powder, Alfa). Nexterion Glass B UV transparent glass plates (Schott, Germany) were used as substrates for polymer layers.

The polymerizations and UV-induced reactions were carried out on an OAI Model 30 deep-UV collimated light source (San Jose, CA) fitted with an USHIO 500 W Hg-xenon lamp (Japan).

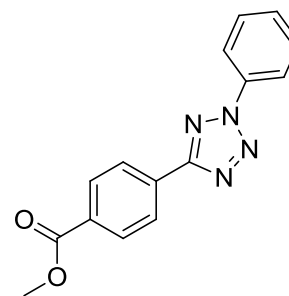
4.4.2 Preparation of 4-(2-phenyl-2H-tetrazol-5-yl)benzoic acid

The synthesis was carried out following a literature procedure.^[66] ¹H NMR (500 MHz, DMSO-d₆) δ 13.25 (s, 1H), 8.29 (d, 2H), 8.16 (t, 4H), 7.70 (t, 2H), 7.63 (t, 1H); ¹³C NMR (125 MHz, DMSO-d₆) δ 166.68, 163.78, 136.11, 132.77, 130.38, 130.27, 130.17, 126.76, 119.95; ESI-MS, calcd. for C₁₄H₉N₄O₂ 266.08 [M-H]⁻, found 265.05.



4.4.3 Preparation of methyl 4-(2-phenyl-2H-tetrazol-5-yl)benzoate 1

The synthesis was carried out by modifying 4-(2-phenyl-2H-tetrazol-5-yl)benzoic acid **2** with methanol via an esterification procedure. 4-(2-phenyl-2H-tetrazol-5-yl)benzoic acid (25 mg, 93 μmol) was dissolved into 10 mL of dichloromethane solution containing methanol (30 mg, 932 μmol) and catalyst 4-(dimethylamino)pyridine (DMAP) (56 mg, 0.46 mmol). Then, the coupling reagent *N,N'*-diisopropylcarbodiimide (DIC) (216 μL, 1.38 mmol) was added to the solution at 0 °C. After stirring the solution at RT for 48 h, the reaction mixture was washed with deionized water and the organic layer was collected. The solvent was removed under reduced pressure to give a crude product which was subsequently purified by Al₂O₃ column chromatography (CH₂Cl₂/hexane 6:4 v/v) to give the corresponding product. ¹H NMR (500MHz, CDCl₃) 8.33 (d, 2H), 8.19 (t, 4H), 7.58 (t, 2H), 7.51 (t, 1H), 3.95 (s, 3H); ¹³C NMR (125 MHz, CDCl₃) δ 166.75, 164.59, 137.02, 132.07, 131.45, 130.45, 130.11, 129.97, 127.2, 120.14, 52.57; ESI-MS, calcd. for C₁₅H₁₃N₄O₂ 280.10 [M+H]⁺, found 281.11.



4.4.4 Kinetic study of UV-induced 1,3-dipolar nucleophilic addition with **1** and **2**

Methyl 4-(2-phenyl-2H-tetrazol-5-yl)benzoate **1** and 2-mercaptoethanol **2** were dissolved in ethyl acetate to obtain concentrations of 20 μM and 100 μM , respectively. Separate reactions were set up by adding 2.5 mL mixture in quartz test tubes. The mixtures were irradiated with a 260 nm UV lamp (intensity, 5 mW cm^{-2}) for 0.5, 1, 2, 3, 4, 5, 6, 7, 8, 10 s, respectively. UV-Vis absorption spectra were recorded after irradiation.

4.4.5 Yield of UV-induced 1,3-dipolar nucleophilic addition with **1** and **2** under different conditions

n(tetrazole):n(thiol)=1:1

Methyl 4-(2-phenyl-2H-tetrazol-5-yl)benzoate **1** (16.5 mg, 59 μmol) and 2-mercaptoethanol **2** (4.2 μL , 59 μmol) were dissolved in 10 mL ethyl acetate or ethanol in a glass vial. Then the solution was bubbled by argon for 10 min. Under stirring, the solution was irradiated with 260-nm, 312-nm UV lamp, respectively (Intensity, 2 mW cm^{-2}) for 120 min. After evaporating the solvent under vacuum, the residue was purified by Al_2O_3 column chromatography (CH_2Cl_2 /ethyl acetate 1:2 v/v) to give the pure product **3**. The product **3** was subsequently weighted and analyzed by MS, ^1H NMR and ^{13}C NMR.

n(tetrazole):n(thiol)=1:5

Methyl 4-(2-phenyl-2H-tetrazol-5-yl)benzoate **1** (16.5 mg, 59 μmol) and 2-mercaptoethanol **2** (21 μL , 295 μmol) were dissolved in 10 mL ethyl acetate or ethanol in a glass vial. Then the solution was bubbled by argon for 10 min. Under stirring, the solution was irradiated with 260-nm, 312-nm and 365-nm UV lamp, respectively (Intensity, 2 mW cm^{-2}) for 120 min. After evaporating the solvent under vacuum, the residue was purified by Al_2O_3 column chromatography (CH_2Cl_2 /ethyl acetate 1:2 v/v) to give the pure product **3**. The product **3** was subsequently weighted and analyzed by MS, ^1H NMR and ^{13}C NMR.

The yields are shown in Table 4.1.

4.4.6 Preparation of PEG-tetrazole 4

The synthesis was carried out by modifying poly(ethylene glycol) methyl ether (MW=5000) with 4-(2-phenyl-2*H*-tetrazol-5-yl)benzoic acid via a standard esterification procedure. Poly(ethylene glycol) methyl ether (309.3 mg) was dissolved into 15 mL of dichloromethane solution containing 4-(2-phenyl-2*H*-tetrazol-5-yl)benzoic acid (27.3 mg, 0.103 mmol) and catalyst 4-(dimethylamino)pyridine (DMAP) (13 mg, 0.105 mmol). Then, the coupling reagent *N,N'*-diisopropylcarbodiimide (DIC) (23.2 μ L, 0.15 mmol) was added to the solution at 0 °C. After stirring the solution at RT for 48 h., 50 mL of cold diethyl ether was added and the precipitate formed was collected and dried under vacuum. The crude product was re-dissolved in dichloromethane and precipitated by adding cold diethyl ether, this procedure was repeated three times. The corresponding product was characterized by GPC and ¹H NMR (Figure 4.8).

4.4.7 UV-induced 1,3-dipolar nucleophilic addition in water

To demonstrate that UV-induced tetrazole-thiol reaction can also proceed in water, PEG-tetrazole **4** (71.6 mg) was used to react with 2-mercaptoethanol (5 eq., 6.0 μ L)) in water under 312 nm UV light for 3 h (Intensity, 2 mW cm⁻²). After evaporating the solvent under vacuum, the residue was redissolved into 2 mL THF. A fine precipitate was formed by adding 12 mL diethyl ether and isolated by centrifugation. Repeat the dissolution and precipitation twice. Conversion was estimated based on NMR spectra (Figure 4.9). Instead of being quenched by H₂O, the nitrilimine intermediate of PEG-tetrazole **4** reacted with 2-mercaptoethanol **2**, giving rise to the thiohydrazone product with 95% conversion. This result proves the practicability of the UV-induced tetrazole-thiol reaction in aqueous solution.

4.4.8 Modification of bovine serum albumin (BSA) by PEG-tetrazole

25 μ L of PEG-tetrazole **4** (5 mg/mL in PBS buffer) or PEG (5 mg/mL in PBS buffer) or PBS buffer were added to 25 μ L solutions of BSA solution (3 mg/mL, PBS buffer) in a 96-well micro plate. After irradiating with a 312-nm UV lamp for 5 min, the solutions were incubated for 2 h at 37 °C. The mixtures were boiled at 95 °C for 5 min after being

added 10 μL 5 \times SDS sample buffer. The samples were then loaded onto a 8% polyacrylamide gel and subjected to protein electrophoresis at 130 V for 2 h. The fluorescent bands in the gel were visualized by illuminating the gel under 365-nm UV light. Afterwards, the same gel was stained with Coomassie blue.

4.4.9 Polymer-polymer coupling

PEG-tetrazole **4** (38 mg) and O-(2-mercaptoethyl)-O'-methylpolyethylene glycol **5** (MW=5000) (36.5 mg) were dissolved in THF (25 mL). Separate reactions were set up by adding 2.5 mL mixture in glass vials. The mixtures were irradiated with a 260 nm UV lamp (Intensity = 5 mW cm^{-2}) under argon for 0 sec, 5 sec, 15 sec, 30 sec, 60 sec, 4 min, 7 min and 10 min, respectively. Solvents were evaporated under vacuum. The residues were redissolved in THF and withdrawn for GPC measurements. A distinct shift of the GPC traces to lower elution volumes (Figure 4.11) indicates successful formation of a higher molecular weight polymer **6** by polymer-polymer conjugation. Half of the starting material already reacted after only 1 min of UV irradiation, and no significant difference was observed for samples taken after 7 min. The remaining small GPC peak corresponding to the starting material could be due to the incomplete tetrazole functionalization of the **4** as well as the non- equimolar ratio of the reactants. These results demonstrate that the UV-induced tetrazole-thiol reaction can also be applied for the conjugation of macromolecules.

4.4.10 Preparation of tetrazole-modified HEMA-EDMA films (tetrazole surface)

Here a published procedure developed in our group to make porous HEMA-EDMA polymer layer was firstly employed.^[47] Briefly, two 12.5 μm -thin strips of Teflon film (American Durafilm Co.) were placed at the edges of one 3-(trimethoxysilyl)propyl methacrylate modified glass-plate and one fluorinated glass slide was clamped on top of it. 70 μL of polymerization mixture of HEMA (24 wt%), EDMA (16 wt%), 1-decanol (12 wt%), cyclohexanol (48 wt%) and 2,2-dimethoxy-2-phenylacetophenone (DMPAP) (photoinitiator, 1 wt% with respect to monomers) were injected in the mold between the glass slides and irradiated for 15 min with 5 mW cm^{-2} 260 nm UV-light. The mold was

then carefully opened using a scalpel. The resulting superficial surface was removed by applying and rapidly removing adhesive film (“Scotch tape”) after separating the plates while the layer was still wetted. A homogeneous porous surface was formed. The plate was washed extensively with ethanol and kept in ethanol for some minutes before drying. Then two glass plates coated with a HEMA-EDMA layer were immersed into 50 mL of dichloromethane solution containing 4-(2-phenyl-2*H*-tetrazol-5-yl)benzoic acid (80 mg, 0.3 mmol) and catalyst 4-(dimethylamino)pyridine (DMAP) (56 mg, 0.46 mmol). Then, the coupling reagent *N,N'*-diisopropylcarbodiimide (DIC) (185.5 μ L, 1.2 mmol) was added to the solution at 0 $^{\circ}$ C. After stirring the solution at RT for 24 h, the plates were washed extensively with acetone, followed by drying.

4.4.11 UV-induced tetrazole-thiol reactions on tetrazole surface

1*H*,1*H*,2*H*,2*H*-perfluorodecanethiol **7 modification:** the tetrazole surface was wetted with an ethyl acetate solution containing 20 vol% 1*H*,1*H*,2*H*,2*H*-perfluorodecanethiol **7**, covered with a photomask, and irradiated by 5 mW cm⁻² 260 nm UV light for different time. After removing the photomask, the tetrazole surface was washed with acetone extensively and dried with a nitrogen gun.

Rhodamine-SH modification: the tetrazole surface was wetted with an acetone solution containing 1 wt% Rhodamine-SH, covered with a photomask, and irradiated by 5 mW cm⁻² 260 nm UV light for 2 min. After removing the photomask, the tetrazole surface was washed with acetone extensively and dried with a nitrogen gun.

1-dodecanethiol modification: 1-dodecanethiol (20 vol%) was dissolved in ethanol, ethyl acetate, acetone, dichloromethane, toluene, and tetrahydrofuran. The tetrazole surface was wetted with one of these thiol solutions, covered with a quartz slide, and irradiated by 5 mW cm⁻² 260 nm UV light for 2 min. After removing the cover, the tetrazole surface was washed with acetone extensively and dried with a nitrogen gun.

4.4.12 Preparation of superhydrophobic-hydrophilic micropatterns via tetrazole-thiol reaction

First, the tetrazole surface was wetted with acetone solution containing 20 vol% 1*H*,1*H*,2*H*,2*H*-perfluorodecanethiol **7**, covered by a photomask, and irradiated by UV

light (5 mW cm^{-2}) for 2 min. After removing the photomask, the surface was washed with acetone and dried. The polymer layer was wetted with an ethanol-water mixture (1:1) containing 20 wt% cysteamine hydrochloride and irradiated by UV light for another 2 min. Finally, the plate was washed extensively with acetone and dried with a nitrogen gun.

4.4.13 Designing a cell microarray on produced superhydrophobic-hydrophilic micropattern

mCherry-expressing rat mammary carcinoma cells were cultured in DMEM containing 10% of fetal bovine serum (FBS). A cell suspension was obtained by trypsinizing a confluent (80% monolayer) culture grown in a Petri dish in an incubator ($37 \text{ }^{\circ}\text{C}$, 5% CO_2) for 2-3 days. For sterilization, the glass substrate with a superhydrophobic-hydrophilic pattern was kept in ethanol for 20 min, dried in air, and placed in a 10 mL Petri dish. 5 mL of cell-suspension was added so that the plate was fully covered (seeding density: 43200 cells/cm^2). The culture medium was changed after culturing the seeded array in the incubator for 5 h. The cell array was cultured for another 25 h.

4.4.14 Immobilization of biotin-PEG-thiol on tetrazole surface and Streptavidin binding

Firstly, the tetrazole surface was wetted by an aqueous solution containing 10 vol% ethanol. Then the plate was washed extensively with pure water to replace the solution in the pores. Excess water was shaken off from the surface. 2 mg/mL biotin-PEG-thiol aqueous solution was dropped on the surface. The polymer layer was irradiated with 365-nm UV light (2 mW cm^{-2}) through a photomask for 10 min. Then, the plate was washed extensively with water. The water wetted surface was then irradiated for another 10 min under 365-nm UV light to decompose the residual tetrazole groups. Substrate surfaces were incubated for 30 min in PBS buffer at $37 \text{ }^{\circ}\text{C}$. Subsequently, the substrates were covered with a solution of streptavidin (Alexa Fluor 594 labeled streptavidin, 1 mg/mL) in PBS buffer. After 30 min, the surfaces were washed with the PBS buffer, rinsed with distilled water and dried with a nitrogen gun.

Chapter 5. Summary and outlook

This PhD work describes three projects aimed at the spatial surface modification by using the classical established or newly developed photo-induced thiol-based reactions.

In the first project, a new method for fabricating superhydrophilic-superhydrophobic micropatterns on an alkyne-modified porous polymer layer via UV-induced thiol-yne reactions is described. Compared with photografting method developed by Zahner et al^[19] in our group, this method is more versatile and facile. A wide variety of thiols including fluorophores or biomolecules is available for the surface modification. The resulting pattern on polymer surface shows high resolution (10 μm), high chemical stability and high mechanical robustness as well, making this modification method a standard protocol for the fabrication of superhydrophilic-superhydrophobic micropatterns in our lab. The water microdroplet arrays formed on the superhydrophilic-superhydrophobic pattern were also used to fabricate freestanding metal-organic framework (MOF) microsheets with designed size and shape.^[221] In addition, the alkyne modified azide-reactive polymer layer was also prepared, allowing for the coupling of molecules functionalized with the azide group via copper(I)-catalyzed azide-alkyne cycloaddition (CuAAC).^[222] Due to the porous structure of the polymer layer and functional groups introduced on the surface, the patterned substrates can potentially be applied in the field of medical diagnostics, such as protein binding.

The superhydrophobic barriers of polymer layer in the first project show perfect water repellency, which enables to formation of arrays of water microdroplets arrays on these surfaces. However, these barriers don't have the ability to resist the wetting from by organic liquids with low surface tension. It is a big challenge to develop a substrate for creating organic microdroplets arrays in combination with facile fabrication, mechanical robustness and high transparency. Thus, in the second project a straightforward two-step approach for the patterning on smooth oxide surfaces based on silanation and UV-induced thiol-ene reactions is developed. This method eliminates the problems of low transparency and complex fabrication, and makes substrates with excellent mechanical stability possible. This patterned surface enables the fabrication of high-density arrays of microdroplets by discontinuous dewetting compatible with organic liquids with low surface tension. In addition, this approach provides a new way for the formation of

homogeneous arrays of hydrophobic nanoparticles and polymer micropads with controlled shapes. The parallel single-step addition of different chemicals into individual organic solvent microdroplets formed on this patterned surface is also demonstrated, showing the possibility of high-throughput screening applications. Thus, I believe this technology would have widely applications in both chemical and biological research fields, e.g., high-throughput synthesis and screening of organic chemical libraries on a chip.

New chemistries are always welcome. Thus the third project mainly focuses on a new photo-induced tetrazole-thiol reaction. The applicability of the UV-induced tetrazole-thiol reaction for small molecules is firstly proved, showing that under UV irradiation this reaction could proceed rapidly at room temperature, with high yields, without a catalyst, and in both polar protic and aprotic solvents. This tetrazole-thiol reaction has been successfully applied for the protein modification, rapid polymer-polymer conjugation and the formation of micropatterns on surfaces. Since the intermediate of tetrazole, nitrilimine, is highly reactive and could react with different nucleophiles such as amine at the same time, this tetrazole-thiol reaction could not be considered as a new photo-click chemistry. However, tetrazole-thiol reaction can yet be regarded as a useful tool for polymer-polymer coupling and surface functionalization. After this work, the reactions between reactive nitrilimine generated by photo photolysis of diaryltetrazoles and some other nucleophiles such as carboxyl group or nitrile group are also investigated by other groups.^[223, 224]

Here I would say cross-linked porous polymethacrylate layer (pore sizes are less than 1000 nm) is a very useful substrate for investigating photo-induced reactions. Due to the existence of hydroxyl groups on the surface, porous HEMA-EDMA polymer layer could be post-modified with different functional groups. This ideal template could offer many advantages: 1) this kind of polymer layers is facile to synthesize; 2) the polymer layer turns into transparent after wetting with solution, which eliminates the drawback of photopatterning that photo-induced reaction only take place on the superficial layer due to the penetration depth of the light into material is limited; 3) the product purification after reaction is simple; 4) it is facilitate the observation and quantification of water contact angle after reactions due to the surface roughness; and 5) compared to strictly 2D surfaces such as silicon wafer or glass, the 3D impregnation of the polymer with a fluorophores leads to considerably higher fluorescence intensities. Alkyne-modified porous HEMA-

EDMA for thiol-yne reactions in the first project^[225], tetrazole-modified porous HEMA-EDMA for tetrazole-thiol reactions in the third project^[175], and bis(2-carboxyethyl) disulfide modified porous HEMA-EDMA for photodynamic disulfide exchange reactions^[226] are all operated on this principle.

Given the above-mentioned advantages of the photo-induced chemistries on solid substrates, I expect these technologies for spatial surface modification based on the photo-induced thiol reactions to find widespread applications among both the materials science and chemistry communities.

References

- [1] A. Lafuma, D. Quere, *Nat Mater* **2003**, *2*, 457.
- [2] T. Darmanin, F. Guittard, *Materials Today* **2015**, *18*, 273.
- [3] H.-C. Flemming, J. Wingender, *Nat Rev Micro* **2010**, *8*, 623.
- [4] V. B. Schwartz, F. Th  iot, S. Ritz, S. P  tz, L. Choritz, A. Lappas, R. F  rch, K. Landfester, U. Jonas, *Advanced Functional Materials* **2012**, *22*, 2376.
- [5] J. Li, T. Kleintschek, A. Rieder, Y. Cheng, T. Baumbach, U. Obst, T. Schwartz, P. A. Levkin, *Acs Applied Materials & Interfaces* **2013**, *5*, 6704.
- [6] D. Rana, T. Matsuura, *Chemical reviews* **2010**, *110*, 2448.
- [7] L. Xiao, J. Li, S. Mieszkina, A. Di Fino, A. S. Clare, M. E. Callow, J. A. Callow, M. Grunze, A. Rosenhahn, P. A. Levkin, *Acs Applied Materials & Interfaces* **2013**, *5*, 10074.
- [8] J. Lv, Y. Song, L. Jiang, J. Wang, *ACS Nano* **2014**, *8*, 3152.
- [9] M. J. Kreder, J. Alvarenga, P. Kim, J. Aizenberg, *Nature Reviews Materials* **2016**, *1*, 15003.
- [10] V. Hejazi, K. Sobolev, M. Nosonovsky, *Scientific Reports* **2013**, *3*, 2194.
- [11] M.-Y. Tsai, C.-Y. Lin, C.-H. Huang, J.-A. Gu, S.-T. Huang, J. Yu, H.-Y. Chen, *Chemical Communications* **2012**, *48*, 10969.
- [12] B. Waterkotte, F. Bally, P. M. Nikolov, A. Waldbaur, B. E. Rapp, R. Truckenm  ller, J. Lahann, K. Schmitz, S. Giselbrecht, *Advanced Functional Materials* **2014**, *24*, 442.
- [13] P. X. Ma, *Advanced drug delivery reviews* **2008**, *60*, 184.
- [14] X. Feng, J. Zhai, L. Jiang, *Angewandte Chemie International Edition* **2005**, *44*, 5115.
- [15] F. Xia, L. Feng, S. Wang, T. Sun, W. Song, W. Jiang, L. Jiang, *Advanced Materials* **2006**, *18*, 432.
- [16] H. Lee, S. M. Dellatore, W. M. Miller, P. B. Messersmith, *Science* **2007**, *318*, 426.
- [17] S. N. Bhatia, D. E. Ingber, *Nat Biotech* **2014**, *32*, 760.
- [18] A. A. Popova, S. M. Schillo, K. Demir, E. Ueda, A. Nesterov-Mueller, P. A. Levkin, *Advanced Materials* **2015**, *27*, 5217.
- [19] D. Zahner, J. Abagat, F. Svec, J. M. J. Fr  chet, P. A. Levkin, *Advanced Materials* **2011**, *23*, 3030.
- [20] D. Samanta, A. Sarkar, *Chemical Society Reviews* **2011**, *40*, 2567.
- [21] B. Kasemo, *Surface Science* **2002**, *500*, 656.
- [22] C. Dorrer, O. Prucker, J. R  he, *Advanced Materials* **2007**, *19*, 456.
- [23] X. Yu, Z. Wang, Y. Han, *Microelectronic Engineering* **2008**, *85*, 1878.
- [24] C. Di Natale, F. A. Davide, A. D'Amico, G. Sberveglieri, P. Nelli, G. Faglia, C. Perego, *Sensors and Actuators B: Chemical* **1995**, *25*, 801.
- [25] Y. Xia, G. M. Whitesides, *Angewandte Chemie International Edition* **1998**, *37*, 550.
- [26] D. Qin, Y. N. Xia, G. M. Whitesides, *Nature Protocols* **2010**, *5*, 491.
- [27] M. Singh, H. M. Haverinen, P. Dhagat, G. E. Jabbour, *Advanced Materials* **2010**, *22*, 673.
- [28] K. Salaita, Y. H. Wang, C. A. Mirkin, *Nature Nanotechnology* **2007**, *2*, 145.
- [29] E. M. Hicks, S. L. Zou, G. C. Schatz, K. G. Spears, R. P. Van Duyne, L. Gunnarsson, T. Rindzevicius, B. Kasemo, M. Kall, *Nano Letters* **2005**, *5*, 1065.

- [30] K. Venkatakrishnan, B. K. A. Ngoi, P. Stanley, L. E. N. Lim, B. Tan, N. R. Sivakumar, *Applied Physics a-Materials Science & Processing* **2002**, 74, 493.
- [31] S.-H. Lee, J. J. Moon, J. L. West, *Biomaterials* **2008**, 29, 2962.
- [32] A. S. Quick, H. Rothfuss, A. Welle, B. Richter, J. Fischer, M. Wegener, C. Barner-Kowollik, *Advanced Functional Materials* **2014**, 24, 3571.
- [33] B. W. Smith, K. Suzuki, *Microlithography: science and technology*, Vol. 126, CRC press, 2007.
- [34] S. A. Ruiz, C. S. Chen, *Soft Matter* **2007**, 3, 168.
- [35] J. L. Wilbur, A. Kumar, E. Kim, G. M. Whitesides, *Advanced Materials* **1994**, 6, 600.
- [36] B. D. Gates, Q. Xu, M. Stewart, D. Ryan, C. G. Willson, G. M. Whitesides, *Chemical reviews* **2005**, 105, 1171.
- [37] A. Quist, E. Pavlovic, S. Oscarsson, *Analytical and Bioanalytical Chemistry* **2005**, 381, 591.
- [38] J. P. Renault, A. Bernard, A. Bietsch, B. Michel, H. R. Bosshard, E. Delamarche, M. Kreiter, B. Hecht, U. P. Wild, *Journal of Physical Chemistry B* **2003**, 107, 703.
- [39] Z. H. Nie, E. Kumacheva, *Nature Materials* **2008**, 7, 277.
- [40] T. Shimoda, K. Morii, S. Seki, H. Kiguchi, *Mrs Bulletin* **2003**, 28, 821.
- [41] J. S. Li, E. Ueda, A. Nallapaneni, L. X. Li, P. A. Levkin, *Langmuir* **2012**, 28, 8286.
- [42] G. M. Gratson, M. Xu, J. A. Lewis, *Nature* **2004**, 428, 386.
- [43] R. D. Piner, J. Zhu, F. Xu, S. Hong, C. A. Mirkin, *Science* **1999**, 283, 661.
- [44] D. S. Ginger, H. Zhang, C. A. Mirkin, *Angewandte Chemie International Edition* **2004**, 43, 30.
- [45] M. Hirtz, M. Lyon, W. Q. Feng, A. E. Holmes, H. Fuchs, P. A. Levkin, *Beilstein Journal of Nanotechnology* **2013**, 4, 377.
- [46] M. A. Tasdelen, Y. Yagci, *Angewandte Chemie-International Edition* **2013**, 52, 5930.
- [47] F. L. Geyer, E. Ueda, U. Liebel, N. Grau, P. A. Levkin, *Angewandte Chemie-International Edition* **2011**, 50, 8424.
- [48] Y. Fan, C. Deng, R. Cheng, F. Meng, Z. Zhong, *Biomacromolecules* **2013**, 14, 2814.
- [49] K. Tadanaga, J. Morinaga, A. Matsuda, T. Minami, *Chemistry of Materials* **2000**, 12, 590.
- [50] X. Zhang, H. Kono, Z. Liu, S. Nishimoto, D. A. Tryk, T. Murakami, H. Sakai, M. Abe, A. Fujishima, *Chemical Communications* **2007**, 0, 4949.
- [51] Y.-K. Lai, Y.-X. Tang, J.-Y. Huang, F. Pan, Z. Chen, K.-Q. Zhang, H. Fuchs, L.-F. Chi, *Sci. Rep.* **2013**, 3.
- [52] K. Liu, L. Jiang, *Nano Today* **2011**, 6, 155.
- [53] R. M. Hensarling, V. A. Doughty, J. W. Chan, D. L. Patton, *Journal of the American Chemical Society* **2009**, 131, 14673.
- [54] H. Trommsdorf, *Ann. Chem. Pharm.* **1834**, 11, 190.
- [55] H. D. Roth, *Angewandte Chemie-International Edition* **1989**, 28, 1193.
- [56] H. C. Kolb, M. G. Finn, K. B. Sharpless, *Angewandte Chemie International Edition* **2001**, 40, 2004.
- [57] M. Meldal, C. W. Tornøe, *Chemical reviews* **2008**, 108, 2952.
- [58] M. A. Tasdelen, Y. Yagci, *Tetrahedron Letters* **2010**, 51, 6945.
- [59] B. J. Adzima, Y. Tao, C. J. Kloxin, C. A. DeForest, K. S. Anseth, C. N. Bowman, *Nat Chem* **2011**, 3, 256.

- [60] R. T. Chen, S. Marchesan, R. A. Evans, K. E. Styan, G. K. Such, A. Postma, K. M. McLean, B. W. Muir, F. Caruso, *Biomacromolecules* **2012**, *13*, 889.
- [61] N. J. Agard, J. A. Prescher, C. R. Bertozzi, *Journal of the American Chemical Society* **2004**, *126*, 15046.
- [62] J. M. Baskin, J. A. Prescher, S. T. Laughlin, N. J. Agard, P. V. Chang, I. A. Miller, A. Lo, J. A. Codelli, C. R. Bertozzi, *Proceedings of the National Academy of Sciences* **2007**, *104*, 16793.
- [63] S. T. Laughlin, J. M. Baskin, S. L. Amacher, C. R. Bertozzi, *Science* **2008**, *320*, 664.
- [64] R. Manova, T. A. van Beek, H. Zuilhof, *Angewandte Chemie International Edition* **2011**, *50*, 5428.
- [65] S. V. Orski, A. A. Poloukhine, S. Arumugam, L. Mao, V. V. Popik, J. Locklin, *Journal of the American Chemical Society* **2010**, *132*, 11024.
- [66] W. Song, Y. Wang, J. Qu, M. M. Madden, Q. Lin, *Angewandte Chemie-International Edition* **2008**, *47*, 2832.
- [67] Y. Wang, W. Song, W. J. Hu, Q. Lin, *Angewandte Chemie-International Edition* **2009**, *48*, 5330.
- [68] J. S. Clovis, A. Eckell, R. Huisgen, R. Sustmann, *Chemische Berichte* **1967**, *100*, 60.
- [69] V. Lohse, P. Leihkauf, C. Csongar, G. Tomaschewski, *Journal für Praktische Chemie* **1988**, *330*, 406.
- [70] S. Arndt, H.-A. Wagenknecht, *Angewandte Chemie International Edition* **2014**, *53*, 14580.
- [71] F. Li, H. Zhang, Y. Sun, Y. Pan, J. Zhou, J. Wang, *Angewandte Chemie-International Edition* **2013**, *125*, 9882.
- [72] W. Song, Y. Wang, J. Qu, Q. Lin, *J. Am. Chem. Soc.* **2008**, *130*, 9654.
- [73] Z. Yu, L. Y. Ho, Q. Lin, *J. Am. Chem. Soc.* **2011**, *133*, 11912.
- [74] R. K. V. Lim, Q. Lin, *Accounts of Chemical Research* **2011**, *44*, 828.
- [75] M. Dietrich, G. Delaittre, J. P. Blinco, A. J. Inglis, M. Bruns, C. Barner-Kowollik, *Adv. Funct. Mater.* **2012**, *22*, 304.
- [76] T. Tischer, C. Rodriguez-Emmenegger, V. Trouillet, A. Welle, V. Schueler, J. O. Mueller, A. S. Goldmann, E. Brynda, C. Barner-Kowollik, *Adv. Mater.* **2014**, 4087.
- [77] E. Blasco, M. Piñol, L. Oriol, B. V. K. J. Schmidt, A. Welle, V. Trouillet, M. Bruns, C. Barner-Kowollik, *Adv. Funct. Mater.* **2013**, *23*, 4011.
- [78] K. N. Houk, J. Sims, C. R. Watts, L. J. Luskus, *Journal of the American Chemical Society* **1973**, *95*, 7301.
- [79] J. Geittner, R. Huisgen, R. Sustmann, *Tetrahedron Letters* **1977**, *18*, 881.
- [80] Y. Wang, W. J. Hu, W. Song, R. K. V. Lim, Q. Lin, *Organic Letters* **2008**, *10*, 3725.
- [81] Z. Yu, T. Y. Ohulchanskyy, P. An, P. N. Prasad, Q. Lin, *J. Am. Chem. Soc.* **2013**, *135*, 16766.
- [82] T. Posner, *Berichte der deutschen chemischen Gesellschaft* **1905**, *38*, 646.
- [83] A. B. Lowe, *Polymer Chemistry* **2010**, *1*, 17.
- [84] C. E. Hoyle, C. N. Bowman, *Angewandte Chemie International Edition* **2010**, *49*, 1540.
- [85] N. B. Cramer, S. K. Reddy, M. Cole, C. Hoyle, C. N. Bowman, *Journal of Polymer Science Part A: Polymer Chemistry* **2004**, *42*, 5817.
- [86] K. L. Killups, L. M. Campos, C. J. Hawker, *Journal of the American Chemical Society* **2008**, *130*, 5062.

- [87] P. Jonkheijm, D. Weinrich, M. Köhn, H. Engelkamp, P. C. M. Christianen, J. Kuhlmann, J. C. Maan, D. Nüsse, H. Schroeder, R. Wacker, R. Breinbauer, C. M. Niemeyer, H. Waldmann, *Angewandte Chemie International Edition* **2008**, *120*, 4493.
- [88] A. Dondoni, *Angewandte Chemie International Edition* **2008**, *47*, 8995.
- [89] H. Bader, L. C. Cross, I. Heilbron, E. R. H. Jones, *Journal of the Chemical Society (Resumed)* **1949**, 619.
- [90] B. D. Fairbanks, T. F. Scott, C. J. Kloxin, K. S. Anseth, C. N. Bowman, *Macromolecules* **2009**, *42*, 211.
- [91] R. Hoogenboom, *Angewandte Chemie International Edition* **2010**, *49*, 3415.
- [92] G. Chen, J. Kumar, A. Gregory, M. H. Stenzel, *Chemical Communications* **2009**, 6291.
- [93] D. Konkolewicz, A. Gray-Weale, S. b. Perrier, *Journal of the American Chemical Society* **2009**, *131*, 18075.
- [94] J. W. Chan, C. E. Hoyle, A. B. Lowe, *Journal of the American Chemical Society* **2009**, *131*, 5751.
- [95] R. K. V. Lim, Q. Lin, *Chemical Communications* **2010**, *46*, 7993.
- [96] E. Albrecht, J. Mattay, S. Steenken, *Journal of the American Chemical Society* **1997**, *119*, 11605.
- [97] K. C. Nicolaou, S. A. Snyder, T. Montagnon, G. Vassilikogiannakis, *Angewandte Chemie International Edition* **2002**, *41*, 1668.
- [98] S. Arumugam, V. V. Popik, *Journal of the American Chemical Society* **2011**, *133*, 5573.
- [99] S. Arumugam, S. V. Orski, J. Locklin, V. V. Popik, *Journal of the American Chemical Society* **2012**, *134*, 179.
- [100] S. Arumugam, V. V. Popik, *Journal of the American Chemical Society* **2011**, *133*, 15730.
- [101] K. Hildebrandt, T. Pauloehrl, J. P. Blinco, K. Linkert, H. G. Börner, C. Barner-Kowollik, *Angewandte Chemie International Edition* **2015**, *54*, 2838.
- [102] T. Pauloehrl, G. Delaittre, V. Winkler, A. Welle, M. Bruns, H. G. Börner, A. M. Greiner, M. Bastmeyer, C. Barner-Kowollik, *Angewandte Chemie International Edition* **2012**, *51*, 1071.
- [103] T. Gruending, K. K. Oehlenschlaeger, E. Frick, M. Glassner, C. Schmid, C. Barner-Kowollik, *Macromolecular Rapid Communications* **2011**, *32*, 807.
- [104] P. J. Wagner, D. Subrahmanyam, B. S. Park, *Journal of the American Chemical Society* **1991**, *113*, 709.
- [105] J. L. Segura, N. Martin, *Chemical reviews* **1999**, *99*, 3199.
- [106] K. K. Oehlenschlaeger, J. O. Mueller, N. B. Heine, M. Glassner, N. K. Guimard, G. Delaittre, F. G. Schmidt, C. Barner-Kowollik, *Angewandte Chemie International Edition* **2013**, *52*, 762.
- [107] M. Glassner, K. K. Oehlenschlaeger, A. Welle, M. Bruns, C. Barner-Kowollik, *Chemical Communications* **2013**, *49*, 633.
- [108] T. Pauloehrl, G. Delaittre, M. Bruns, M. Meißler, H. G. Börner, M. Bastmeyer, C. Barner-Kowollik, *Angewandte Chemie-International Edition* **2012**, *51*, 9181.
- [109] K. Schaper, M. Etinski, T. Fleig, *Photochemistry and Photobiology* **2009**, *85*, 1075.
- [110] S. Park, M. N. Yousaf, *Langmuir* **2008**, *24*, 6201.
- [111] S. Arumugam, V. V. Popik, *Journal of the American Chemical Society* **2012**, *134*, 8408.

- [112] T. Pauloehrl, A. Welle, K. K. Oehlenschlaeger, C. Barner-Kowollik, *Chemical Science* **2013**, *4*, 3503.
- [113] I. V. Zavarzin, V. N. Yarovenko, A. V. Shirokov, N. G. Smirnova, A. A. Es'kov, M. M. Krayushkin, *Arkivoc* **2003**, 205.
- [114] M. Kaupp, A. S. Quick, C. Rodriguez-Emmenegger, A. Welle, V. Trouillet, O. Pop-Georgievski, M. Wegener, C. Barner-Kowollik, *Advanced Functional Materials* **2014**, *24*, 5649.
- [115] H. Staudinger, *Berichte der deutschen chemischen Gesellschaft* **1907**, *40*, 1145.
- [116] F. A. Leibfarth, M. Kang, M. Ham, J. Kim, L. M. Campos, N. Gupta, B. Moon, C. J. Hawker, *Nat Chem* **2010**, *2*, 207.
- [117] M. A. Tasdelen, V. Kumbaraci, S. Jockusch, N. J. Turro, N. Talinli, Y. Yagci, *Macromolecules* **2008**, *41*, 295.
- [118] O. Soltani, J. K. De Brabander, *Angewandte Chemie-International Edition* **2005**, *44*, 1696.
- [119] G. Yilmaz, V. Kumbaraci, N. Talinli, P. Tatar, A. L. Demirel, Y. Yagci, *Journal of Polymer Science Part A: Polymer Chemistry* **2012**, *50*, 2517.
- [120] L. Li, J. Li, X. Du, A. Welle, M. Grunze, O. Trapp, P. A. Levkin, *Angewandte Chemie-International Edition* **2014**, *53*, 3835.
- [121] É. Hideg, C. Barta, T. Káai, I. Vass, K. Hideg, K. Asada, *Plant and Cell Physiology* **2002**, *43*, 1154.
- [122] L.-H. Liu, M. Yan, *Accounts of Chemical Research* **2010**, *43*, 1434.
- [123] S. J. Pastine, D. Okawa, B. Kessler, M. Rolandi, M. Llorente, A. Zettl, J. M. J. Fréchet, *Journal of the American Chemical Society* **2008**, *130*, 4238.
- [124] T. Young, *Philosophical Transactions of the Royal Society of London* **1805**, *95*, 65.
- [125] R. N. Wenzel, *Industrial & Engineering Chemistry* **1936**, *28*, 988.
- [126] A. Cassie, S. Baxter, *Transactions of the Faraday Society* **1944**, *40*, 546.
- [127] J. Jopp, H. Grüll, R. Yerushalmi-Rozen, *Langmuir* **2004**, *20*, 10015.
- [128] E. Ueda, P. A. Levkin, *Adv. Mater.* **2013**, *25*, 1234.
- [129] S. Wang, L. Jiang, *Advanced Materials* **2007**, *19*, 3423.
- [130] X.-M. Li, D. Reinhoudt, M. Crego-Calama, *Chemical Society Reviews* **2007**, *36*, 1350.
- [131] W. Barthlott, C. Neinhuis, *Planta* **1997**, *202*, 1.
- [132] X. F. Gao, L. Jiang, *Nature* **2004**, *432*, 36.
- [133] L. Feng, S. Li, Y. Li, H. Li, L. Zhang, J. Zhai, Y. Song, B. Liu, L. Jiang, D. Zhu, *Advanced Materials* **2002**, *14*, 1857.
- [134] T. Sun, L. Feng, X. Gao, L. Jiang, *Accounts of Chemical Research* **2005**, *38*, 644.
- [135] Y. Tian, L. Jiang, *Nat Mater* **2013**, *12*, 291.
- [136] C. W. Guo, S. T. Wang, H. Liu, L. Feng, Y. L. Song, L. Jiang, *Journal of Adhesion Science and Technology* **2008**, *22*, 395.
- [137] E. A. Vogler, *Advances in Colloid and Interface Science* **1998**, *74*, 69.
- [138] P. Roach, N. J. Shirtcliffe, M. I. Newton, *Soft Matter* **2008**, *4*, 224.
- [139] X. Zhang, F. Shi, J. Niu, Y. G. Jiang, Z. Q. Wang, *Journal of Materials Chemistry* **2008**, *18*, 621.
- [140] D. Quere, *Annual Review of Materials Research* **2008**, *38*, 71.
- [141] D. Wu, F. Xu, B. Sun, R. Fu, H. He, K. Matyjaszewski, *Chemical reviews* **2012**, *112*, 3959.
- [142] J. Urban, P. Jandera, *Journal of Separation Science* **2008**, *31*, 2521.
- [143] C. Viklund, F. Svec, J. M. J. Fréchet, K. Irgum, *Chemistry of Materials* **1996**, *8*, 744.

- [144] C. Yu, M. H. Davey, F. Svec, J. M. J. Fréchet, *Analytical Chemistry* **2001**, *73*, 5088.
- [145] P. A. Levkin, F. Svec, J. M. J. Fréchet, *Advanced Functional Materials* **2009**, *19*, 1993.
- [146] F. Svec, *Journal of Separation Science* **2004**, *27*, 747.
- [147] Q. Luo, H. Zou, X. Xiao, Z. Guo, L. Kong, X. Mao, *Journal of Chromatography A* **2001**, *926*, 255.
- [148] R. Wang, K. Hashimoto, A. Fujishima, M. Chikuni, E. Kojima, A. Kitamura, M. Shimohigoshi, T. Watanabe, *Nature* **1997**, 388, 431.
- [149] E. Ueda, F. L. Geyer, V. Nedashkivska, P. A. Levkin, *Lab on a Chip* **2012**, *12*, 5218.
- [150] E. Ueda, P. A. Levkin, *Advanced Healthcare Materials* **2013**, n/a.
- [151] V. Jokinen, R. Kostianen, T. Sikanen, *Advanced Materials* **2012**, *24*, 6240.
- [152] S. P. R. Kobaku, A. K. Kota, D. H. Lee, J. M. Mabry, A. Tuteja, *Angewandte Chemie International Edition* **2012**, *51*, 10109.
- [153] H. Mertaniemi, V. Jokinen, L. Sainiemi, S. Franssila, A. Marmur, O. Ikkala, R. H. A. Ras, *Advanced Materials* **2011**, *23*, 2911.
- [154] W. Song, A. C. Lima, J. F. Mano, *Soft Matter* **2010**, *6*, 5868.
- [155] S. Xing, R. S. Harake, T. Pan, *Lab on a Chip* **2011**, *11*, 3642.
- [156] Y. Han, P. Levkin, I. Abarientos, H. Liu, F. Svec, J. M. J. Fréchet, *Analytical Chemistry* **2010**, *82*, 2520.
- [157] S. Nishimoto, H. Sekine, X. Zhang, Z. Liu, K. Nakata, T. Murakami, Y. Koide, A. Fujishima, *Langmuir* **2009**, *25*, 7226.
- [158] L. Sainiemi, V. Jokinen, A. Shah, M. Shpak, S. Aura, P. Suvanto, S. Franssila, *Advanced Materials* **2011**, *23*, 122.
- [159] V. Jokinen, L. Sainiemi, S. Franssila, *Advanced Materials* **2008**, *20*, 3453.
- [160] R. P. Garrod, L. G. Harris, W. C. E. Schofield, J. McGettrick, L. J. Ward, D. O. H. Teare, J. P. S. Badyal, *Langmuir* **2006**, *23*, 689.
- [161] L. Zhai, M. C. Berg, F. Ç. Cebeci, Y. Kim, J. M. Milwid, M. F. Rubner, R. E. Cohen, *Nano Letters* **2006**, *6*, 1213.
- [162] Y. K. Lai, F. Pan, C. Xu, H. Fuchs, L. F. Chi, *Advanced Materials* **2013**, *25*, 1682.
- [163] S. M. Kang, I. You, W. K. Cho, H. K. Shon, T. G. Lee, I. S. Choi, J. M. Karp, H. Lee, *Angewandte Chemie International Edition* **2010**, *49*, 9401.
- [164] U. Manna, A. H. Broderick, D. M. Lynn, *Advanced Materials* **2012**, *24*, 4291.
- [165] B. D. Fairbanks, T. F. Scott, C. J. Kloxin, K. S. Anseth, C. N. Bowman, *Macromolecules* **2008**, *42*, 211.
- [166] N. S. Bhairamadgi, S. Gangarapu, M. A. Caipa Campos, J. M. J. Paulusse, C. J. M. van Rijn, H. Zuilhof, *Langmuir* **2013**, *29*, 4535.
- [167] M. Guerrouache, S. Mahouche-Chergui, M. M. Chehimi, B. Carbonnier, *Chemical Communications* **2012**, *48*, 7486.
- [168] C. Wendeln, S. Rinnen, C. Schulz, H. F. Arlinghaus, B. J. Ravoo, *Langmuir* **2010**, *26*, 15966.
- [169] C. Wendeln, I. Singh, S. Rinnen, C. Schulz, H. F. Arlinghaus, G. A. Burley, B. J. Ravoo, *Chemical Science* **2012**, *3*, 2479.
- [170] A. N. Efremov, E. Stanganello, A. Welle, S. Scholpp, P. A. Levkin, *Biomaterials* **2013**, *34*, 1757.
- [171] R. J. Jackman, D. C. Duffy, E. Ostuni, N. D. Willmore, G. M. Whitesides, *Analytical Chemistry* **1998**, *70*, 2280.

- [172] S. P. R. Kobaku, G. Kwon, A. K. Kota, R. G. Karunakaran, P. Wong, D. H. Lee, A. Tuteja, *Acs Applied Materials & Interfaces* **2015**, *7*, 4075.
- [173] Y. Xia, D. Qin, Y. Yin, *Current Opinion in Colloid & Interface Science* **2001**, *6*, 54.
- [174] S.-W. Hu, B.-Y. Xu, W.-k. Ye, X.-H. Xia, H.-Y. Chen, J.-J. Xu, *Acs Applied Materials & Interfaces* **2015**, *7*, 935.
- [175] W. Feng, L. Li, C. Yang, A. Welle, O. Trapp, P. A. Levkin, *Angewandte Chemie International Edition* **2015**, *54*, 8732.
- [176] W. Feng, L. Li, E. Ueda, J. Li, S. Heißler, A. Welle, O. Trapp, P. A. Levkin, *Adv. Mater. Inter.* **2014**, DOI: 10.1002/admi.201400269.
- [177] H. Li, Q. Yang, G. Li, M. Li, S. Wang, Y. Song, *Acs Applied Materials & Interfaces* **2015**, *7*, 9060.
- [178] Y. Du, M. Ghodousi, E. Lo, M. K. Vidula, O. Emiroglu, A. Khademhosseini, *Biotechnology and Bioengineering* **2010**, *105*, 655.
- [179] H. A. Biebuyck, G. M. Whitesides, *Langmuir* **1994**, *10*, 2790.
- [180] A. Tuteja, W. Choi, M. Ma, J. M. Mabry, S. A. Mazzella, G. C. Rutledge, G. H. McKinley, R. E. Cohen, *Science* **2007**, *318*, 1618.
- [181] X. Deng, L. Mammen, H. J. Butt, D. Vollmer, *Science* **2012**, *335*, 67.
- [182] K. Golovin, D. H. Lee, J. M. Mabry, A. Tuteja, *Angewandte Chemie-International Edition* **2013**, *52*, 13007.
- [183] P. Silberzan, L. Leger, D. Ausserre, J. J. Benattar, *Langmuir* **1991**, *7*, 1647.
- [184] K. M. Smyth, Massachusetts Institute of Technology, 2010.
- [185] T. L. Liu, C.-J. C. Kim, *Science* **2014**, *346*, 1096.
- [186] J. P. Zhang, S. Seeger, *Angewandte Chemie-International Edition* **2011**, *50*, 6652.
- [187] D. F. Cheng, C. Urata, B. Masheder, A. Hozumi, *Journal of the American Chemical Society* **2012**, *134*, 10191.
- [188] D. F. Cheng, C. Urata, M. Yagihashi, A. Hozumi, *Angewandte Chemie-International Edition* **2012**, *51*, 2956.
- [189] C. Urata, B. Masheder, D. F. Cheng, D. F. Miranda, G. J. Dunderdale, T. Miyamae, A. Hozumi, *Langmuir* **2014**, *30*, 4049.
- [190] T.-S. Wong, S. H. Kang, S. K. Y. Tang, E. J. Smythe, B. D. Hatton, A. Grinthal, J. Aizenberg, *Nature* **2011**, *477*, 443.
- [191] N. Vogel, R. A. Belisle, B. Hatton, T. S. Wong, J. Aizenberg, *Nature Communications* **2013**, *4*.
- [192] J. Huang, F. Kim, A. R. Tao, S. Connor, P. Yang, *Nat Mater* **2005**, *4*, 896.
- [193] J. Huang, R. Fan, S. Connor, P. Yang, *Angewandte Chemie International Edition* **2007**, *46*, 2414.
- [194] H. Yang, B. Yuan, X. Zhang, O. A. Scherman, *Accounts of Chemical Research* **2014**, *47*, 2106.
- [195] X. Shen, C.-M. Ho, T.-S. Wong, *The Journal of Physical Chemistry B* **2010**, *114*, 5269.
- [196] S. Sun, H. Zeng, D. B. Robinson, S. Raoux, P. M. Rice, S. X. Wang, G. Li, *Journal of the American Chemical Society* **2004**, *126*, 273.
- [197] N. J. Turro, *Modern molecular photochemistry*, University Science Books, 1991.
- [198] H. Okabe, **1978**.
- [199] S. L. Murov, I. Carmichael, G. L. Hug, *Handbook of photochemistry*, CRC Press, 1993.
- [200] J. P. Knowles, L. D. Elliott, K. I. Booker-Milburn, *Beilstein J. Org. Chem.* **2012**, *8*, 2025.

- [201] K. A. Mosiewicz, L. Kolb, A. J. van der Vlies, M. M. Martino, P. S. Lienemann, J. A. Hubbell, M. Ehrbar, M. P. Lutolf, *Nat Mater* **2013**, *12*, 1072.
- [202] C. Li, A. Glidle, X. Yuan, Z. Hu, E. Pulleine, J. Cooper, W. Yang, H. Yin, *Biomacromolecules* **2013**, *14*, 1278.
- [203] T. A. Martin, S. R. Caliarì, P. D. Williford, B. A. Harley, R. C. Bailey, *Biomaterials* **2011**, *32*, 3949.
- [204] Y. Li, B. H. San, J. L. Kessler, J. H. Kim, Q. Xu, J. Hanes, S. M. Yu, *Macromolecular Bioscience* **2015**, *15*, 52.
- [205] C.-M. Chan, T.-M. Ko, H. Hiraoka, *Surface science reports* **1996**, *24*, 1.
- [206] L. Spanhel, M. Haase, H. Weller, A. Henglein, *J. Am. Chem. Soc.* **1987**, *109*, 5649.
- [207] Y. Ikada, *Biomaterials* **1994**, *15*, 725.
- [208] J. A. Rogers, K. E. Paul, R. J. Jackman, G. M. Whitesides, *Applied Physics Letters* **1997**, *70*, 2658.
- [209] A. B. Lowe, C. E. Hoyle, C. N. Bowman, *Journal of Materials Chemistry* **2010**, *20*, 4745.
- [210] R. K. V. Lim, Q. Lin, *Acc. Chem. Res.* **2011**, *44*, 828.
- [211] Z. P. Yu, L. Y. Ho, Q. Lin, *J. Am. Chem. Soc.* **2011**, *133*, 11912.
- [212] R. Huisgen, J. Sauer, M. Seidel, *Chemische Berichte* **1961**, *94*, 2503.
- [213] R. Huisgen, R. Grashey, M. Seidel, H. Knupfer, R. Schmidt, *Justus Liebigs Annalen der Chemie* **1962**, *658*, 169.
- [214] J. Wang, W. Zhang, W. Song, Y. Wang, Z. Yu, J. Li, M. Wu, L. Wang, J. Zang, Q. Lin, *J. Am. Chem. Soc.* **2010**, *132*, 14812.
- [215] C.-C. Lin, A. Raza, H. Shih, *Biomaterials* **2011**, *32*, 9685.
- [216] M. Glassner, K. K. Oehlenschlaeger, T. Gruending, C. Barner-Kowollik, *Macromolecules* **2011**, *44*, 4681.
- [217] Y. Z. Wang, W. J. Hu, W. J. Song, R. K. V. Lint, Q. Lin, *Organic Letters* **2008**, *10*, 3725.
- [218] A. Svenson, J. Carlsson, *Biochimica et Biophysica Acta (BBA)-Protein Structure* **1975**, *400*, 433.
- [219] M. Oblak, A. Prezelj, S. Pecar, T. Solmajer, *Zeitschrift Fur Naturforschung C-a Journal of Biosciences* **2004**, *59*, 880.
- [220] C. D. Wagner, *Journal of Electron Spectroscopy and Related Phenomena* **1983**, *32*, 99.
- [221] M. Tsotsalas, H. Maheshwari, S. Schmitt, S. Heißler, W. Feng, P. A. Levkin, *Advanced Materials Interfaces* **2016**, *3*, n/a.
- [222] M. Hirtz, W. Feng, H. Fuchs, P. A. Levkin, *Advanced Materials Interfaces* **2016**, n/a.
- [223] Z. Li, L. Qian, L. Li, J. C. Bernhammer, H. V. Huynh, J.-S. Lee, S. Q. Yao, *Angewandte Chemie International Edition* **2016**, *55*, 2002.
- [224] S. Zhao, J. Dai, M. Hu, C. Liu, R. Meng, X. Liu, C. Wang, T. Luo, *Chemical Communications* **2016**, *52*, 4702.
- [225] W. Q. Feng, L. X. Li, E. Ueda, J. S. Li, S. Heissler, A. Welle, O. Trapp, P. A. Levkin, *Advanced Materials Interfaces* **2014**, *1*.
- [226] X. Du, J. Li, A. Welle, L. Li, W. Feng, P. A. Levkin, *Advanced Materials* **2015**, *27*, 4997.

**Eidesstattliche Versicherung gemäß § 8 der Promotionsordnung
der Naturwissenschaftlich-Mathematischen Gesamtfakultät
der Universität Heidelberg**

1. Bei der eingereichten Dissertation zu dem Thema

handelt es sich um meine eigenständig erbrachte Leistung.

2. Ich habe nur die angegebenen Quellen und Hilfsmittel benutzt und mich keiner unzulässigen Hilfe Dritter bedient. Insbesondere habe ich wörtlich oder sinngemäß aus anderen Werken übernommene Inhalte als solche kenntlich gemacht.

3. Die Arbeit oder Teile davon habe ich wie folgt/bislang nicht¹⁾ an einer Hochschule des In- oder Auslands als Bestandteil einer Prüfungs- oder Qualifikationsleistung vorgelegt.

Titel der Arbeit: _____

Hochschule und Jahr: _____

Art der Prüfungs- oder Qualifikationsleistung: _____

4. Die Richtigkeit der vorstehenden Erklärungen bestätige ich.

5. Die Bedeutung der eidesstattlichen Versicherung und die strafrechtlichen Folgen einer unrichtigen oder unvollständigen eidesstattlichen Versicherung sind mir bekannt.

Ich versichere an Eides statt, dass ich nach bestem Wissen die reine Wahrheit erklärt und nichts verschwiegen habe.

Ort und Datum

Unterschrift

¹⁾ Nicht Zutreffendes streichen. Bei Bejahung sind anzugeben: der Titel der andernorts vorgelegten Arbeit, die Hochschule, das Jahr der Vorlage und die Art der Prüfungs- oder Qualifikationsleistung.

Eidesstattliche Versicherung

Belehrung

Die Universitäten in Baden-Württemberg verlangen eine Eidesstattliche Versicherung über die Eigenständigkeit der erbrachten wissenschaftlichen Leistungen, um sich glaubhaft zu versichern, dass der Promovend die wissenschaftlichen Leistungen eigenständig erbracht hat.

Weil der Gesetzgeber der Eidesstattlichen Versicherung eine besondere Bedeutung beimisst und sie erhebliche Folgen haben kann, hat der Gesetzgeber die Abgabe einer falschen eidesstattlichen Versicherung unter Strafe gestellt. Bei vorsätzlicher (also wissentlicher) Abgabe einer falschen Erklärung droht eine Freiheitsstrafe bis zu 3 Jahren oder eine Geldstrafe.

Eine fahrlässige Abgabe (also Abgabe, obwohl Sie hätten erkennen müssen, dass die Erklärung nicht den Tatsachen entspricht) kann eine Freiheitsstrafe bis zu einem Jahr oder eine Geldstrafe nach sich ziehen.

Die entsprechenden Strafvorschriften sind in **§ 156 StGB** (falsche Versicherungen an Eides Statt) und in **§ 161 StGB** (fahrlässiger Falscheid, fahrlässige falsche Versicherung an Eides Statt) wiedergegeben.

§ 156 StGB: Falsche Versicherung an Eides Statt

Wer vor einer zur Abnahme einer Versicherung an Eides Statt zuständigen Behörde eine solche Versicherung falsch abgibt oder unter Berufung auf eine solche Versicherung falsch aussagt, wird mit Freiheitsstrafe bis zu drei Jahren oder mit Geldstrafe bestraft.

§ 161 StGB: Fahrlässiger Falscheid, fahrlässige falsche Versicherung an Eides Statt:

Abs. 1: Wenn eine der in den § 154 bis 156 bezeichneten Handlungen aus Fahrlässigkeit begangen worden ist, so tritt Freiheitsstrafe bis zu einem Jahr oder Geldstrafe ein.

Abs. 2: Strafflosigkeit tritt ein, wenn der Täter die falsche Angabe rechtzeitig berichtigt. Die Vorschriften des § 158 Abs. 2 und 3 gelten entsprechend.

Ort und Datum

Unterschrift